Effect of Electrostatic Charge on the Deposition of Monodisperse Uniformly Charged Particles in Idealized Extrathoracic Airway of an Adult, Child and Infant

by

Mehdi Azhdarzadeh

A thesis submitted in partial fulfillment of the requirements for the degree of

Doctor of Philosophy

Department of Mechanical Engineering
University of Alberta

Abstract

An *in vitro* study was performed on the effect of electrostatic charge on the deposition of monodisperse uniformly charged particles in the extrathoracic airway. An atomizer was designed and prototyped to generate particles using controlled Plateau-Rayleigh breakup, and charge via induction. Experiments were conducted in three phases for adult oral-extrathoracic, child oral-extrathoracic (children aged 6-14 years), and infant nasal-extrathoracic (infants aged 3-18 months) airways.

For the adult case, the Alberta idealized mouth-throat was used to mimic the oral-extrathoracic airway. Experiments covered particles with aerodynamic diameters of 3-6 μm, at flow rates of 15-30 L/min and charge per particle range of 0-25,000 e.

Tests for the deposition of particles in the child oral-extrathoracic airway were conducted using the Alberta idealized child mouth-throat and particles having aerodynamic diameters of 3-6 μm. Volume flow rate of inhaled gas was set to 10-20 L/min and charge of particles was in the range of 0-10,000 e per particle.

The Alberta idealized infant nose-throat model was utilized for the infant case, while aerodynamic diameters of particles were 3-6 μm at flow rates of 7.5-15 L/min and the charge level of particles varying between 0-10,000 e/particle.

The conductive version of the replicas was utilized to avoid any repulsion between the charge of the particles accumulated on the internal walls of the airway and the aerosol particles passing through the airway.

For each case, nonlinear least squares minimization was used to develop a different empirical equation, including electrostatic effects for predicting the deposition of particles in the airway.

Preface

This thesis is an original work done by Mehdi Azhdarzadeh, under the supervision of Dr. Warren H. Finlay, Dr. Reinhard Vehring, and Dr. Jason S. Olfert, and is prepared in 6 chapters.

Chapter 1 is the introduction to the research topic.

Chapter 2 explains theory and details of the design and protyping of an atomizer, particle charger, and a Faraday cup.

Chapter 3 has been published as Azhdarzadeh, M., Olfert, J. S., Vehring, R., Finlay, W. H. (2014). Effect of electrostatic charge on oral-extrathoracic deposition for uniformly charged monodisperse aerosols. Journal of Aerosol Science, 68:38-45.

Chapter 4 has been published as Azhdarzadeh, M., Olfert, J. S., Vehring, R., Finlay, W. H. (2014). Effect of Induced Charge on Deposition of Uniformly Charged Particles in a Pediatric Oral-Extrathoracic Airway. Aerosol Science and Technology, 48:508-514.

Chapter 5 has been published as Azhdarzadeh, M., Olfert, J. S., Vehring, R., Finlay, W. H. (2014). Effect of Electrostatic Charge on Deposition of Uniformly Charged Monodisperse Particles in the Nasal Extrathoracic Airways of an Infant. Journal of Aerosol Medicine and Pulmonary Drug Delivery, 27:1-5.

Chapter 6 contains the conclusions and summaries of the findings in the previous chapters.

Appendix A and B include drawings and details of assembling parts of the atomizer, particle charger and Faraday cup.

All design and building of the setup, data collection and data analysis were performed by me under the supervision of my supervisors.

Dedication

To my parents

An endless source of support and inspiration.

Acknowledgements

I would like to express my deepest appreciation to my supervisors Dr. Warren H. Finlay, Dr. Reinhard Vehring and Dr. Jason S. Olfert. Dr. Finlay, thank you for your valuable advice and endless support throughout the project. Dr. Vehring, I appreciate all the great things I learned from you, and your kind guidance. Dr. Olfert, I am grateful to you for your support, encouragement and valuable help. I am proud to have such scholars as my supervisors.

I sincerely acknowledge Dr. Vehring, Tarek Mohammad and Jeffery Fong for the initial idea of designing a monodisperse particle generator based on controlled Plateau-Rayleigh jet breakup and James Ivey for helping me to learn how to work with the spray dryer.

I need to thank all the machine shop and office support staff. Bernie Faulkner for his smart hints, Rick Bubenko for doing a great job in building required parts, and Rick Conrad for helping with electrical design of the setup.

I would like to thank Ms. Helena Orszanska and all my current and former colleagues in the ARLA lab, the Particle Engineering lab and Dr. Olfert's research group, especially Andriy Roshchenko, Connor Ruzycki, Nicholas Carrigy, Chelsea Morin, Laleh Golshahi, Emadeddin Javaheri, Azadeh Akhavan, Abouzar Shamsaddini, Tyler Johnson, Alberto Baldelli, Hui Wang, Dr. Mohammed Boraey and Dr. Susan Hoe for their friendship and valuable discussions regarding the research project. I also thank Dr. Andrew Martin for his kind advice and encouragement.

I want to express my special gratitude to my parents, my sister Zhaleh and my brothers Ebrahim and Ramin.

Finally, the financial support of the Alberta Lung Association through a studentship award and NSERC through a Collaborative Health Research Projects (CHRP) grant is acknowledged.

Mehdi Azhdarzadeh

March 17nd, 2014

Edmonton, AB, Canada

Table of Contents

List of Tables

List of Figures

List of Symbols

a	undisturbed radius of jet, (m)
A_{GS}	Gaussian surface, (m^2)
A_j	surface of disturbed jet, (m^2)
A_{j0}	surface of undisturbed jet, (m^2)
A_s	surface of airway, (m^2)
b_1, b_2	Coefficients of Paschen equation
c	disturbance growth rate, (1/s)
$\bar{c}_i$	mean thermal speed of ions (m/s)
C	electrical capacity, (F)
C_c	Cunningham correction factor
C_V	volume concentration of solution
d_a	aerodynamic diameter, (m)
d_c	characteristic diameter of airway, (m)
d_d	geometric diameter of droplet, (m)
d_j	diameter of jet, (m)
d_p	geometric diameter of particle, (m)
$d_{Rayleigh}$	Rayleigh diameter, (m)
d_{sd}	diameter of spinning disk, (m)
d_w	diameter of wire, (m)
D	diameter of orifice, (m)
D_h	hydraulic diameter of airway, (m)
D_{mean}	mean diameter of airway, (m)
e	charge of an electron, (C)
E	electrical field intensity, (V/m)
E_b	electrical field intensity at electrical breakdown, (V/m)
E_L	surface electrical field intensity needed for ion emission, (V/m)
f	Frequency, (1/s)

h	disintegration length, (m)
H	gap between orifice and induction plate, (m)
Inc	induced charge number
k	wave number, (1/m)
k_B	Boltzmann constant
L	centerline path length of airway, (m)
n	charge in elementary unit (e)
n_{Rayleigh}	Rayleigh charge limit
n_{s}	saturation charge of particle
N_{i}	concentration of ions
Oh	Ohnesorge number
p	thermodynamic pressure, (N/m^2)
q	charge, (C)
q_0	spraying charge, (C)
Q	volume flow rate of inhaled gas, (m^3/s)
r	radius of jet, (m)
Re	Reynolds number
Stk	Stokes number
t	time, (s)
T	absolute temperature, (K)
U_{mean}	mean velocity of gas in airway based on D_{mean}, (m/s)
v_{j}	initial velocity of jet, (m/s)
V	electrical potential, (V)
$\dot{V}$	volume flow rate of jet, (m^3/s)
$\bar{V}$	volume of the airway, (m^3)
W_{p}	potential energy, (J)
We	Weber number
$\acute{x}$	nondimensionalized distance of particle from wall
x, $\hat{x}$ and $\tilde{x}$	introduced deposition parameters

x_{d}	droplet spacing, (m)
z	space coordinate in Cartesian system
Z_{i}	electrical mobility of ion, (m^2/V.s)
α	correction factor for non-uniformity of electrical field
β	induction coefficient, (C/V)
γ	surface tension, (N/m)
γ_{L}	surface tension of liquid, (N/m)
δ	amplitude of disturbance, (m)
ε	relative permittivity
ε_0	permittivity of free space, (F/m)
η	particle deposition for referenced studies
λ_{max}	maximum wavelength, (m)
λ_{min}	minimum wavelength, (m)
λ_{opt}	optimum wavelength, (m)
μ	dynamic viscosity, (Pa.s)
ρ	density, (kg/m^3)
ρ^*	reference density of 1000 kg/m^3
ρ_{L}	density of liquid, (kg/m^3)
ρ_{p}	particle density, (kg/m^3)
σ	electrical conductivity, (S/m)
τ	droplet formation time, (s)
ω_{sd}	speed of spinning disk, (rad/s)

Chapter 1. Introduction

1.1. Background

The extrathoracic region is defined as the respiratory tract region proximal to trachea, which includes the following areas (Finlay 2001b; Stahlhofen et al. 1980; Stahlhofen et al. 1983):

- The oral cavity
- The nasal cavity
- The larynx, which is located in the entrance to the trachea and includes the vocal cords
- The pharynx, which is the area between the larynx and either oral cavity or nasal cavity. This region is divided into the oropharynx, which includes the area between larynx and month, and the nasopharynx (nose). The larynx and pharynx together are called throat.
- The proximal region of the trachea

The extrathoracic region is the first area that deposition of inhaled aerosols, either therapeutic or toxic, takes place. This region acts like a coarse filter, especially for micron-sized particles, for which impaction is the dominant deposition parameter. Deposition in this region can dramatically affect the dose of therapeutic medicine that reaches the lungs (Borgström et al. 2006b), so there is a lot of interest in studies that can give a predictive understanding of the problem. Particle deposition in the extrathoracic region is a complex problem dependent on many parameters such as morphological configuration, aerodynamic diameter of particles, volume flow rate of inhaled gas, electrostatic effects, and inter-subject variability, among others.

There are numerous studies on the deposition of aerosols in the extrathoracic airways of adults (Borgström et al. 2006b; Bowes and Swift 1989; Brancatisano et al. 1983; Chan and Lippmann 1980; DeHaan and Finlay 2001; 2004; Heenan et al. 2004; Zhou et al. 2011), children (Becquemin et al. 1991; Golshahi et al. 2012) and infants (Javaheri et al. 2013; Laube et al. 2010b; Storey-Bishoff et al. 2008a), but the aforementioned studies have ignored electrostatic effects in deposition.

Studies on some commercial respiratory drug delivery devices reported high charge levels on the emitted aerosol particles (Hoe et al. 2009b; Kwok et al. 2005a; Kwok et al. 2010). Kwok et al. (2005a) noticed higher than 40,000 e per particle for particles produced by a commercial metered dose inhaler (MDI). They used a modified electrical low pressure impactor (ELPI) to measure net charge of particles in each stage of impactor. Their results showed different charge polarities at various particle diameters for Intal Forte, Tilade and Flixotide and unipolar charge distribution for Ventolin and QVAR. Kwok et al. (2005a) and Kwok et al. (2010), using an ELPI and Hoe et al. (2009b), using electrical next generation impactor (eNGI), only reported net charge of particles at different size bins and their experimental setup were not able to answer the question of charge polarity for a given size bin. This means that individual particles may have higher bipolar charge levels. O'Leary et al. (2008) and O'Leary et al. (2008) designed an apparatus based on electrical precipitation to demonstrate the magnitude and polarity of charge for particles. Their apparatus is composed of two electrical precipitator columns, each precipitator column including different stages that classifies particles based on their electrical mobility. The aerosol is split in the inlet into the precipitators. Each column has an electrode, with different polarity, in the middle that causes a radial electrical field and drives particles with

opposite polarity toward the walls of the column which act as measuring electrodes. O'Leary et al. (2008) selected a pMDI that showed unipolar charge behavior across the aerosol size distribution, measured by ELPI, and showed that each size bin is composed of particles with different polarities. Saini et al. (2007) using an electrical single-particle aerodynamic relaxation time (E-SPART) analyzer showed that particles emitted from two sets of MDIs and dry powder inhalers (DPIs) carry bipolar charges. Kulon and Balachandran (2001) developed an apparatus mainly composed of two “D” shape electrical precipitators with different polarities to separate particles, based on the polarity of their charge, and measure total charge of particles with each polarity. Balachandran et al. (2003) used the aforementioned apparatus to demonstrate the bipolar charge distribution of two pharmaceutical powders. Kulon et al. (2003) utilized phase doppler anemometry in the presence of a DC electrical field to measure charge and polarity of nebulized dioctyl phthalate (DOP) particles. Beleca et al. (2010) conducted similar experiments on lactose powders. Both studies reported a bipolar charge distribution for particles.

High charge levels and the lack of sufficient data in the literature about the effect of electrostatic charges on deposition in the respiratory tract emphasize the importance and need for studies in this field.

Most of the studies that looked into the effect of electrostatic charge on deposition either targeted the whole respiratory tract of humans or qualitatively treated particles as charged or uncharged, which makes it difficult to have a predictive understanding of the problem (Ali et al. 2009; Ali et al. 2008; Bailey et al. 1998; Balachandran et al. 1997; Hashish 1992; Hashish et al. 1994; Majid et al. 2012a; Melandri et al. 1983c; Saini et al. 2004b; Saini et al. 2002b). Ali et al.

(2008) and Ali et al. (2009) investigated deposition of charged particles generated from nebulizers, metered dose inhalers (MDIs) and dry powder inhalers (DPIs) in the mouth-throat and reported increased deposition due to electrostatic forces by comparing charged and uncharged particles. Bailey et al. (1998) developed a lung model and along with some clinical data concluded that deposition targeting is possible by control of breathing, particle aerodynamic diameter and particle electrostatic charge. Balachandran et al. (1997) developed a computer model to predict deposition in the whole respiratory tract and reported deposition enhancement by increasing the charge level of particles. Hashish (1992) and Hashish et al. (1994) developed a mathematical model for controlling and targeting deposition of particles in the lung. Majid et al. (2012a) employed a stochastic human lung model to examine the deposition increase in the lung and concluded that with the application of charged particles more control on targeting the particles is possible. Melandri et al. (1983c) conducted *in vivo* experiments by using unipolar charges of both polarities and a particle size range of 0.3-1 μm, and reported increased deposition in human airways due to image forces between the particle and walls of the airways. Saini et al. (2004b) employed an Anderson cascade impactor to model the lung and noticed that the deposition rate in the upper stages of the cascade impactor was higher for charged particles than for neutral particles, implying that the deposition of charged particles was enhanced. Saini et al. (2002b) introduced particles generated from a spinning disk aerosol generator to a glass bead lung model and found enhanced deposition in the lung as a result of particles' electrostatic charge.

The fraction of particles deposited in the extrathoracic region is dependent on the age of subjects, i.e., adult, child or infant. This is due to the fact that the geometry of the airway and

the preferred route of inhalation are different for adults, children, and infants. The preferred inhalation route for adults and children is oral inhalation due to less deposition compared to nasal inhalation (Finlay and Martin 2008), while nasal inhalation is the preferred route for infants, because they are obligate nose breathers (Janssens et al. 2001b; Sasaki et al. 1977b). Achieving cooperation from subjects, especially for children and infants, is causing more restrictions for *in vivo* studies. To avoid such issues, *in vitro* experiments using the ideal replicas of the human airway can be a valuable option. Ideal models are the simplified version of the replicas which do not include unnecessary convolutions of the airway but still comply with the average deposition patterns for the airway. The Aerosol Research Laboratory of Alberta research group has developed three different ideal model of the extrathoracic airway, i.e., the Alberta idealized mouth-throat model for adults (Stapleton et al. 2000), the Alberta idealized child mouth-throat model for children (Golshahi and Finlay 2012), and the Alberta idealized infant nose-throat model for infants (Javaheri et al. 2013).

1.2. Objectives

This research is mainly a quantitative *in vitro* study on the effect of induced electrostatic charge on the deposition of particles in the extrathoracic airway and developing empirical relations to predict the aforementioned deposition. In this study the effect of particle aerodynamic diameter, flow rate of inhaled gas, and electrostatic charge of particles on the deposition of particles in the extrathoracic airway was studied. The study was performed in three different phases for adults, children and infants. To produce monodisperse uniformly charged particles for *in vitro* testing, an atomizer and a charger were designed and prototyped. The

measurement of the particles' charges was conducted using a designed and prototyped custom Faraday cup.

1.3. Thesis structure

This thesis is prepared in a mixed format. The first chapter is a brief introduction which describes the previous studies in the field and objectives of the present research. The second chapter looks into the theory of particle generation and particle charging, along with the design and prototyping of an atomizer and a charger for our *in vitro* experiments. Chapters three, four and five are our three published papers which investigate the effect of electrostatic charge on deposition of particles in the extrathoracic airway of adults, children and infants, respectively. Chapter six covers the conclusion and summary of the findings and developed empirical relations. Appendix A and B include the drawings, assembling of parts and trouble shooting of the atomizer, charger, and Faraday cup.

Bibliography

Ali, M., Mazumder, M. K., Martonen, T. B. (2009). Measurements of electrodynamic effects on the deposition of MDI and DPI aerosols in a replica cast of human oral – pharyngeal – laryngeal airways. Journal of Aerosol Medicine, 22:35-44.

Ali, M., Reddy, R. N., Mazumder, M. K. (2008). Electrostatic charge effect on respirable aerosol particle deposition in a cadaver based throat cast replica. Journal of Electrostatics, 66:401-406.

Bailey, A. G., Hashish, A. H., Williams, T. J. (1998). Drug delivery by inhalation of charged particles. Journal of Electrostatics, 44:3-10.

Balachandran, W., Kulon, J., Koolpiruck, D., Dawson, M., Burnel, P. (2003). Bipolar charge measurement of pharmaceutical powders. Powder technology, 135:156-163.

Balachandran, W., Machowski, W., Gaura, E., Hudson, C. (1997). Control of drug aerosol in human airways using electrostatic forces. Journal of Electrostatics, 40-41:579-584.

Becquemin, M., Swift, D., Bouchikhi, A., Roy, M., Teillac, A. (1991). Particle deposition and resistance in the noses of adults and children. European Respiratory Journal, 4:694-702.

Beleca, R., Abbod, M., Balachandran, W., Miller, P. R. (2010). Investigation of electrostatic properties of pharmaceutical powders using phase Doppler anemometry. IEEE Transactions on Industry Applications, 46:1181-1187.

Borgström, L., Olsson, B., Thorsson, L. (2006). Degree of throat deposition can explain the variability in lung deposition of inhaled drugs. Journal of Aerosol Medicine, 19:473-483.

Bowes, S. M. and Swift, D. L. (1989). Deposition of inhaled particles in the oral airway during oronasal breathing. Aerosol Science and Technology, 11:157-167.

Brancatisano, T., Collett, P. W., Engel, L. A. (1983). Respiratory movements of the vocal cords. Journal of Applied Physiology, 54:1269-1276.

Chan, T. L. and Lippmann, M. (1980). Experimental measurements and empirical modelling of the regional deposition of inhaled particles in humans. American Industrial Hygiene Association Journal, 41:399-409.

DeHaan, W. H. and Finlay, W. H. (2001). In vitro monodisperse aerosol deposition in a mouth and throat with six different inhalation devices. Journal of Aerosol Medicine, 14:361-367.

DeHaan, W. H. and Finlay, W. H. (2004). Predicting extrathoracic deposition from dry powder inhalers. Journal of Aerosol Science, 35:309-331.

Finlay, W. H. (2001). The Mechanics of Inhaled Pharmaceutical Aerosols: An Introduction. Academic Press, London.

Finlay, W. H. and Martin, A. R. (2008). Recent advances in predictive understanding of respiratory tract deposition. Journal of aerosol medicine and pulmonary drug delivery, 21:189-206.

Golshahi, L. and Finlay, W. H. (2012). An Idealized Child Throat that Mimics Average Pediatric Oropharyngeal Deposition. Aerosol Science and Technology, 46:i-iv.

Golshahi, L., Noga, M. L., Finlay, W. H. (2012). Deposition of inhaled micrometer-sized particles in oropharyngeal airway replicas of children at constant flow rates. Journal of Aerosol Science, 49:21-31.

Hashish, A. H. (1992). Selective deposition of pulsed aerosols in the human lung. Journal of Aerosol Science, 23:473-476.

Hashish, A. H., Bailey, a. G., Williams, T. J. (1994). Modelling the effect of charge on selective deposition of particles in a diseased lung using aerosol boli. Physics in Medicine and Biology, 39:2247-2262.

Heenan, A. F., Finlay, W. H., Grgic, B., Pollard, A., Burnell, P. K. P. (2004). An investigation of the relationship between the flow field and regional deposition in realistic extra-thoracic airways. Journal of Aerosol Science, 35:1013-1023.

Hoe, S., Traini, D., Chan, H. K., Young, P. M. (2009). Measuring charge and mass distributions in dry powder inhalers using the electrical Next Generation Impactor (eNGI). European Journal of Pharmaceutical Sciences, 38:88-94.

Janssens, H. M., de Jongste, J. C., Fokkens, W. J., Robben, S. G., Wouters, K., Tiddens, H. A. (2001). The Sophia Anatomical Infant Nose-Throat (Saint) model: a valuable tool to study aerosol deposition in infants. Journal of aerosol medicine, 14:433-441.

Javaheri, E., Golshahi, L., Finlay, W. H. (2013). An idealized geometry that mimics average infant nasal airway deposition. Journal of Aerosol Science, 55:137-148.

Kulon, J. and Balachandran, W. (2001). The measurement of bipolar charge on aerosols. Journal of Electrostatics, 51:552-557.

Kulon, J., Malyan, B. E., Balachandran, W. (2003). Simultaneous measurement of particle size and electrostatic charge distribution in DC electric field using phase Doppler anemometry. IEEE Transactions on Industry Applications, 39:1522-1528.

Kwok, P. C. L., Glover, W., Chan, H.-K. (2005). Electrostatic charge characteristics of aerosols produced from metered dose inhalers. Journal of Pharmaceutical Sciences, 94:2789-2799.

Kwok, P. C. L., Trietsch, S. J., Kumon, M., Chan, H.-K. (2010). Electrostatic charge characteristics of jet nebulized aerosols. Journal of aerosol medicine and pulmonary drug delivery, 23:149-159.

Laube, B. L., Sharpless, G., Shermer, C., Nasir, O., Sullivan, V., Powell, K. (2010). Deposition of albuterol aerosol generated by pneumatic nebulizer in the Sophia Anatomical Infant Nose-Throat (SAINT) model. Pharmaceutical research, 27:1722-1729.

Majid, H., Madl, P., Hofmann, W., Alam, K. (2012). Implementation of Charged Particles Deposition in Stochastic Lung Model and Calculation of Enhanced Deposition. Aerosol Science and Technology, 46:547-554.

Melandri, C., Tarroni, G., Prodi, V., Zaiacomo, T. D., Formignani, M., Lombardi, C. C. (1983). Deposition of charged particles in the human airways. Journal of Aerosol Science, 14:657-669.

O'Leary, M., Balachadran, W., Rogueda, P., Chambers, F. (2008). The bipolar nature of charge resident on supposedly unipolar aerosols, in Journal of Physics: Conference Series, IOP Publishing, 012022.

O'Leary, M., Blachandran, W., Chambers, F. (2008). Electrical mobility profiling used to illustrate the bipolar nature of pharmaceutical aerosol charge. Respiratory Drug Delivery.

Saini, D., Biris, a. S., Srirama, P. K., Mazumder, M. K. (2007). Particle size and charge distribution analysis of pharmaceutical aerosols generated by inhalers. Pharmaceutical Development and Technology, 12:35-41.

Saini, D., Gunamgari, J., Zulaloglu, C., Sims, R. A., Mazumder, M. K. (2004). Effect of electrostatic charge and size distributions on respirable aerosol deposition in lung model, in Industry Applications Conference, 2004. 39th IAS Annual Meeting, Seattle, 948-952.

Saini, D., Yurteri, C. U., Grable, N., Sims, R. A., Mazumder, M. K. (2002). Drug delivery studies on electrostatically charged dry powder inhaler aerosols using a glass bead lung model, in Industry Applications Conference, 2002. 37th IAS Annual Meeting, Pittsburgh, PA, 2451-2453.

Sasaki, C. T., Levine, P. A., Laitman, J. T., Crelin, E. S. (1977). Postnatal Descent of the Epiglottis in Man: A Preliminary Report. Archives of Otolaryngology - Head and Neck Surgery, 103:169-171.

Stahlhofen, W., Gebhart, J., Heyder, J. (1980). Experimental determination of the regional deposition of aerosol particles in the human respiratory tract. American Industrial Hygiene Association journal, 41:385-398a.

Stahlhofen, W., Gebhart, J., Heyder, J., Scheuch, G. (1983). New regional deposition data of the human respiratory tract. Journal of Aerosol Science, 14:186-188.

Stapleton, K. W., Guentsch, E., Hoskinson, M. K., Finlay, W. H. (2000). On the suitability of k–ε turbulence modeling for aerosol deposition in the mouth and throat: a comparison with experiment. Journal of Aerosol Science, 31:739-749.

Storey-Bishoff, J., Noga, M., Finlay, W. H. (2008). Deposition of micrometer-sized aerosol particles in infant nasal airway replicas. Journal of Aerosol Science, 39:1055-1065.

Zhou, Y., Sun, J., Cheng, Y. S. (2011). Comparison of deposition in the USP and physical mouth-throat models with solid and liquid particles. Journal of Aerosol Medicine and Pulmonary Drug Delivery, 24:277-284.

Chapter 2. Generating Monodisperse Uniformly Charged Particles

2.1. Introduction

The use of monodisperse uniformly charged particles offers many advantages in quantitative studies of various phenomena when considering the effects of aerodynamic diameter and electrostatic charge. In contrast, polydisperse or non-uniform particles can make it more difficult to understand data from a study. Lacking specific information on the power of a given parameter in a phenomenon, e.g., whether a phenomenon is proportional to a diameter linearly or rather proportional to its square root, polydisperse particles can mask effects that would be readily observed with a monodisperse aerosol. Particle monodispersity and charge uniformity help to ensure uniform, unbiased particle losses, eliminating approximations in calculations. Particle sampling is also simplified considerably for monodisperse uniformly charged particles.

There are various methods of producing particles and charging them, but most are not capable of producing uniformly charged monodisperse particles. In addition, many of the methods used in particle generation are not compatible with those used to charge particles. In this chapter the fundamentals of common methods for particle generation and charging are briefly reviewed, with the most suitable method for experiments selected for further consideration. The theory and details of regarding the design and prototyping of an atomizer, charger and Faraday cup are then explained in the remainder of the chapter.

2.1.1. Generating Monodisperse Particles

2.1.1.1. Condensation Monodisperse Aerosol Generation

In condensation monodisperse aerosol generation, heated vapor of a given substance is condensed on nuclei present in the aerosol. An atomizer produces the initial particle nuclei, which are then dried using a suitable desiccant such as silica gel in a drying container. The aerosol consisting of dried particle nuclei is then mixed with the heated vapor of a given substance, which condenses on the nuclei during transit through a condensation column in laminar flow. The initial nuclei are not necessarily monodisperse, but they compose only the core of final particles. Particle size is mainly controlled by the concentration of heated vapor, which is itself governed by the saturation ratio at a specific temperature and the dilution rate of the vapor by makeup gas. The concentration of particles in the aerosol is directly controlled by the concentration of nuclei and the dilution ratio with makeup gas. Generated particles typically have a geometric diameter in the range of 0.03 to 2 μm, with a geometric standard deviation (GSD) of less than 1.3. This method is known to generate a high concentration of particles, i.e. 10^{13} particles/m^3. Key parameters that control the quality of monodispersity and the concentration of particles produced with this method include the uniformity of the aerosol temperature profile, having a sufficient concentration of nuclei and vapor, and ensuring a long residence time in the condensation column (Kulkarni et al. 2011).

Condensation monodisperse aerosol generation has been developed and utilized successfully for generating particles from a variety of substances (Tomaides et al. 1971; Tu 1982). Tomaides et al. (1971) used four liquid substances: di-2-ethyl-hexyl phthalate (DEP), oleic acid (OA), glycerin (GL), dioctyl phthalate (DOP) and 2 solid materials: stearic acid (SA) and

triphenyl phosphate (TPP) to generate particles, achieving a high quality of monodispersity for DOP and TPP with GSDs ranging from 1.06 to 1.12. The median diameter of generated particles ranged from 0.9-1.1 μm, with a particle concentration of 10^{12} particles/m^3. Tomaides et al. (1971) also improved upon previous versions of condensation aerosol generators by adding a neutralization chamber. Tu (1982) designed a compact condensation monodisperse aerosol generator and produced particles of carnauba wax, stearic acid and ammonium bisulfate with geometric diameters ranging from 0.01 to 2 μm and number concentrations of 10^{10}-10^{12} particle/m^3.

2.1.1.2. Spinning Disk Monodisperse Aerosol Generator

Spinning disk aerosol generators provide another method for the production of monodisperse particles. In this method, a liquid jet, consisting of an aqueous suspension or solution, is directed on the center of a disk rotating with constant speed. The liquid is spread over the disk and creates a thin film, which accumulates on the disk until centrifugal forces on the growing liquid mass overcome capillary forces, leading to the release of a droplet (Kulkarni et al. 2011; May 1949; Mitchell 1984; Walton and Prewett 1949). The droplet size, d_{d}, is a fuction of disk diameter, d_{sd}(μm), and the speed of the rotating disk , ω_{sd} (rpm), as follows (Kulkarni et al. 2011):

$$d_{\mathrm{d}} = \left(W\gamma_{\mathrm{L}}/\rho_{\mathrm{L}}\omega_{\mathrm{sd}}^2 d_{\mathrm{sd}}\right)^{1/2} \qquad (2.1)$$

where γ_{L} and ρ_{L} are the surface tension and density of the liquid and *W* is a parameter depending on the design of the spinning disk and the liquid used for producing particles.

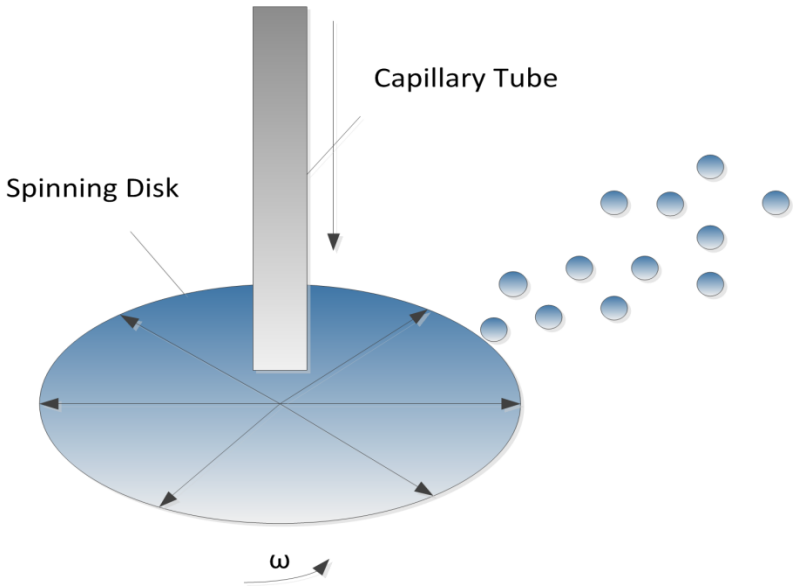

Figure 2.1. Schematic of spinning disk monodisperse aerosol generator

One disadvantages of spinning disk method is the presence of undesirable satellites in the generated aerosol. Moreover, the variability of *W* is not a favorable characteristic.

Walton and Prewett (1949) used a spinning disk aerosol generator to produce particles in the geometric diameter range of 15-3000 μm, reporting that to have a good quality of monodispersity the liquid feed must be central to the disk and continuous, and that the surface of the disk must be completely wetted to avoid an uneven film formation associated with non-uniform droplet sizes. May (1949) modified the aerosol generator of Walton and Prewett (1949), to partially eliminate satellites. Mitchell (1984) also modified May's spinning disk to remove satellites more efficiently from the produced aerosol, and produced particles with a geometric diameter of 0.4-10 μm with a standard deviation of less than 1.1 and maximum number concentration of 2×10^{8} particle/m^3.

2.1.1.3. Electro-spraying technique for generating monodisperse particles

Electro-spraying involves the generation of particles by running a semi-conductive liquid through a capillary tube while establishing a high electrical potential difference (in excess of a couple of thousands volts) between the tip of capillary tube and a coaxial plate (Kulkarni et al. 2011). This electrical potential difference creates a strong electrical field between the tip of the capillary tube and the conductive plate, resulting in an electrical force on the liquid emerging from the tube. Several modes of liquid stream breakup are observed depending on the strength of the electrical field, hydrodynamic parameters, and the physical properties of the working fluid (Kulkarni et al. 2011). In some conditions (Cloupeau and Prunet-Foch 1994; M. Cloupeau and Prunet-Foch 1989) the emerging liquid meniscus establishes a conical shape before breakup. The emerging jet, under the action of charge-carrying varicose instabilities, breaks up into droplets with diameters roughly twice the diameter of the jet, but much smaller than the

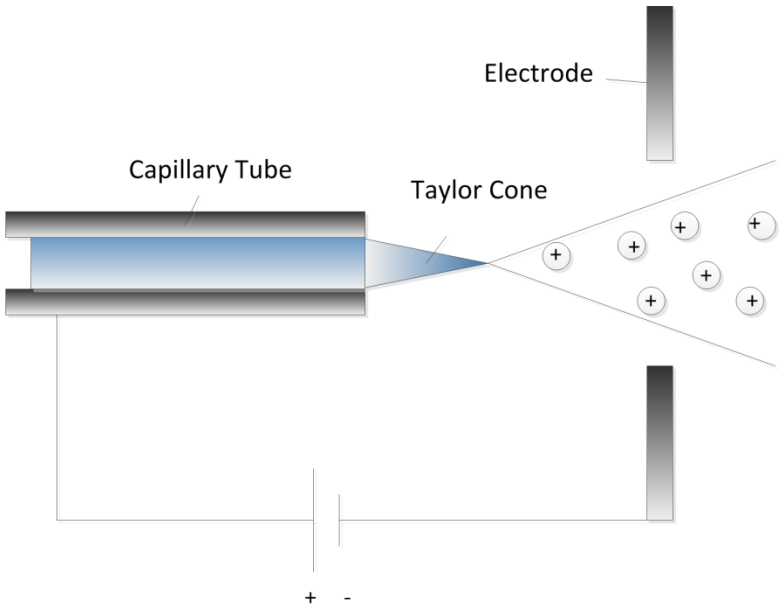

Figure 2.2. Schematic of monodisperse electro-spray

diameter of capillary tube (Kulkarni et al. 2011; Rosell-Llompart and Mora 1994; Tang and Gomez 1994). The mean droplet diameter is usually in the range of 0.3-50 μm, though it can be reduced significantly to 10 nm. The size of generated particles is a function of tube diameter, flow rate, electrical field strength, current, physical properties of working fluid such as surface tension, electrical conductivity and viscosity (Kulkarni et al. 2011).

Tang and Gomez (1994) utilized the electro-spraying method to produce monodisperse droplets in the geometric diameter range of 2-12 μm with GSD of 1.15 and 1.05 for smaller and larger droplets, respectively. Tang and Gomez (1994) controlled droplet size mainly through the feed rate of working fluid, but they also noticed that increasing conductivity of the liquid by adding sodium chloride (NaCl) reduced the geometric diameter of droplets to below 5 μm. Around the same time, Rosell-Llompart and Mora (1994) generated droplets with geometric diameters in the range of 0.3-4 μm and a GSD of 1.1 using the electrospraying technique. The range of particle sizes generated by this method can be extended to the nanometer range if volatile solvents are used. Satellite particles can reduce the monodispersity of aerosol generated with this method, necessitating the removal of these small residual droplets from the stream for truly monodisperse application.

2.1.1.4. Controlled Plateau–Rayleigh jet breakup

This method, also known as vibrating-orifice (Berglund and Liu 1973), is capable of generating monodisperse particles in the geometric diameter range of 0.5-50 μm and geometric standard deviation (GSD) below 1.2 (Kulkarni et al. 2011). In the vibrating-orifice method, a working fluid is forced through a micron-sized orifice by action of a syringe actuated by a step-motor (Kulkarni et al. 2011) or a pressurized reservoir (Lin et al. 1990). The emerging jet is exposed to

a mechanical disturbance caused by a piezoelectric actuator which results in capillary waves on the jet. For some particular frequencies and amplitudes this disturbance can result in monodisperse breakup of the jet (Plateau 1873; Rayleigh 1879). To produce smaller particles, a volatile solvent can be used, which evaporates, leaving the nonvolatile solute behind. In practice, maximum particle size is not well defined, and the limiting factor for the minimum particle size is the purity of the solvent. To produce high quality monodisperse particles the stream of particles needs to be dispersed before coagulation occurs (Anders et al. 1992). Particles generated by this method can carry a substantial amount of charge which may cause high losses, so it is common to neutralize them using a radioactive source. The radioactive source creates charged ions which will be attracted to the charged particles of opposite polarity, resulting in a Boltzmann distribution for the charge of the particles. Here, Boltzmann distribution of charge for particles is mainly due to the fact that mechanism of charging is diffusion charging. This method is explained in section 2.1.2.1. The common radioactive sources for this purpose use beta emitters such as ^{85}Kr or tritium and alpha emitters like ^{210}Po or ^{241}Am (Kulkarni et al. 2011).

2.1.2. Charging Particles

2.1.2.1. Diffusion Charging

Diffusion charging involves exposing aerosol particles to ions, whether unipolar or bipolar, where, due to Brownian motion of particles and ions, they collide with each other which results in charge being acquired by the particles. This method of charging does not need an external electrical field as a driving mechanism and does not depend on the particle material (Hinds 1999). For unipolar charging, the rate of charging is decreased with time. This is due to the

repulsive force between the charge on the particle and ions close to the particle, hence ions need higher speeds to reach the particle. This rate never reaches zero since ions in equilibrium have velocities following a Boltzmann distribution (Tolman 1938) which does not have a nonrelativistic upper limit. The following expression shows the approximate charge, in elementary charge unit (*e*), for a given geometric diameter, d_{p}, at time *t* suggested by Hinds (1999),

$$n(t) = \frac{2\pi\varepsilon_0 d_{\mathrm{p}} kT}{e^2} \ln\left[1 + \frac{4\pi^2 \varepsilon_0 d_{\mathrm{p}} \bar{c}_{\mathrm{i}} e^2 N_{\mathrm{i}} t}{kT}\right] \quad (2.2)$$

Here $\varepsilon_0 = 8.85 \times 10^{-12}\mathrm{C}V^{-1}\mathrm{m}^{-1}$and $k = 1.38 \times 10^{-23}\mathrm{m}^2\mathrm{kgs}^{-2}\mathrm{K}^{-1}$ are the permittivity of free space and Boltzmann constant, respectively. *T* is the gas temperature, N_{i} shows the concentration of ions and $\bar{c}_{\mathrm{i}}$ represents the mean thermal speed of ions.

2.1.2.2. Field Charging

In field charging, particles are charged by unipolar ions in the presence of an electrical field. Ions are accelerated in the electrical field along the electrical field lines and collide with the particles. Neglecting diffusion charging, the charge acquired by particles by field charging is (Hinds 1999),

$$n(t) = \left(\frac{3\varepsilon}{\varepsilon + 2}\right)\left(\frac{\pi\varepsilon_0 E d^2}{e}\right)\left(\frac{4\pi^2 e Z_{\mathrm{i}} N_{\mathrm{i}} t}{1 + 4\pi^2 e Z_{\mathrm{i}} N_{\mathrm{i}} t}\right) \quad (2.3)$$

Here ε is the relative permittivity of the particle, Z_{i} is the mobility of ions and *E* is the intensity of electrical field. As ions accumulate on the particle, field lines do not converge on the particle's surface and charge saturation happens at (Hinds 1999),

$$n_s = \left(\frac{3\varepsilon}{\varepsilon + 2}\right)\left(\frac{\pi\varepsilon_0 E d^2}{e}\right) \qquad (2.4)$$

2.1.2.3. Tribo-electrification and contact charging

The charge acquired by particles when contacting a surface of different material is usually known as tribo-electrification. The observations show that friction enhances this phenomenon (Moore 1973). To predict their charges after being in contact with each other, materials are arranged in tribo-electric series (Kwetkus 1998). Reproducibility of experimental results are usually poor (Castle 1997; Kwetkus 1998), and the physics of this phenomenon is not totally understood. There are no universal tribo-electric series and the series published by different authors have many inconsistencies (Castle 1997; Kwetkus 1998). There are different theories to explain this phenomenon; some consider electrons as the charge carriers and some ions, but most of the studies assume electrons as the charge carrier and relate the net charge after separating the materials to the electron work function of the materials. For metals the electron work function is defined as the minimum energy required to release an electron from a solid and bring it to the infinite distance (Kwetkus 1998).

2.1.2.4. Field emission charging

When particles are exposed to a strong electrical field, this field can cause extraction of some electrons from the particle which results in a net charge on the particles. This phenomenon occurs at very strong electrical fields, which makes it almost impossible for aerosols since breakdown of the gas usually happens at lower strength of electrical field. Paschen (1889) conducted experiments on breakdown of different gases between parallel plates at different

pressure of gas and various gap lengths and suggested following equation for their breakdown potential difference,

$$V_{\mathrm{b}} = \frac{b_1 p\Delta}{\ln(p\Delta) + b_2} \tag{2.5}$$

Here p is the thermodynamic pressure in Bar and Δ is the gap between parallel plates in meter. b_1 and b_2 are constants depending on the composition of the gas between the plates.

Field emission charging is mainly limited to a particle in vacuum or in an insulating liquid environment (Moore 1973).

2.1.2.5. Photoelectric Charging

Light can impart energy to the electrons on the surface of a particle and cause them to release electron from the surface which is known as photoelectric charging (Moore 1973).

2.1.2.6. Induction Charging

If a conductive liquid is exposed to an electrical field during disintegration, the resulting particles will carry a net charge. This is due to the induced charge on the surface of liquid which cancels out the electrical field inside the liquid (Moore 1973). When the liquid is disintegrated while the electrical field is maintained, this charge is trapped on the particles. The charge that particles acquire in this process depends on the strength of the electrical field, disintegration time, particle diameter and conductivity of the liquid. The charge which particles carry in electro-spraying is also a result of induction in the liquid, but in electro-spraying the electrical field is so strong that it overcomes surface tension and enhances the disintegration of liquid. The order of charge that particles acquire in electro-spraying is higher than induction charging (Moore 1973).

2.1.2.7. Corona Discharge

One of the common methods to charge particles is passing aerosol through a region including ions. Since the life time of ions is usually very short, this method needs a source for continuously producing ions. Ions can be created in the air by radioactive discharge, ultraviolet radiation, flames, and corona discharge (Hinds 1999). Corona discharge is capable of producing a continuous stream of ions at high concentration which makes it more favorable for most charging apparatuses. Corona discharge requires strong non-uniform electrical fields similar to the one between a needle and a plate or a concentric thin wire and a tube.

Air and other gases are normally good insulators but in regions with high gradient of electrical field they can undergo an electrical break down and become conductive. The strength of electrical field required to cause breakdown, E_{b}, depends on the diameter of the wire, d_{w}. The following empirical equation predicts this electrical field in air (Hinds 1999),

$$E_{\mathrm{b}} = 3000 + 127 d_{\mathrm{w}}^{-1/2} \ \mathrm{kV/m} \qquad (2.6)$$

In this region the previously present ions under action of electrical fields accelerate and acquire high velocities. These ions collide with other molecules and create positive ions and free electrons (Hinds 1999; Moore 1973) which result in an avalanche of ions. Positive ions and electrons move in opposite directions, one moving toward the cathode and others toward the anode. This direction depends on the polarity of the corona which is a function of electrical potential difference between the electrode and plate. Depending on the polarity of corona, a wind of positive ions or electrons will be produced. Positive and negative coronas have different properties, for example in the positive corona the region around the wire seems bluish-green and is stable but for the negative corona the glow seems like dancing brushes or

tufts. Since the negative corona produces about 10 times higher ozone than the positive corona, the use of positive corona is mostly preferred. Clean air at high velocities is blown through the tube which will carry the ions and mix them with aerosol particles by diffusion charging (Hinds 1999).

2.1.3. Choosing a method to produce monodisperse particles and charge them uniformly

Among the aforementioned charging methods the only one which can produce particles with uniform charge is induction charging. Diffusion charging results in a Boltzmann distribution of charge for particles and tribo-electrification is not easily controlled. The only method of particle generation which is compatible with induction charging is controlled Plateau-Rayleigh jet breakup. This method was first used by Reischl et al. (1977) for producing uniformly charged monodisperse particles. The uniformity of charge distribution is dependent on the monodispersity of the particles since the diameter of the droplets determines the capacitance which will be charged. In this method the dispersion cap of the atomizer is replaced by an induction cap which creates a uniform electrical field in the disintegration region of the droplets. Theory and detail of the method is explained in section 2.2.

In the present study, an atomizer based on controlled Plateau–Rayleigh jet breakup theory, similar to the one built by Berglund and Liu (1973), was designed and built. The atomizer is also equipped with a charging cap to charge particles uniformly. To measure the charge of particles, a custom Faraday cup was also designed and built.

2.2. Theory

2.2.1. Controlled Plateau–Rayleigh jet breakup

Controlled Plateau-Rayleigh jet breakup essentially involves disintegrating a jet under action of capillary waves, usually produced by a piezoelectric transducer. The first observations of jet breakup into droplets were reported by Savart (1833). Although surface tension was known at that time, Savart (1833) did not recognize it as the source of jet instability. The first theoretical work in this field was conducted by Plateau (1873), but since his notes were not in English most of the references in this area go to Rayleigh's work (Rayleigh 1879). Plateau (1873) studied an infinite cylinder of fluid. This is an unstable form of equilibrium based on the surface energy concept, and prefers to turn into a more stable form, consisting of spherical droplets that have smaller total surface. By forcing the frequency of the jet disintegration, Plateau (1873) showed that the effect of viscosity increases the wavelength of breakup disturbance, hence increasing the volume of the droplets. Rayleigh (1879) conducted an infinitesimal disturbance growth analysis on the instability of jets which is briefly outlined here. Assuming an undisturbed radius of jet, a, axis of jet z, and an average infinitesimal disturbance with an amplitude of δ and wave number of $k = 2\pi/\lambda$ where λ is the wave length of disturbance, the radius of jet at a specific time reads,

$$r = a + \delta \cos kz \qquad (2.7)$$

Comparing the surface of the disturbed jet, A_j, and undisturbed jet, A_{j0},

$$A_j - A_{j0} = \frac{\pi\delta^2}{2a}(k^2a^2 - 1) \qquad (2.8)$$

To have an unstable system which tends to disintegrate, the final surface must be smaller than the initial one, which is the case when ka is less than unity. This means that the jet disintegrates into droplets when the wave length of the disturbance is larger than the circumference of the jet, i.e., $\lambda > 2\pi a$. This statement can be expressed as a function of orifice diameter, *D*, assuming approximately equal diameter for the jet, d_{j}, and the orifice,

$$f < \frac{4\dot{V}}{\pi^2 D^3} \qquad (2.9)$$

Here f is the frequency of the disturbance and $\dot{V}$ is the volume flow rate of the jet. This equation does not consider any lower bound for the frequency range. Schneider and Hendricks (1964) recommended the wave length range of $7a < \lambda < 14a$ for the monodisperse droplets generated from a capillary tube under the action of disturbances generated by a piezoelectric transducer, which can be rewritten as follows,

$$\frac{4\dot{V}}{7\pi D^3} \leq f \leq \frac{4\dot{V}}{3.5\pi D^3} \qquad (2.10)$$

Rayleigh (1879) assumed that the disturbance, δ, is proportional to e^{ct}, where *c* is the growth rate of the disturbance. After calculating potential surface energy and kinetic energy of the jet, he derived an equation for growth rate versus wave number. Growth rate has a maximum at the following wave length, which is assumed to be the optimum disintegration wave length.

$$\lambda_{\mathrm{opt}} = 4.508 \times 2a \qquad (2.11)$$

The initial droplet diameter can be estimated by the volume of the liquid in one wavelength as follows,

$$d_{\mathrm{d}} = \sqrt[3]{\frac{6\dot{V}}{\pi f}} \tag{2.12}$$

Hence, for the most unstable waves, or at the optimum frequencies, droplet geometric diameter would be,

$$d_{\mathrm{d}} = 3.78a \tag{2.13}$$

Assuming a jet velocity of $V_{\mathrm{j}} = C_{\mathrm{d}}\sqrt{\frac{2\Delta p}{\rho}}$, droplet spacing, x_{d}, reads

$$\frac{x}{d_{\mathrm{d}}} = \frac{V_{\mathrm{j}}}{f d_{\mathrm{d}}} = \left(\frac{4C_{\mathrm{d}}^2 \Delta p}{3\rho d_{\mathrm{d}}^2 f^2}\right)^{1/3} \tag{2.14}$$

Here C_{d}, Δp and ρ are the discharge coefficient of the jet, pressure drop and density of fluid, respectively. Rayleigh also looked into disintegration of a viscous jet under the action of surface tension which resulted in complicated equations which indicate that the effect of viscosity is to shift the most unstable waves to longer wave lengths (McCarthy and Molloy 1974).

Weber (1931) also conducted a study on jet instability. His findings for minimum and optimum wave lengths for disintegration of an inviscid jet are,

$$\lambda_{\min} = \pi\, d_{\mathrm{j}} \tag{2.15}$$

$$\lambda_{\mathrm{opt}} = \sqrt{2}\pi d_{\mathrm{j}} \approx 4.44 d_{\mathrm{j}} \tag{2.16}$$

When including the effect of viscosity,

$$\lambda_{\min} = \pi d_{\mathrm{j}} \tag{2.17}$$

$$\lambda_{\text{opt}} = \sqrt{2}\pi d_{\text{j}}\left(1 + \frac{3\mu}{\sqrt{\rho\gamma d_{\text{j}}}}\right) \quad (2.18)$$

Here, μ is dynamic viscosity and γ is surface tension. These results imply that viscosity does not have any effect on the minimum wave length of disturbance but pushes the optimum wave length to higher values.

Weber also looked into the effect of the relative velocity of the emerging jet and ambient fluid. His findings showed the effect of relative velocity is to decrease the wave lengths of both minimum and optimum disturbance waves. For instance, at a relative velocity of 15 m/s

$$\lambda_{\text{min}} = 2.2 d_{\text{j}} \quad (2.19)$$

$$\lambda_{\text{opt}} = 2.8 d_{\text{j}} \quad (2.20)$$

Ohnesorge (1936) classified jet disintegration regimes based on Reynolds number and Ohnesorg number, $Oh = {\sqrt{We}}/{Re} = {\mu}/{\rho\gamma d_{\text{j}}}$, into three regions.

1. At low Reynolds numbers the jet disintegrates into approximately uniform drops.
2. At intermediate Reynolds numbers, the jet breakup is based on its axial oscillation and results in a wide range of droplet sizes.
3. At high Reynolds numbers, disintegration happens in a short distance after the jet emerges.

Physically Ohnesorge number includes viscous, inertial and surface forces and can be written as

$$Oh = \frac{Viscous\ Forces}{\sqrt{Inertial\ Forces . Surface\ tension\ forces}} \quad (2.21)$$

Although, due to the simplifications and assumptions made in the theoretical works or difference in experimental conditions, these formulas may not totally comply with the experimental outputs; however, they are useful in giving an understanding and a guide for adjusting parameters while designing and building of the atomizer.

Figure 2.3 shows the initial velocity of the jet emerging from the atomizer vs. the pressure of the feed line assuming an approximate discharge coefficient of $C_{\mathrm{d}} = 1.0$. Figures 2.4 shows the monodisperse disintegration region for the jet according to the empirical relation, Eq. (2.10), suggested by Schneider and Hendricks (1964) and corresponding expected droplet size and droplet spacing for ethanol droplets. As seen in Fig. 2.4, at a constant pressure, increasing the frequency results in finer droplets. Another observation is that higher pressures require higher disintegration frequencies. It is also noticed that at higher frequencies normalized spacing of the droplets decreases. This information can be useful in dealing with droplet coalescence which threatens the monodispersity of the particles.

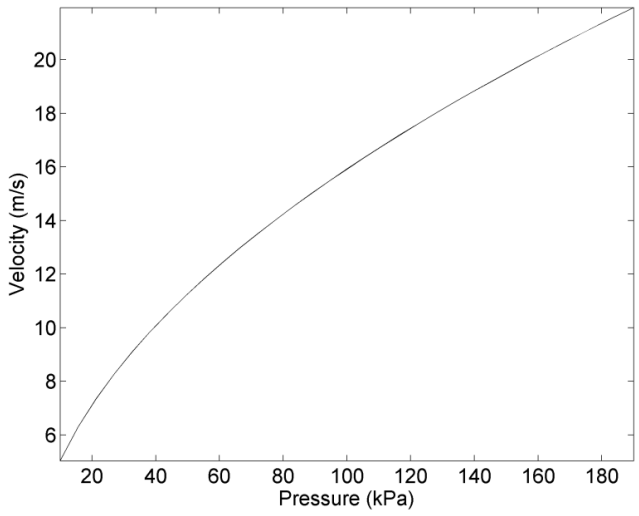

Figure 2.3. Initial velocity of the jet vs. reservoir pressure, *D*=20 μm and $C_{\mathrm{d}} = 1.0$

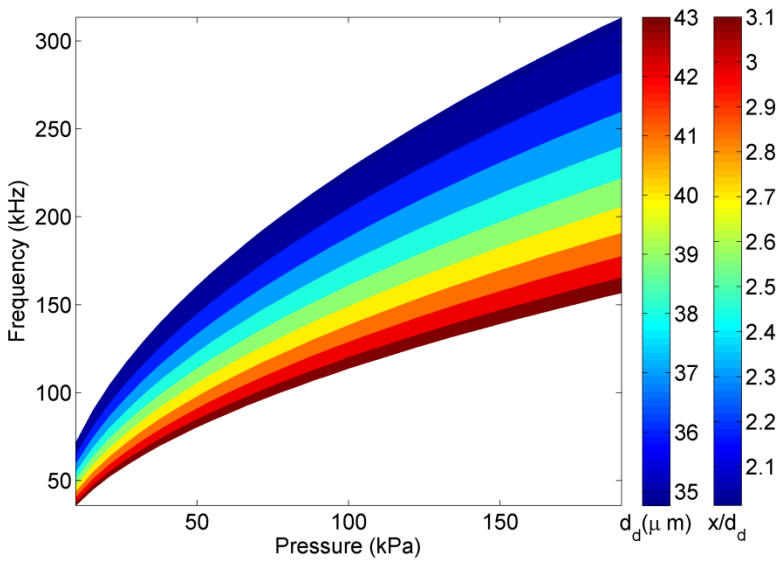

Figure 2.4. Droplet size variation and droplet spacing vs. Pressure and Frequency on monodisperse disintegration region for orifice size $D = 20\ \mu\text{m}$ and $C_\text{d} = 1.0$, based on Eqs. (2.10), (2.12) and (2.14) (Schneider and Hendricks 1964)

2.2.2. Preventing droplet coalescence

After breaking a jet into uniformly sized droplets, it is essential to avoid droplet coalescence to keep the quality of monodispersity. The chain of produced droplets travelling in a straight line decelerates and droplet coalescence is probable. This requires an understanding of the coherence length for the monodisperse chain of droplets (Anders et al. 1992). Anders et al. (1992) related this phenomenon to the internal disturbances of some droplets which results in their change of velocity. This velocity change affects the spacing of the droplets and enhances droplet collision and coalescence. Anders et al. (1992) believe that external disturbances contribute to this tendency and only in very controlled conditions can this spacing be kept large (Orme and Muntz 1990).

One practical approach to avoid droplet coalescence is to decrease the possibility of droplet collision by dispersing the droplet stream, which is most commonly performed via a turbulent air stream. To disperse the chain, a cap is placed after the atomizer head and a turbulent air stream is passed through the cap which disperses the jet. The optimum flow rate for the stream can be adjusted by monitoring monodispersity of the produced particles.

2.2.3. Drying initial droplets

Spray drying is a broad field with many applications (Masters 1991; Pradip et al. 2011; Vehring et al. 2007), but here we will focus on the aspects needed for the production of monodisperse Di(2-ethylhexyl) sebacate (DEHS) particles needed for our experiment. DEHS is widely used in aerosol investigations due to its high stability as a result of low vapor pressure. As discussed in the section 2.2.1 a rough estimate for the initial droplet diameter in controlled Plateau-Rayleigh jet break up is twice the orifice diameter. To have finer particles, a solution composed of volatile and nonvolatile phases is used as the working fluid for the atomizer, and initial droplets are dried to their final sizes.

The evaporation of a droplet while spraying is mainly a coupled heat and mass transfer problem. The driving force of this process is the difference between the vapor pressure of the solvent and their partial pressure in the gas phase (Vehring et al. 2007). Rate of evaporation depends on the balance of heat transfer on the surface of the droplet and required vaporization enthalpy. An important consideration while dealing with a chain of droplets rather than a single droplet is their mutual interaction during the evaporation process, which hinders the process considerably. This is mainly due to increased solvent vapor pressure in the area close to the

chain of droplets, so one approach to avoid this condition is to increase the spacing of droplets by dispersing them.

Assuming no volume change on mixing, i.e. ideal solution, in this method the final size of the particles depends on the initial droplet size and the concentration of the solution as follows,

$$d_{\mathrm{p}} = d_{\mathrm{d}} \sqrt[3]{C_{\mathrm{V}}} \qquad (2.22)$$

Here d_{p}, d_{d} and C_{V} are the geometric diameter of the particle, geometric diameter of the droplet and volume concentration of the solution.

Design of a drying column needs careful consideration of the time required for drying initial droplets, which is a complex function of droplet surface area, the difference of vapor pressure of solvent and their partial pressure in ambient gas, properties of sheath flow surrounding the jet, relative velocity of the jet, mutual interaction of droplets in the chain which may affect the partial pressure of the solvent in ambient gas, and effective drag force droplet experience while travelling in the column (Liu and Frohn 1988a), among others.

Practically, to have an efficient and fast drying process, it is preferable to use a solvent with high vapor pressure to enhance the evaporation of the volatile phase. Using a small orifice can also help by making the initial diameter of droplets closer to the final particle diameter. Considering approximately constant spacing of the droplets, $x = V/f$, while the diameter of particles are reduced for a smaller orifice, the adverse mutual effect of droplets, due to affecting partial vapor pressure of the solvent in ambient gas and drag force, will also be decreased. The disadvantages of using smaller orifices is their higher probability of getting clogged which is also enhanced by the higher concentration of the solution needed for a

specific final diameter of particle with smaller orifices. Dispersion of the droplet chain is the most recommended strategy which can decrease the mutual effect of droplets and as already mentioned; it is the key for keeping the quality of particle monodispersity. The main effect of particle dispersion is decreasing the possibility of particle coagulation and later decreasing the mutual particle-particle interaction by changing the partial vapor pressure of the solvent in the surrounding gas.

2.2.4. Induction charging of liquid droplets

Induction charging can place a uniform and controlled amount of charge on the particles. Here the theory will be applied to the present atomizer.

At height h, breakup point of the jet, the electrical potential will be

$$\acute{V} = \frac{\alpha V h}{H} \qquad (2.23)$$

Here α, V and *H* are constant coefficient that corrects for the non-uniformity of the electrical field, the electrical potential between the induction plate and orifice, and the length of the gap between the induction plate and orifice, respectively.

Considering the droplets before disintegration as a capacitor, the charge on a droplet in elementary charges *q* will be,

$$q = -\frac{C\acute{V}}{e} \qquad (2.24)$$

where *C* and *e* are the electrical capacity of the droplet and elementary charge.

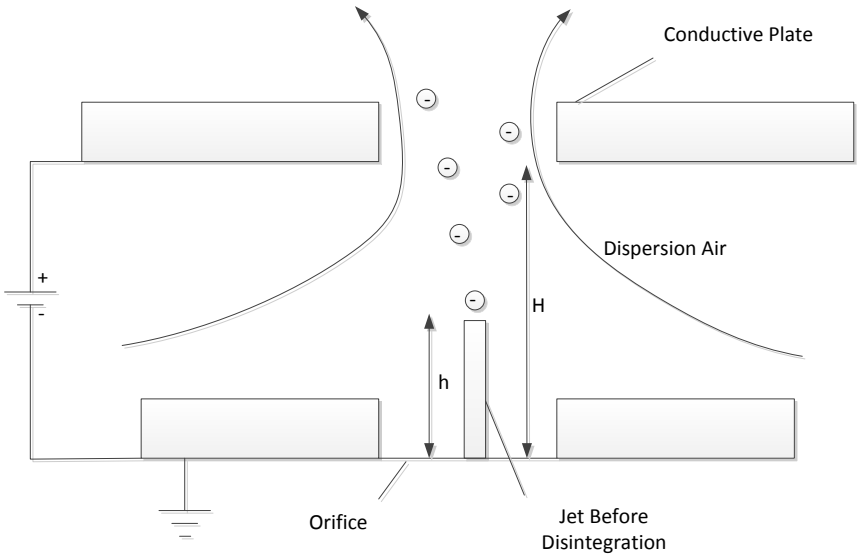

Figure 2.5. Schematic of induction charging and droplet dispersion using charging cap

To calculate the capacitance of a droplet, consider Fig. 2.6, which shows a spherical capacitor. By assuming a Gaussian surface, A_{GS}, in the area $a < r < b$, the strength of the electrical field is calculated as,

$$E = \frac{\Phi}{A_{\mathrm{GS}}} = \frac{q}{\varepsilon_0 4\pi r^2} \qquad (2.25)$$

Here q is the charge of capacitor and $\varepsilon_0 = 8.842 \times 10^{-12}\ \mathrm{C/Vm}$ is the permittivity of free space.

Then the electrical potential difference of the capacitor is,

$$\Delta V = \int_a^b E\ \mathrm{d}r \qquad (2.26)$$

$$= \frac{q}{4\pi\varepsilon_0}\left(\frac{1}{r_1} - \frac{1}{r_2}\right)$$

The capacitance of a capacitor is defined as,

$$C = \frac{q}{\Delta V} \qquad (2.27)$$

Hence for the present geometry the capacitance, *C*, would be,

$$C = \frac{4\pi\varepsilon_0}{\left(\frac{1}{r_1} - \frac{1}{r_2}\right)} \qquad (2.28)$$

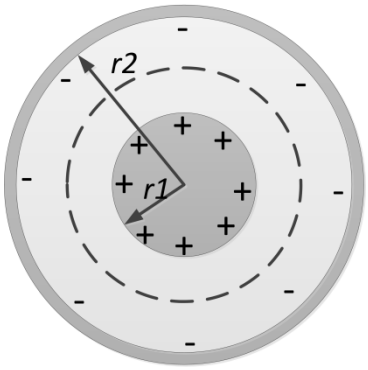

Figure 2.6. Calculating capacitance of an spherical capacitor

For a conductive droplet with geometric diameter of d_d, $r_1 = d_\mathrm{d}/2$ and $r_2 \to \infty$,

$$C = 2\pi\varepsilon_0 d_\mathrm{d} \qquad (2.29)$$

Hence, the resulting induced charge on each droplet would be,

$$q = -\frac{2\pi\varepsilon_0 \alpha d_\mathrm{d} V h}{eH} \qquad (2.30)$$

In this method, the charge that the droplets carry is the sum of q_0, the charge created while spraying (Moore 1973), and the induced part βV, so,

$$q = q_0 + \beta V \quad (2.31)$$

Here β is a constant depending on the geometry of the induction cap,

$$\beta = -\frac{2\pi\varepsilon_0\alpha d_{\mathrm{d}} h}{eH} \quad (2.32)$$

In this technique, the droplets can be neutralized by inducing a charge equal but with opposite sign of q_0.

For liquids with very low conductivities the final charge will also be dependent on the length of charging time (Reischl et al. 1977). The following is the equation for charging of a capacitor. In this case, the capacitor is the droplet,

$$q = q_0 + \beta V\left(1 - e^{-\tau/RC}\right) \quad (2.33)$$

$$\tau \cong \frac{1}{f} \quad (2.34)$$

$$R = \frac{4L}{\pi d_{\mathrm{d}}^2 \sigma} \quad (2.35)$$

Here τ is the droplet formation time, which is equal to the inversion of the frequency, f, by the assumption that there is no satellite droplet formation. L and σ are disintegration length and electrical conductivity of the solution.

2.2.5. Charge Limits

There are limits on the amount of charge that can be placed on a particle with a given size (Hinds 1999). The most common ones applicable to controlled Plateau-Rayleigh jet breakup are electron field emission and Rayleigh limits. For particles with negative charge, the maximum charge limit is reached when the electrical field resulting from the charge on its surface causes

spontaneous emission of electrons. This limit depends on the particle shape and, for particles with sharper edges, is lower. For spherical particles this limit is (Hinds 1999),

$$n_{\mathrm{L}} = \frac{4\pi\varepsilon_0 d_{\mathrm{p}}^2 E_{\mathrm{L}}}{4e} \qquad (2.36)$$

Here $E_{\mathrm{L}} = 9.0 \times 10^8\ \mathrm{V/m}$ is the surface field strength needed for the emission of electrons. There is also a similar limit for positively charged particles with $E_{\mathrm{L}} = 2.1 \times 10^{10}\ \mathrm{V/m}$. As is noticeable, the charge limit for positive ions is much higher. It is due to the fact that a much stronger field is required to extract a positive ion from a particle.

For liquid droplets there is also a limit known as the Rayleigh limit. The limit is mainly based on the mutual repulsion of electric charge on the droplet which may overcome the cohesion force of surface tension, σ, and result in the breakup of droplet. As already was shown in section 2.2.4, a conductive droplet can be considered as a capacitor with $C = 2\pi\varepsilon_0 d_{\mathrm{d}}$. The corresponding energy stored in droplet as a capacitor and surface energy are $\frac{q^2}{2C} = \frac{q^2}{4\pi\varepsilon_0 d_{\mathrm{d}}}$ and $\pi\sigma d_{\mathrm{d}}^2$ respectively (Frohn and Roth 2000), resulting in total potential energy of droplet as follows,

$$W_{\mathrm{P}} = \frac{q^2}{4\pi\varepsilon_0 d_{\mathrm{d}}} + \pi\gamma d_{\mathrm{d}}^2 \qquad (2.37)$$

For a given charge this function has a minimum for the so-called Rayleigh diameter,

$$d_{\mathrm{Rayleigh}} = \sqrt[3]{\frac{q^2}{8\pi^2\varepsilon_0\gamma}} \qquad (2.38)$$

The corresponding charge for a given diameter is known as Rayleigh limit for droplets (Frohn and Roth 2000; Hinds 1999),

$$n_{\text{Rayleigh}} = \left(\frac{8\pi^2 \varepsilon_0 \gamma d_{\text{d}}^3}{e^2}\right)^{1/2} \qquad (2.39)$$

This limit is lower than the electron field emission limit for droplets with geometric diameter larger than about $0.1\ \mu\text{m}$ (Hinds 1999).

2.3. Design and Building

2.3.1. Atomizer with Charging Cap

An atomizer based on the theory of controlled jet break up and compatible with a commercial spray dryer (Buchi B-190, Buchi Labortechnik AG, Flawil, Switzerland), was designed and prototyped. The schematic design of the atomizer with its main components is depicted in the Fig. 2.7. For drawings of the atomizer and assembly details, please refer to appendix A. Figure 2.8 shows the finished atomizer ready to be incorporated into the commercial spray dryer.

Uniform breakup of the jet was achieved through capillary waves produced by actuation of a piezoelectric ring (Ferroperm PiezoCeramics, 105261, Pz26) using a function generator (15 MHz Synthesized Function Generator, Model DS340, Stanford Research Systems, California, USA) at optimum frequencies and amplitudes. These optimum frequencies and amplitudes were found by monitoring the particle generation by an Aerosol Particle Sizer (APS 3321, TSI, Minneapolis, USA). Figure 2.9 shows the output file of the APS for one of the samplings with an orifice diameter of $20\ \mu\text{m}$ (TSI, 393530, Minneapolis, USA), while actuation frequency and amplitude of the function generator was set to 110 kHz and 2 V peak to peak (sinusoidal wave) and

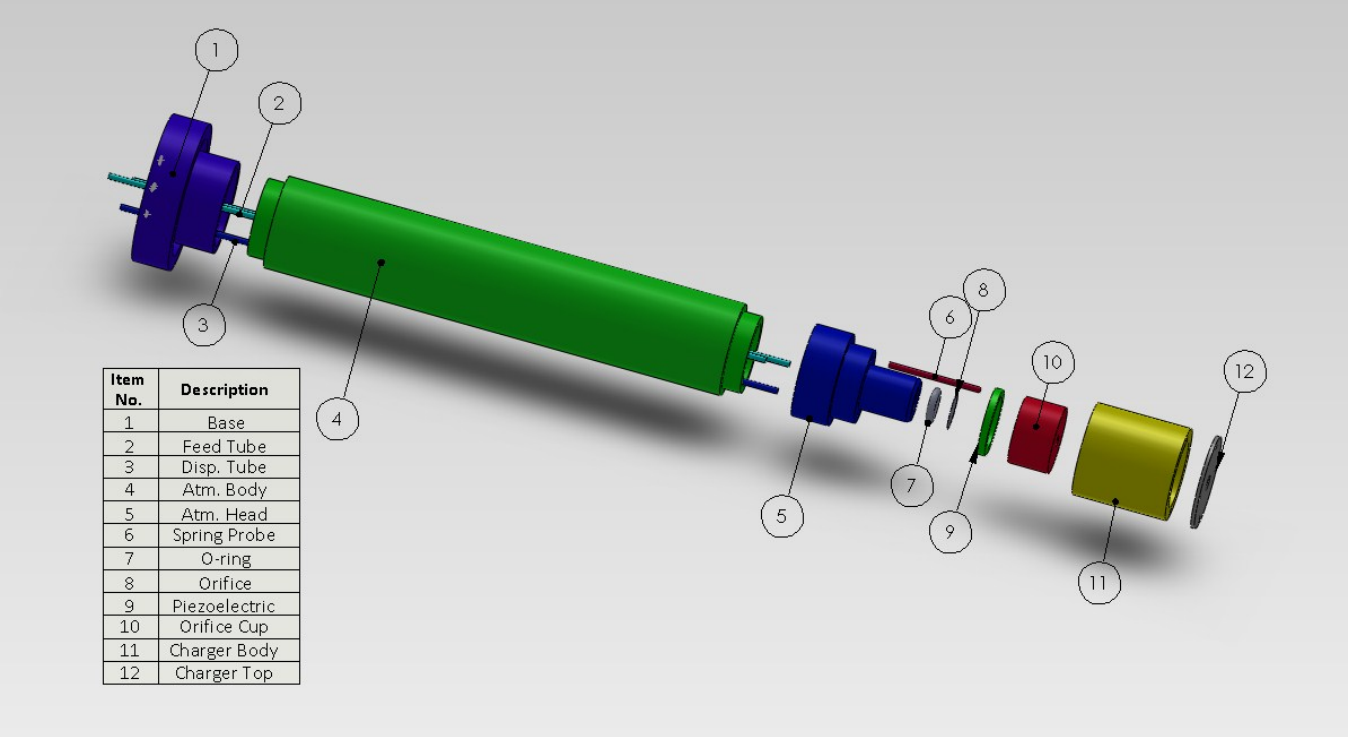

Item No.	Description
1	Base
2	Feed Tube
3	Disp. Tube
4	Atm. Body
5	Atm. Head
6	Spring Probe
7	O-ring
8	Orifice
9	Piezoelectric
10	Orifice Cup
11	Charger Body
12	Charger Top

Figure 2.7. Schematic of the designed atomizer for controlled Plateau-Rayleigh jet break up

Figure 2.8. Finished atomizer ready to be inserted into commercial spray dryer (Buchi B-190, Buchi Labortechnik AG, Flawil, Switzerland)

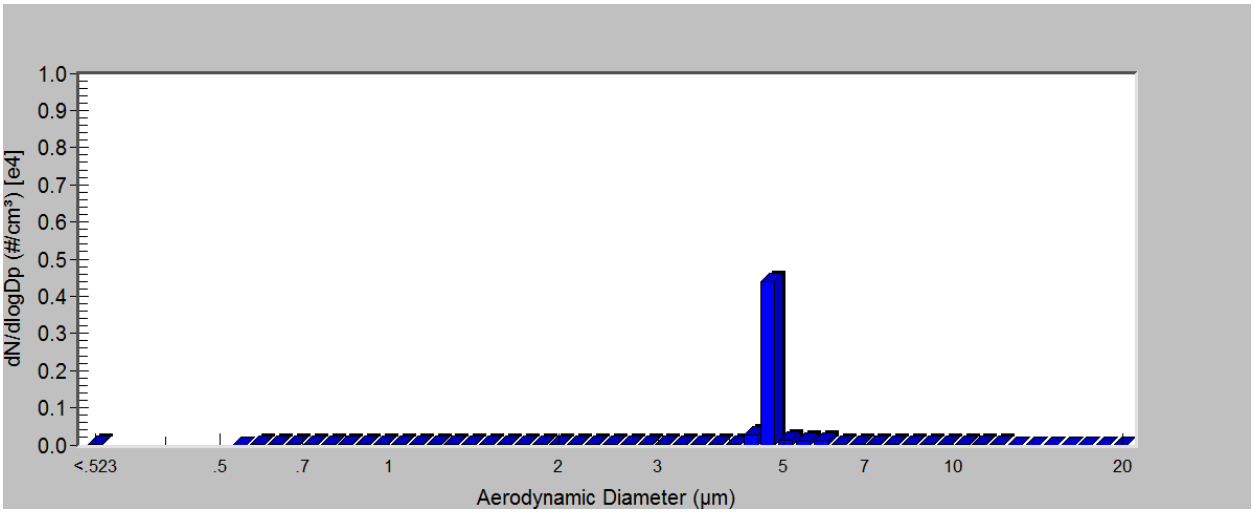

Figure 2.9. Monitoring particles leaving spray dryer by Aerosol Particle Sizer (APS 3321, TSI, Minneapolis, USA), f=110 kHz, V=2 V peak to peak, sinus wave, $p_{res} = 100\ kPa$

pressure was 100 kPa. It is recommended to keep the pressure of the reservoir as low as possible since at higher pressures the velocity of the jet increases, shortening the residence time of droplets in the spray dryer, hence requiring a longer spray-dryer column. Particles were made from Di(2-ethylhexyl) sebacate (DEHS) (ACROS, 269920010, 97%, USA) due to its very low vapor pressure and high stability; reagent alcohol (A995-4, HPLC grade, Fisher Scientific, United States) was utilized as a solvent and the volume concentration of DEHS in the reagent alcohol was 0.0021.

The next step was placing a uniform charge on the particles, which requires the jet to be made from a conductive solution; however, the solution of DEHS in alcohol is not conductive. To provide the required conductivity for the solution, a very small amount of aqueous solution of sodium chloride (NaCl) was added to the solution of DEHS in the reagent alcohol, the amount depending on the desired charge, the concentration of DEHS in ethanol, the gap between the

orifice and the conductive plate, and applied electrical potential difference. These values are mentioned for each experiment in the following chapters.

The charging cap is essentially a conductive plate separated from the rest of the setup by electrical insulation (optically clear and cast acrylic, McMaster-Carr, 8528K36, Illinois, USA). By applying a potential difference (Circuit Specialist, Programmable DC Power Supply 0-72V,0-1.5A, CSI3646A, USA) between the conductive plate and orifice, an approximately uniform field is established in the gap between the orifice and conductive plate, which induces the emerging jet and results in a net charge on the droplets during disintegration.

2.3.2. Feed line of Atomizer

To supply the atomizer with pressurized liquid, a feed line, Fig. 2.10, was designed and built. To avoid fluctuation in feed rate, a reservoir (Swagelok, 304L SS Double-Ended DOT-Compliant Sample Cylinder, 304L-HDF4-300, USA) was used to feed the atomizer (Lin et al. 1990) instead of a syringe and step-motor. The reservoir was fed from the top and Compressed Dry Air (CDA) was utilized to pressurize the solution. Although the feed line was also equipped with two stainless steel frit type filters (SS-4TF-05 housing, SS-4F-K4-05 0.5 micron filter, Swagelok, Edmonton, AB, Canada), one for the CDA line and one just before the atomizer, to prevent the micron-sized orifice being clogged by contaminants in the system, the solution was filtered before filling reservoir.

The check valve in the CDA line prevents any return of solution to the airline, and the exhaust valve in the system makes it possible to exhaust the reservoir and fill it with another solution. The reservoir was also equipped with a sight glass to see the amount of solution in the reservoir. It is useful for troubleshooting when the jet dies, which may have different causes

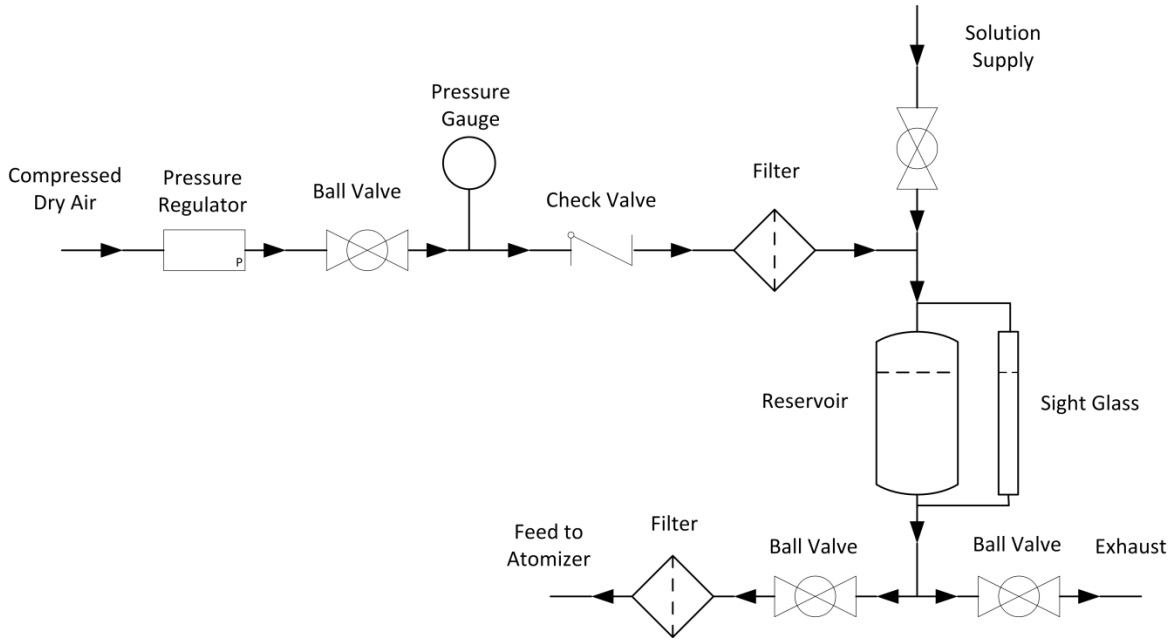

Figure 2.10. Schematic diagram of feed-line designed to supply the atomizer with pressurized solution

such as orifice blockage, low pressure in the system or an empty reservoir. The pressure regulator after the CDA supply adjusts the feed rate (for a given orifice) by controlling the reservoir pressure. The feed line diameter before the reservoir (airline) and after the reservoir (solution line) was 1/4 and 1/8 inch respectively.

2.3.3. Faraday Cup

To measure the charge of particles, a Faraday cup was designed and prototyped, and was connected to a high accuracy electrometer (Keithley 6517A, Ohio, USA). The Faraday cup and its internal structure are shown in Figs. 2.11 and 2.12, respectively. Particles are collected in the internal conductive cup (in this case, copper) and their charge is discharged to the electrometer through a low noise coaxial cable (Keithley, 4801, USA). Use of low noise cable is highly recommended due to the low level charge measurements. The intermediate cup is made from electrical insulation (McMaster, UHMW Polyethylene, USA) and the external cup is another

Figure 2.11. Designed and prototyped Faraday cup to measure particle's charge

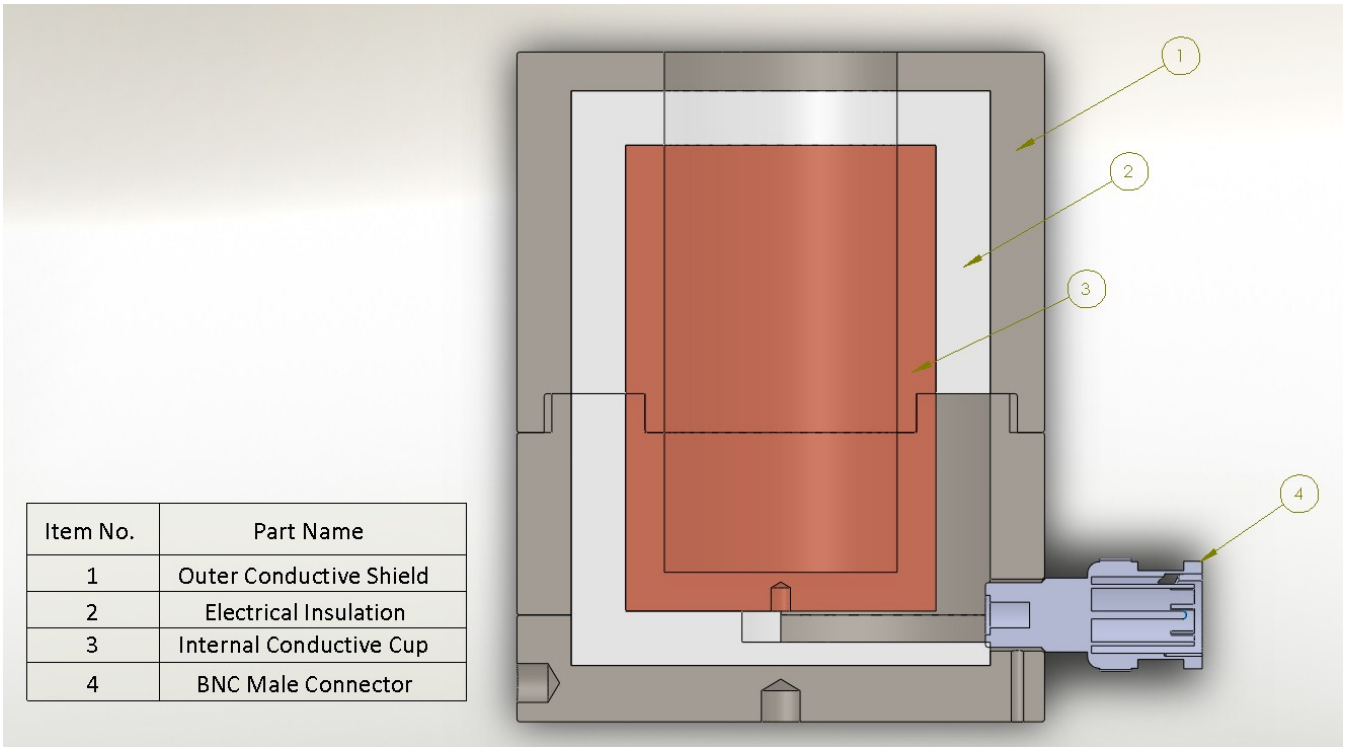

Item No.	Part Name
1	Outer Conductive Shield
2	Electrical Insulation
3	Internal Conductive Cup
4	BNC Male Connector

Figure 2.12. Internal structure of designed Faraday cup to measure particles' charge

conductive cup (in this case, Stainless Steel) to eliminate any external electric or electromagnetic fields which may result in an induced charge in the internal cup and cause noise in the measurements. The cup is designed in a fashion to be easily dismantled for cleaning and troubleshooting purposes. For drawings and more details please refer to Appendix B. Assuming uniform charge of particles for induction charging (Reischl et al. 1977), then due to the monodispersity of particles and uniform constant electrical fields experienced by the droplets, the charge of an individual particle can be easily calculated by dividing the total charge by the total number of particles generated in the chosen sampling time, which is equal to the frequency of the function generator (Ashgriz and Yarin 2011).

2.4. Conclusions

A custom atomizer and Faraday cup were designed and built to produce monodisperse uniformly charged particles (Berglund and Liu 1973; Rayleigh 1879; Reischl et al. 1977) and measure their charge. These particles were essential for our *in vitro* quantitative study of particle deposition in human airways.

Bibliography

Anders, K., Roth, N., Frohn, A. (1992). Operation Characteristics of Vibrating-Orifice Generators: The coherence length. Particle & Particle Systems Characterization, 9:40-43.

Ashgriz, N. and Yarin, A. L. (2011). Handbook of Atomization and Sprays. Springer, New York.

Berglund, R. N. and Liu, B. Y. H. (1973). Generation of monodisperse aerosol standards. Environmental Science & Technology, 7:147-153.

Castle, G. S. P. (1997). Contact charging between insulators. Journal of Electrostatics, 40–41:13-20.

Cloupeau, M. and Prunet-Foch, B. (1994). Electrohydrodynamic spraying functioning modes: a critical review. Journal of Aerosol Science, 25:1021-1036.

Frohn, A. and Roth, N. (2000). Dynamics of droplets. Springer.

Hinds, W. C. (1999). Aerosol Technology: Properties, Behavior, and Measurement of Airborne Particles. Wiley-Interscience, New York.

Kulkarni, P., Baron, P. A., Willeke, K. (2011). Aerosol Measurement: Principles, Techniques, and Applications, . John Wiley & Sons. Inc.

Kwetkus, B. A. (1998). Particle triboelectrification and its use in the electrostatic separation process. Particulate Science and Technology, 16:55-68.

Lin, H. B., Eversole, J. D., Campillo, A. J. (1990). Vibrating orifice droplet generator for precision optical studies. Review of Scientific Instruments, 61:1018-1018.

Liu, D. Y. and Frohn, A. (1988). Drag coefficients of single droplets moving in an infinite droplet chain on the axis of a tube, 14:217-232.

M. Cloupeau and Prunet-Foch, B. (1989). Electrostatic spraying of liquids in cone-jet mode. Journal of Electrostatics, 22:135-159.

Masters, K. (1991). Spray drying handbook:725.

May, K. R. (1949). An Improved Spinning Top Homogeneous Spray Apparatus. Journal of Applied Physics, 20:932.

McCarthy, M. J. and Molloy, N. A. (1974). Review of stability of liquid jets and the influence of nozzle design. The Chemical Engineering Journal, 7:1-20.

Mitchell, J. P. (1984). The production of aerosols from aqueous solutions using the spinning top generator. Journal of aerosol Science, 15:35-45.

Moore, A. D. (1973). Electrostatics and Its Applications. Wiley, New York.

Ohnesorge, W. v. (1936). Formation of drops by nozzles and the breakup of liquid jets. Z. Angew. Math. Mech, 16:355-358.

Orme, M. and Muntz, E. P. (1990). The manipulation of capillary stream breakup using amplitude-modulated disturbances: A pictorial and quantitative representation. Physics of Fluids A: Fluid Dynamics, 2:1124.

Paschen, F. (1889). Ueber die zum Funkenübergang in Luft, Wasserstoff und Kohlensäure bei verschiedenen Drucken erforderliche Potentialdifferenz (On the potential difference required for spark initiation in air, hydrogen, and carbon dioxide at different pressures). Annalen der Physik, 273:69-75.

Plateau, J. A. F. (1873). Statique expérimentale et théorique des liquides soumis aux seules forces moléculaires. Gauthier-Villars.

Pradip, Nandiyanto, A. B. D., Okuyama, K. (2011). Progress in developing spray-drying methods for the production of controlled morphology particles: From the nanometer to submicrometer size ranges. Advanced Powder Technology, 22:1-19.

Rayleigh, L. (1879). On the instability of jets. Proceedings of London Mathematical Society, 10:3-14.

Reischl, G., John, W., Devor, W. (1977). Uniform electrical charging of monodisperse aerosols. Journal of Aerosol Science, 8:55-65.

Rosell-Llompart, J. and Mora, J. F. d. l. (1994). Generation of monodisperse droplets 0.3 to 4 µm in diameter from electrified cone-jets of highly conducting and viscous liquids. Journal of Aerosol Science, 25:1093-1119.

Savart, F. (1833). Mémoire sur la constitution des veines liquides lancées par des orifices circulaires en mince paroi. Ann. Chim. Phys, 53:1833.

Schneider, J. M. and Hendricks, C. D. (1964). Source of Uniform-Sized Liquid Droplets. Review of Scientific Instruments, 35:1349-1350.

Tang, K. and Gomez, A. (1994). Generation by electrospray of monodisperse water droplets for targeted drug delivery by inhalation. Journal of Aerosol Science, 25:1237-1249.

Tolman, R. C. (1938). The Principles of Statistical Mechanics. Dover Publications.

Tomaides, M., Liu, B. Y. H., Whitby, K. T. (1971). Evaluation of the condensation aerosol generator for producing monodispersed aerosols. Journal of Aerosol Science, 2:39-46.

Tu, K.-W. (1982). A condensation aerosol generator system for monodisperse aerosols of different physicochemical properties. Journal of Aerosol Science, 13:363-371.

Vehring, R., Foss, W. R., Lechuga-Ballesteros, D. (2007). Particle formation in spray drying. Journal of Aerosol Science, 38:728-746.

Walton, W. H. and Prewett, W. C. (1949). The Production of Sprays and Mists of Uniform Drop Size by Means of Spinning Disc Type Sprayers. Proceedings of the Physical Society. Section B, 62:341-350.

Chapter 3. Effect of Electrostatic Charge on Oral-Extrathoracic Deposition for Uniformly Charged Monodisperse Aerosols

This chapter has been published as:

Azhdarzadeh, M., Olfert, J. S., Vehring, R., Finlay, W. H. (2014). Effect of Electrostatic Charge on Oral-Extrathoracic Deposition for Uniformly Charged Monodisperse Aerosols. Journal of Aerosol Science, 68, 38-45.

3.1. Introduction

Inhaled aerosol deposition in the mouth-throat region is an important consideration in the design of pharmaceutical inhalers. Knowledge of mouth-throat deposition allows for the design of high efficiency drug delivery methods to the pulmonary region, reducing the dose of drug needed for a specific treatment while limiting deleterious side effects and lowering the cost of treatment. Exposure to toxic and harmful aerosols in environmental and work places can also be a concern for people dealing with human health risk assessments. The extrathoracic region functions as a coarse particle filter, affecting the amount of aerosol, either therapeutic or toxic, that reaches the lung.

The deposition of aerosols in the respiratory tract is a complex function of many parameters, such as aerodynamic particle diameter, volume flow rate, morphological configuration, charge of aerosols, among others (Finlay 2001b). Numerous studies have investigated the effects of aerosol particle size, volume flow rate, and morphological configuration on particle deposition (Borgström 1999; Bowes and Swift 1989; Cass et al. 1999; Chan and Lippmann 1980; DeHaan and Finlay 2001; 2004; Emmett et al. 1982; Foord et al.

1978; Grgic et al. 2004a; Grgic et al. 2004b; Heenan et al. 2004; Stahlhofen et al. 1980; Stahlhofen et al. 1983; Stahlhofen et al. 1984; Zhou et al. 2011). Most deposition studies do not consider the effect of aerosol charge, and instead often use neutralized aerosols. A limited number of numerical and *in vivo* studies have examined the effect of electrostatic charge on total respiratory tract deposition (Bailey 1997; Bailey et al. 1998; Balachandran et al. 1997; Majid et al. 2012a; Melandri et al. 1983a). Bailey (1997) and Bailey et al. (1998) used a lung model and clinical data and came to the conclusion that by careful control of breathing, particle size and particle charge, deposition targeting of particles in the human airways is achievable. Balachandran et al. (1997) developed a computer model for investigating deposition of inhaled particles as a result of different deposition mechanisms in human airways and found a significant increase in deposition due to the charge that particles carry. They also noticed that particles with high charge were mostly deposited in the upper airways. Majid et al. (2012a) carried out a study on deposition enhancement in the stochastic human lung model IDEAL (Inhalation, Deposition and Exhalation of Aerosols in the Lung) for the particle size range of 0.3-1 μm. They reported that deposition enhancement in the human airways reaches a saturation point in alveolar region which depends on the particle size and flow condition. Melandri et al. (1983a) conducted *in vivo* experiments with particle diameters in the range of 0.3-1 μm and reported increased deposition due to electrostatic effects. Previous *in vitro* work conducted in the mouth-throat with charged aerosols (Ali et al. 2009; Ali et al. 2008; Chan et al. 1978) categorized particles as charged and uncharged rather than quantifying the charge of each particle, complicating the development of a fully predictive understanding of electrostatic effects. Chang et al. (2012) looked into the penetration of monodisperse particles (1 μm

diameter) with uniform charge through metallic tubes, and reported an increase in deposition with increasing particle charge and tube length. Yu (1985) has also looked into the effect of electrostatic charge in deposition of aerosols in human airways theoretically.

Electrostatic measurements of pharmaceutical aerosols show significant charge levels on particles generated by commercial respiratory drug delivery devices (Byron et al. 1997; Hoe et al. 2009b; Kwok et al. 2005b). Kwok et al. (2005b) reported more than 40,000 elementary charges per particle for particles with 6.0 μm diameter emitted from commercial MDI's. This high charge levels reveals the need for investigating electrostatic induced charge effect on deposition of particles in human airways.

In the current work, the effects on mouth-throat deposition of aerodynamic particle diameter (using monodisperse particles), volume flow rate and charge of particles (using uniformly charged particles) over a wide range of charge per particle (0-25,000 e) were investigated quantitatively. These effects were incorporated into a dimensionless empirical relation for deposition of particles in the mouth-throat of human adults that reduces to a previously published correlation (Grgic et al. 2004a) in the case of neutral particles.

3.2. Methods

A schematic of the setup for investigating the effect of particle charge, aerodynamic diameter of particle and volume flow rate on deposition in the oral-extrathoracic airway of an adult mouth-throat replica is depicted in Fig. 3.1. The Alberta Idealized Throat based on Stapleton et al. (2000), was used to mimic the oral-extrathoracic airway of a human adult in this experiment.

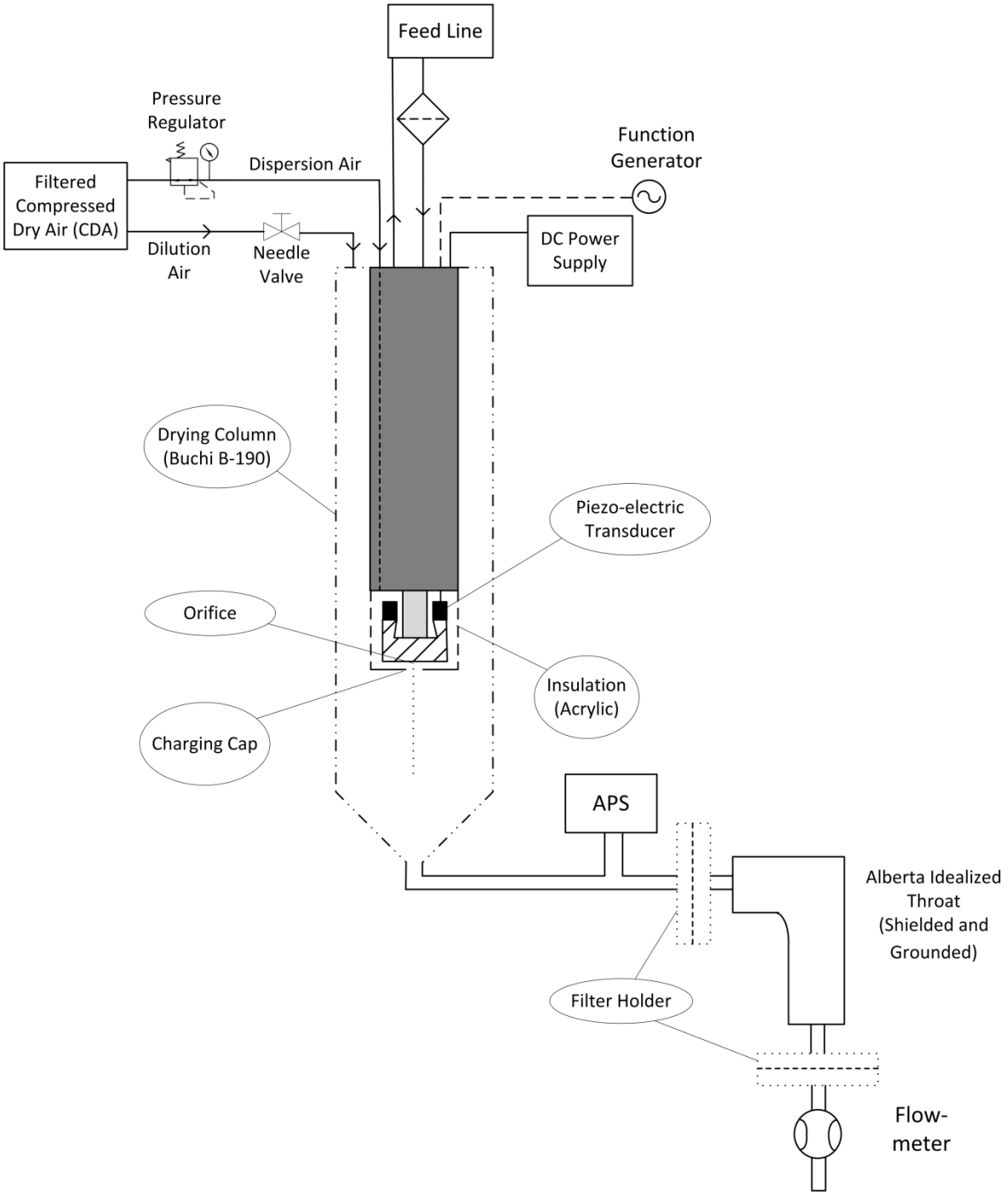

Figure 3.1. Schematic of the experimental set up to investigate the effect of particle charge, aerodynamic diameter of particle and volume flow rate on deposition in the oral-extrathoracic region of a human adult upper airway replica

This replica has been successful in mimicking mouth-throat deposition in adults (Grgic et al. 2004a; Grgic et al. 2004b; Zhang et al. 2007; Zhou et al. 2011). For mouth-throat replicas manufactured from nonconductive materials, the accumulation of electrostatic charge on the inside surface, mostly as a result of deposition from previous particles, could result in a repulsive force on particles in the aerosol flow passing through the airway, potentially altering their trajectory and changing deposition patterns in the throat. For this reason, a grounded, shielded and conductive aluminum version of the replica was utilized to avoid any such electrostatic or electromagnetic effects.

To investigate the effect of electrostatic forces for various particle aerodynamic diameters and different flow rates, it is useful to generate monodisperse particles carrying uniform charge. One of the most accurate methods capable of producing monodisperse aerosols is via continuous jet break up. This method is based on the uniform disintegration of a jet under the action of capillary waves generated by a piezo-electric transducer (Berglund and Liu 1973; Rayleigh 1879). A purpose-built atomizer based on this method was designed and a feed line to supply a constant flow with very low pressure fluctuations (Lin et al. 1990), maintained by using a pressurized reservoir instead of the commonly used step motors in commercial counterparts, was utilized. The feed line consists of a reservoir connected to a compressed dry air (CDA) line with a pressure regulator (Festo, LR-D-MINI-A543, Germany) to provide the required pressure to build up a jet and control its flow rate. A stainless steel frit-type filter (SS-2TF-05, 0.5 micron, Swagelok, USA) was placed before the atomizer to prevent particles from entering the atomizer and clogging the micron-sized orifice. A solution of Di(2-ethylhexyl) sebacate (DEHS) (ACROS,

269920010, 97%, USA) in ethanol (HPLC grade, Fisher Scientific, New Jersey, USA) was utilized for stable particle generation.

Electrostatic induction was used to charge the droplets uniformly (Reischl et al. 1977). In this method, an induction cap (charging cap) located immediately after the orifice creates a small gap between the orifice and the cap. Acrylic (optically clear and cast acrylic, McMaster-Carr, 8528K36, Illinois, USA) insulation is utilized to insulate the cap from the atomizer. By applying an electrical potential difference between the cap and orifice, an approximately uniform electrical field is established in the gap. If the solution used to create the jet is conductive, an inductive charge will be built up on the jet, and consequently the generated droplets will carry a net charge. This charge is the sum of q_0, the charge related to spraying, and the induced charge, βV, which add up to a total charge of q (Reischl et al. 1977):

$$q = q_0 + \beta V \tag{3.1}$$

Here β is a constant that depends on the physical properties of the working fluid and the geometry of the cap, while V is the electrical potential difference between the cap and the orifice. For a liquid with very low conductivity, the charging process will also depend on the time length of charging (Reischl et al. 1977).

Figure 3.2 confirms Eq. (3.1) for DEHS droplets, where 17.5 mL of aqueous sodium chloride solution with a volume concentration of 0.001 has been added to 140 mL DEHS solution in ethanol with volume concentration of 0.0022 to provide the required conductivity for the solution. The reservoir pressure was set to 1 bar, and a 20 μm orifice (TSI, 393530, Minneapolis, USA) was chosen for droplet generation. Droplet production frequency was controlled by a

function generator (15 MHz Synthesized Function Generator, Model DS340, Stanford Research Systems, California, USA) that was set to 91 kHz sinusodial wave with amplitude of 2 V peak to peak. The gap between charging cap and orifice was 1 mm. The test was repeated three times and a linear least squares fit was used for the data fitting.

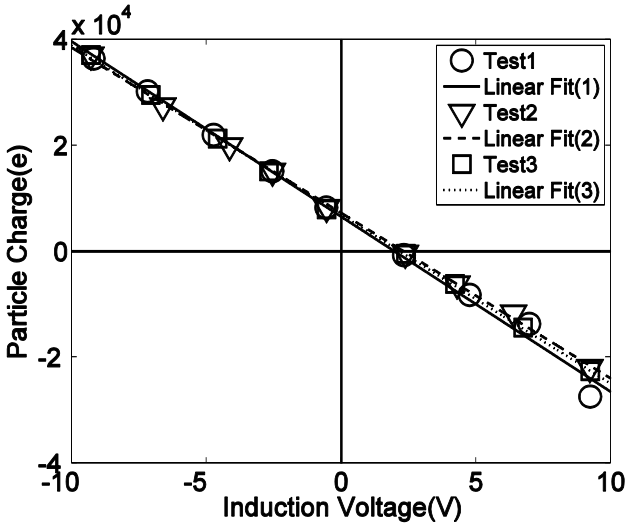

Figure 3.2. Charge vs. Induction voltage for DEHS droplets (geometric diameter of particle, d_p =5.22 μm), confirming the behavior expected by Eq. (3.1)

To measure individual droplet charge, droplets were collected in a Faraday cup over a sampling time of 20 sec. The Faraday cup was connected to a high accuracy electrometer (Keithley 6517A, Ohio, USA) reading the total charge of droplets collected in the cup over the sampling time. To minimize any possible loss of droplets, the cup was placed immediately after the charging cap. To check for variations in experimental conditions, a charge measurement was performed before and after each sampling. Knowing the droplet generation rate, which is equal to the actuation frequency of the piezoelectric (Ashgriz and Yarin 2011), and assuming no satellite droplets, the charge of each individual droplet was then determined by assuming uniform charging (Reischl et al. 1977). The study by Reischl et al. (1977) found charge variation

to be proportional to the variation in droplet diameter, since the droplet diameter governs the electrical capacity to be charged. They also report good uniformity in the charge and mention that the charge variation between the droplets is so small that it could not be measured by their method (a mobility analyzer).

By passing a turbulent air stream through the charging cap, it also served as a dispersion cap. The optimum volume flow rate for the dispersion air stream was adjusted, for different experimental settings, by a pressure regulator (Norgren, R72G-2AT-RMG, Queretaro, Mexico) upstream of the dispersion line. The optimum volume flow rate was chosen based on monitoring the particles size by an aerodynamic particle sizer (APS 3321, TSI, Minneapolis, USA). This turbulent air stream disperses the chain of droplets and minimizes the coalescence of droplets which would cause polydispersity.

To produce DEHS particles, a solution of DEHS in ethanol, with volume concentration depending on desired particle size, was prepared. The atomizer was coupled with a commercial spray dryer (Buchi B-190, Buchi Labortechnik AG, Flawil, Switzerland) to dry the initial droplets to their final size in a drying column. Assuming Rayleigh breakup (Rayleigh 1879)**,** the initial geometric diameter of the droplets is approximately twice the orifice diameter. The final diameter of a particle depends on volume concentration of solution and initial droplet diameter. Real time measurement of the aerodynamic diameter of the particles was conducted by APS immediately after the dryer column.

All the deposition experiments were conducted using monodisperse particles with a measured GSD less than 1.1. The particles were collected on a non-hygroscopic filter membrane

(47 mm, TX40HI20WW, Pall, USA) mounted on a filter holder (47 mm, XX4404700, Milipore, Massachusetts, USA). An ultra-microbalance (Mettler Toledo UMX2, 11115545, Ohio, USA) with a maximum capacity of 2.1 g and a readability of 0.1 μg was utilized to measure the weight of the particles collected on the filter membrane. To avoid any error in measurement due to electrostatic charge on the filter membrane, an anti-electrostatic gun (Zerostat 3, Milty, Hertfordshire, UK) was utilized to neutralize the membrane before measuring the filter.

As depicted in Fig. 3.1, the filter holder was first placed before the throat, and particles collected over a sampling time of either 420, 180 or 120 seconds, depending on particle size. Keeping the experimental conditions constant, the filter holder was moved to the output of the throat, and particles were collected over the same length of time. To increase the accuracy of the measurement and to check for variations of experimental conditions during the deposition tests, the filter holder was again placed at the inlet and the measurement was repeated. The average increase in filter mass for the first and third sampling (filter holder at inlet) was considered as the mass of particles entering the inlet and the increase in filter mass for the second sampling (filter holder at outlet) was considered as the mass of particles entering the outlet. The difference in mass entering the inlet and outlet, which is the mass deposited in the replica, over the measured mass entering the inlet was considered as deposition fraction. The volume flow rate of air was monitored by a flow meter (Model 4000, TSI, Minneapolis, USA) after the throat and altered by changing the flow volume entering the spray dryer which itself was adjusted by a needle valve (Penutrol, N30BK, Antrim, Ireland).

To check the accuracy of the ultra-microbalance setup, the experiment was conducted with filtered air, expecting no mass change in the filter membrane. When repeated 10 times, the maximum deviation was less than 4 μg. Comparing this value with the smallest sample masses, which were about 100 μg, the relative error of the gravimetric method was expected to be less than 4% in all cases.

3.3. Results and Discussion

For validation, results obtained with the current set up, Fig. 3.1, for neutralized particles were compared with values based on (DeHaan and Finlay 2004) calculated using the ARLA Deposition Calculator, which is available online (http://www.mece.ualberta.ca/arla/deposition_calculator.html); this comparison is shown in Table 3.1 for different particle aerodynamic diameters and flow rates. The comparison shows good agreement between the results.

Table 3.1. Comparison of deposition in the Alberta Idealized Throat based on DeHaan and Finlay (2004) with the current experimental data for neutralized particles

	DeHaan & Finlay (2004)	Current Setup
$d_a = 3.3\ \mu m, Q_{air} = 15\ L/min$	4%	4%
$d_a = 3.3\ \mu m, Q_{air} = 30\ L/min$	12%	12%
$d_a = 4.6\ \mu m, Q_{air} = 15\ L/min$	11%	10.5%
$d_a = 4.6\ \mu m, Q_{air} = 30\ L/min$	31%	28%
$d_a = 5.9\ \mu m, Q_{air} = 15\ L/min$	23%	22.5%
$d_a = 5.9\ \mu m, Q_{air} = 30\ L/min$	55%	54%

Figures 3.3, 3.4 and 3.5 show the effect of particle charge on deposition at two different flow rates (15 and 30 L/min), for particles with aerodynamic diameters of 3.3, 4.6, and 5.9 μm, respectively. The increase in deposition, compared to neutral particles, can be explained by induced charge effects at the walls of the airway which result in a Coulomb force between the particle and wall that enhances deposition (Bailey et al. 1998; Finlay 2001b). The other electrostatic effect known as the space charge effect (Wilson, 1947) was unimportant in our experiments, since the aerosol number concentration was lower than 10^3 /cm^3.

The enhancement in deposition with charge was larger for smaller particles. This can be explained by considering the ratio of the two dimensionless numbers governing the two main

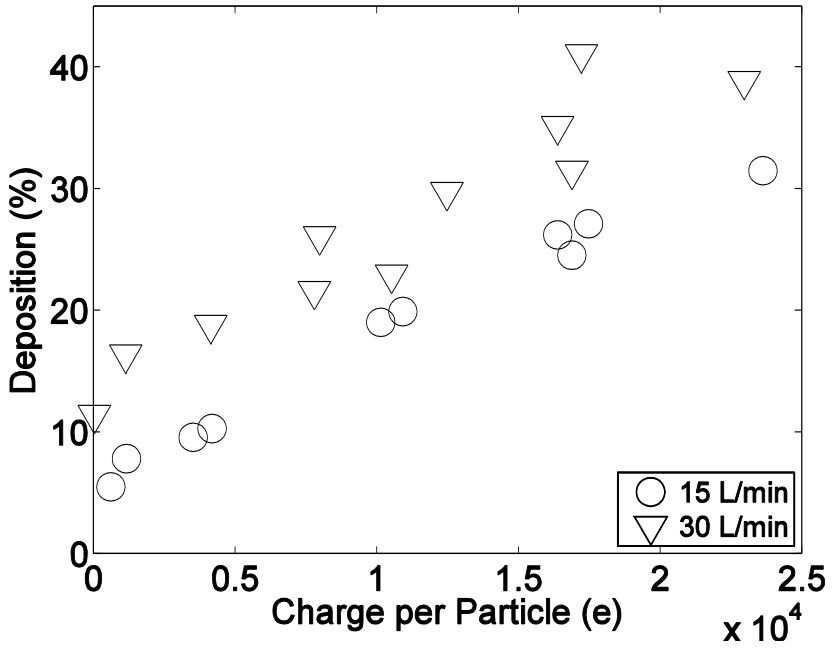

Figure 3.3. Deposition in the Alberta Idealized Throat vs. charge at two different flow rates for DEHS particles (d_a=3.3 μm)

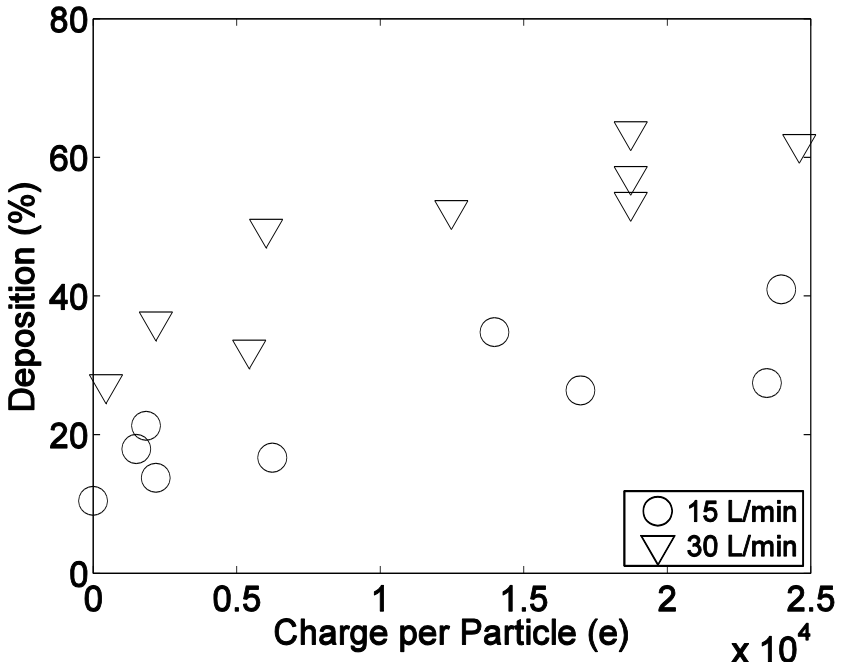

Figure 3.4. Deposition in the Alberta Idealized Throat vs. charge at two different flow rates for DEHS particles (d_a=4.6 μm)

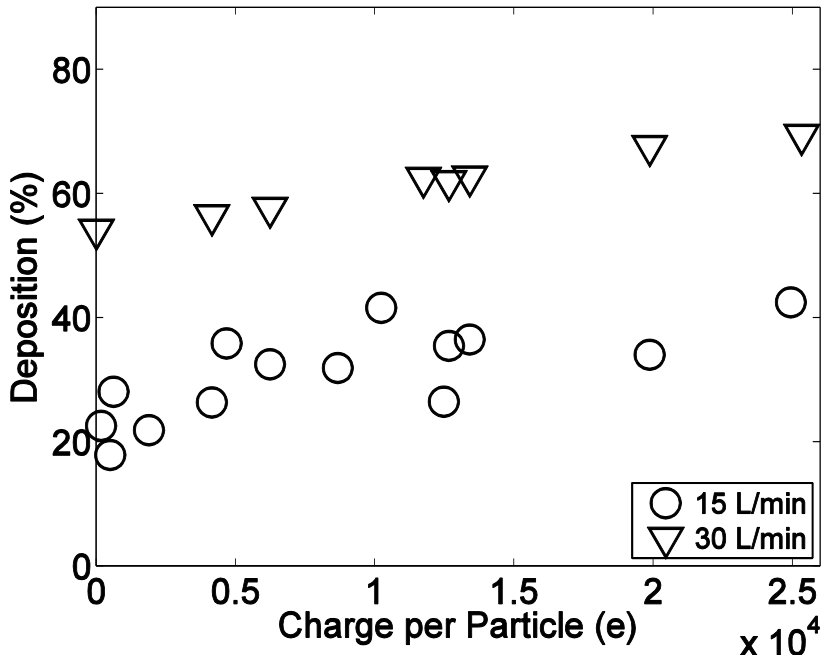

Figure 3.5. Deposition in the Alberta Idealized Throat vs. charge at two different flow rates for DEHS particles (d_a=5.9 μm)

deposition mechanisms here i.e. electrostatic induction and impaction. The deposition mechanisms of diffusion and sedimentation are not important here since diffusion is mostly important for particle with aerodynamic diameter smaller than 1 μm while sedimentation becomes important for more distal human airways, where the residence time is larger (Finlay 2001b).

Neglecting Cunningham slip factors, which is reasonable for the particle sizes considered here, the dimensionless number governing electrostatic induction is (Finlay 2001b)

$$Inc = \frac{\sqrt{\rho_{\mathrm{p}}/\rho^*}}{3\pi\mu U_{\mathrm{mean}} d_{\mathrm{a}}} \frac{e^2}{16\pi\varepsilon_0 D_{\mathrm{mean}}^2} \frac{n^2}{\acute{x}^2} = \frac{\sqrt{\rho_{\mathrm{p}}/\rho^*}\ e^2 n^2}{192\pi\mu d_{\mathrm{a}} \varepsilon_0 Q \acute{x}^2} \quad (3.2)$$

Here ρ_{p}, ρ^*, e, n and $\varepsilon_0 = 8.85 \times 10^{-12}\ \mathrm{C^2 N^{-1} m^{-2}}$ are particle density, reference density of 1000 kg/m^3, elementary charge, number of elementary charges on each particle, and permittivity of free space, respectively. The variable $x' = {x_{\mathrm{p}}}/{D_{\mathrm{mean}}}$, is the nondimensional distance of the particle from the wall. A value of $\acute{x}$=0.025 as suggested by Finlay (2001b) was utilized in the present work.

The dimensionless parameter governing inertial impaction is

$$Stk = \frac{\rho^* d_{\mathrm{a}}^2 U_{\mathrm{mean}}}{18\mu D_{\mathrm{mean}}} = \frac{\rho^* d_{\mathrm{a}}^2 Q}{36\mu} \sqrt{\frac{\pi L^3}{\bar{V}^3}} \quad (3.3)$$

An equivalent mean diameter ($D_{\mathrm{mean}} = 2\sqrt{\bar{V}/\pi L}$) and corresponding velocity ($U_{\mathrm{mean}} = 4Q/\pi D_{\mathrm{mean}}^2$) similar to what Grgic et al. (2004a) defined, is utilized in the aforementioned numbers. Here $\bar{V}$=76.8 cm^3 for mouth throat volume, *L*=18.8 cm for centerline path length were utilized to remain consistent with the aforementioned work of Grgic et al. (2004a). These values are based on average value for seven realistic geometries. *Q*, μ and d_{a} are volume flow rate of inhaled gas, dynamic viscosity of inhaled gas and aerodynamic diameter of the particles.

These two dimensionless numbers can be derived by nondimensionalizing the equation of motion for a particle, including the Coulomb force. The ratio of the two dimensionless numbers, *Inc/Stk*, determines the relative importance of induced charge effects. This ratio is larger for smaller particle sizes, and explains the larger effect of charge on deposition for the smaller particles in Fig. 3.3 vs. larger particles in Fig. 3.4 and Fig. 3.5.

Less deposition enhancement for larger particles does not necessarily mean that this effect will always be less important for larger particles, since the Rayleigh limit (Hinds 1999) and field emission limit for larger particles are larger, so that the maximum charge they can carry is higher. In addition, for monodisperse aerosols with a given charge per unit mass of aerosol, larger particles will have higher charge levels.

It is beneficial to present deposition as a function of the dimensionless numbers governing the problem. Grgic et al. (2004a) suggested an empirical relation including Reynolds and Stokes

number, *Re* and *Stk*, for deposition of neutralized particles in the mouth-throat airways as follows:

$$\eta(\%) = \left[1 - \frac{1}{(1 + 11.5x^{1.912})}\right] \times 100 \quad (3.4)$$

Here $x = StkRe^{0.37}$ is the deposition parameter defined in the Grgic et al. (2004a) study. Reynolds number used in the aforementioned work was:

$$Re = \frac{\rho_{\mathrm{g}} U_{\mathrm{mean}} D_{\mathrm{mean}}}{\mu} = \frac{2\rho_{\mathrm{a}} Q}{\mu}\sqrt{\frac{L}{\pi \bar{V}}} \quad (3.5)$$

Here ρ_{g} is the density of inhaled gas. In the current work, a more general empirical relation that captures electrostatic effects is suggested as follows:

$$\bar{\eta}(\%) = \left[1 - \frac{1}{(1 + 11.5\bar{x}^{1.912})}\right] \times 100 \quad (3.6)$$

where,

$$\bar{x} = (0.3956\, Inc^{0.2680} + Re^{0.37} Stk)(1 + 2.4452 Inc^{0.0045}) \quad (3.7)$$

The aforementioned relation was obtained using a nonlinear least squares algorithm. For the case of a neutral particle, it reduces to the equation suggested by Grgic et al. (2004a). Figure 3.6 shows the resulting equation plotted versus the presently defined deposition parameter $\bar{x}$, compared with the experimental data obtained using the setup presented in Fig. 3.1. The coefficient of determination of the fitting, R^2, and root mean square error are 0.88 and 5 respectively.

Equation (3.6) includes both inertial and induced charge deposition parameters that are involved in the mouth-throat deposition in a dimensionless form, and can be used to predict deposition due to both deposition mechanisms. It is worth mentioning that Eq. (3.6) is intended to predict the combined effects of induced charge and inertial impaction only for the parameter range of the present experimental data, i.e., dilute, charged aerosols at flow rates of 15-30 L/min with aerodynamic particle diameters in a range of 3-6 μm; extrapolation outside this range of values is of course not recommended.

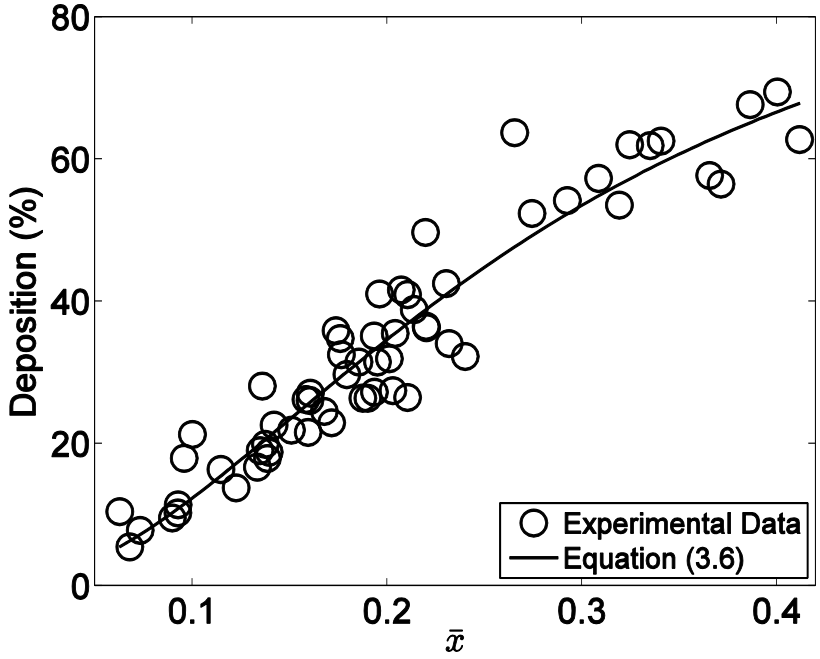

Figure 3.6. Suggested dimensionless equation for deposition on mouth throat of human adults including inertial and induced charge electrostatic effects, Eq. (3.6)

3.4. Conclusions

The effect of particle charge on deposition in a mouth-throat mimic (the Alberta Idealized Throat) was investigated at different particle aerodynamic diameters and volume flow rates. As expected, particle charge affects deposition substantially, especially for smaller sizes where the

impaction mechanism of deposition is less dominant. An empirical dimensionless relation is suggested to predict average deposition in the mouth-throat that includes the three relevant dimensionless numbers: Stokes number, Reynolds number and induced charge number. This correlation allows prediction of the combined effect of charge and inertial impaction on deposition in the oral-extrathoracic airways.

Bibliography

Ali, M., Mazumder, M. K., Martonen, T. B. (2009). Measurements of electrodynamic effects on the deposition of MDI and DPI aerosols in a replica cast of human oral – pharyngeal – laryngeal airways. Journal of Aerosol Medicine, 22:35-44.

Ali, M., Reddy, R. N., Mazumder, M. K. (2008). Electrostatic charge effect on respirable aerosol particle deposition in a cadaver based throat cast replica. Journal of Electrostatics, 66:401-406.

Ashgriz, N. and Yarin, A. L. (2011). Handbook of Atomization and Sprays. Springer, New York.

Bailey, A. G. (1997). The Inhalation and Deposition of Charged Particles Within the Human Lung. Journal of Electrostatics, 42:25-32.

Bailey, A. G., Hashish, A. H., Williams, T. J. (1998). Drug delivery by inhalation of charged particles. Journal of Electrostatics, 44:3-10.

Balachandran, W., Machowski, W., Gaura, E., Hudson, C. (1997). Control of drug aerosol in human airways using electrostatic forces. Journal of Electrostatics, 40-41:579-584.

Berglund, R. N. and Liu, B. Y. H. (1973). Generation of monodisperse aerosol standards. Environmental Science & Technology, 7:147-153.

Borgström, L. (1999). In vitro, ex vivo, in vivo veritas. Allergy, 54:88-92.

Bowes, S. M. and Swift, D. L. (1989). Deposition of inhaled particles in the oral airway during oronasal breathing. Aerosol Science and Technology, 11:157-167.

Byron, P. R., Peart, J., Staniforth, J. N. (1997). Aerosol Electrostatics I: Properties of Fine Powders Before and After Aerosolization by Dry Powder Inhalers. Pharmaceutical Research, 14:698-705.

Cass, L. M. R., Brown, J., Pickford, M., Fayinka, S., Newman, S. P., Johansson, C. J., Bye, A. (1999). Pharmacoscintigraphic evaluation of lung deposition of inhaled zanamivir in healthy volunteers. Clinical Pharmacokinetics, 36:21-31.

Chan, T. L. and Lippmann, M. (1980). Experimental measurements and empirical modelling of the regional deposition of inhaled particles in humans. American Industrial Hygiene Association Journal, 41:399-409.

Chan, T. L., Lippmann, M., Cohen, V. R., Schlesinger, R. B. (1978). Effect of electrostatic charges on particle deposition in a hollow cast of the human larynx-tracheobronchial tree. J. Aerosol Sci., 9:463-468.

Chang, K. N., Chen, Y. K., Huang, S. H., Chen, C. W., Lai, C. Y., Chen, C. C. (2012). Penetration of charged particles through metallic tubes. Journal of Aerosol Science, 48:10-17.

DeHaan, W. H. and Finlay, W. H. (2001). In vitro monodisperse aerosol deposition in a mouth and throat with six different inhalation devices. Journal of Aerosol Medicine, 14:361-367.

DeHaan, W. H. and Finlay, W. H. (2004). Predicting extrathoracic deposition from dry powder inhalers. Journal of Aerosol Science, 35:309-331.

Emmett, P. C., Aitken, R. J., Hannan, W. J. (1982). Measurements of the total and regional deposition of inhaled particles in the human respiratory tract. Journal of Aerosol Science, 13:549-560.

Finlay, W. H. (2001). The Mechanics of Inhaled Pharmaceutical Aerosols: An Introduction. Academic Press, London.

Foord, N., Black, A., Walsh, M. (1978). Regional deposition of 2.5–7.5 µm diameter inhaled particles in healthy male non-smokers. Journal of Aerosol Science, 9:343-357.

Grgic, B., Finlay, W. H., Burnell, P. K. P., Heenan, A. F. (2004a). In vitro intersubject and intrasubject deposition measurements in realistic mouth–throat geometries. Journal of Aerosol Science, 35:1025-1040.

Grgic, B., Finlay, W. H., Heenan, A. F. (2004b). Regional aerosol deposition and flow measurements in an idealized mouth and throat. Journal of Aerosol Science, 35:21-32.

Heenan, A. F., Finlay, W. H., Grgic, B., Pollard, A., Burnell, P. K. P. (2004). An investigation of the relationship between the flow field and regional deposition in realistic extra-thoracic airways. Journal of Aerosol Science, 35:1013-1023.

Hinds, W. C. (1999). Aerosol Technology: Properties, Behavior, and Measurement of Airborne Particles. Wiley-Interscience, New York.

Hoe, S., Traini, D., Chan, H. K., Young, P. M. (2009). Measuring charge and mass distributions in dry powder inhalers using the electrical Next Generation Impactor (eNGI). European Journal of Pharmaceutical Sciences, 38:88-94.

Kwok, P. C. L., Glover, W., Chan, H.-K. (2005). Electrostatic charge characteristics of aerosols produced from metered dose inhalers. Journal of Pharmaceutical Sciences, 94:2789-2799.

Lin, H. B., Eversole, J. D., Campillo, A. J. (1990). Vibrating orifice droplet generator for precision optical studies. Review of Scientific Instruments, 61:1018-1018.

Majid, H., Madl, P., Hofmann, W., Alam, K. (2012). Implementation of Charged Particles Deposition in Stochastic Lung Model and Calculation of Enhanced Deposition. Aerosol Science and Technology, 46:547-554.

Melandri, C., Tarroni, G., Prodi, V., De Zaiacomo, T., Formignani, M., Lombardi, C. C. (1983). Deposition of charged particles in the human airways. Journal of Aerosol Science, 14:657-669.

Rayleigh, L. (1879). On the instability of jets. Proceedings of London Mathematical Society, 10:3-14.

Reischl, G., John, W., Devor, W. (1977). Uniform electrical charging of monodisperse aerosols. Journal of Aerosol Science, 8:55-65.

Stahlhofen, W., Gebhart, J., Heyder, J. (1980). Experimental determination of the regional deposition of aerosol particles in the human respiratory tract. American Industrial Hygiene Association journal, 41:385-398a.

Stahlhofen, W., Gebhart, J., Heyder, J., Scheuch, G. (1983). New regional deposition data of the human respiratory tract. Journal of Aerosol Science, 14:186-188.

Stahlhofen, W., Gebhart, J., Heyder, J., Scheuch, G., Juraske, P. (1984). Particle deposition in extrathoracic airways of healthy subjects and of patients with early stages of laryngeal carcinoma. Journal of Aerosol Science, 15:215-217.

Stapleton, K. W., Guentsch, E., Hoskinson, M. K., Finlay, W. H. (2000). On the suitability of k–ε turbulence modeling for aerosol deposition in the mouth and throat: a comparison with experiment. Journal of Aerosol Science, 31:739-749.

Yu, C. P. (1985). Theories of electrostatic lung deposition of inhaled aerosols. Annals of Occupational Hygiene, 29:219-227.

Zhang, Y., Gilbertson, K., Finlay, W. H. (2007). In vivo–in vitro comparison of deposition in three mouth–throat models with Qvar® and turbuhaler® inhalers. Journal of Aerosol Medicine:227-235.

Zhou, Y., Sun, J., Cheng, Y. S. (2011). Comparison of deposition in the USP and physical mouth-throat models with solid and liquid particles. Journal of Aerosol Medicine and Pulmonary Drug Delivery, 24:277-284.

Chapter 4. Effect of Induced Charge on Deposition of Uniformly Charged Particles in a Pediatric Oral-extrathoracic Airway

This chapter has been published as:

Azhdarzadeh, M., Olfert, J. S., Vehring, R., Finlay, W. H. (2014). Effect of Induced Charge on Deposition of Uniformly Charged Particles in a Pediatric Oral-extrathoracic Airway. Aerosol Science and Technology, 48:508-514.

4.1. Introduction

Extrathoracic deposition affects the variability of both toxic and pharmaceutical aerosols that reach the lungs (Borgström et al. 2006b). Knowledge of deposition in the extrathoracic airways as a function of the relevant parameters is helpful in the design of new drug delivery devices to the respiratory tract, as well as in the study and regulation of environmental aerosol exposure.

Most of the mouth-throat deposition data in the literature are for human adults and uncharged particles (Borgström 1999; Bowes and Swift 1989; Brancatisano et al. 1983; Cass et al. 1999; Chan and Lippmann 1980; DeHaan and Finlay 2001; 2004; Emmett et al. 1982; Foord et al. 1978; Grgic et al. 2004a; Grgic et al. 2004b; Stahlhofen et al. 1983; Zhou et al. 2011). A number of authors have examined deposition of charged aerosols in adults (Ali et al. 2009; Ali et al. 2008; Azhdarzadeh et al. 2014a; Bailey et al. 1998; Balachandran et al. 1997; Hashish 1992; Hashish et al. 1994; Majid et al. 2012a; Melandri et al. 1983a; Saini et al. 2004a; Saini et al. 2002a). However, there is comparatively little data on oral airway deposition for children (Becquemin et al. 1991; Below et al. 2013; Bennett and Zeman 2004; Bickmann et al. 2008; Golshahi et al. 2012; Golshahi et al. 2013; Mitchell and Nagel 1997b; Schueepp et al. 2009), and

all previous pediatric work is for uncharged aerosols. Despite the importance of the existing studies for adult subjects, the lack of data for child subjects may arise from additional ethical considerations regarding experiments with children and also the difficulty of achieving cooperation from young children during experiments. To avoid such issues, *in vitro* experiments using models of children's airways are a valuable alternative. To reduce the number of experiments needed, idealized models that mimic average deposition are useful (Bickmann et al. 2008; Golshahi and Finlay 2012; Stapleton et al. 2000).

Electrostatic charge measurements for pharmaceutical inhalers have revealed high charge levels on the particles emitted from some commercial respiratory drug delivery devices (Byron et al. 1997; Hoe et al. 2009b; Kwok and Chan 2009; Kwok et al. 2005c). Kwok et al., 2005 reported charge levels higher than 40,000 e per particle for particles generated by a commercial Metered Dose Inhaler (MDI). These high charge levels on particles and the lack of comprehensive data on child mouth-throat deposition highlights the need for studies on the effect of electrostatic charge on deposition of particles in pediatric oral extrathoracic airways. Electrostatic charge of particles can alter particles trajectory through induced charge and space charge effects. Since water accounts for most of the weight of the human body (Hall 2011), the order of magnitude for its dielectric constant is expected to be similar to that of water. For such high dielectric constants, the force exerted on the particle from the airway wall would be similar to the force from a mirror image particle with equal magnitude but opposite sign. This effect is known as the induced charge effect. The space charge effect, instead caused by Columbic repulsion of nearby particles with the same charge polarity, is important only for an aerosol with high concentration. Both effects can alter particle trajectories compared to neutral

particles, pushing them toward the walls of the airways, so that both induced charge and space charge effects result in increased deposition (Finlay 2001c).

In the present work, a quantitative study on the effect of induced electrostatic charge on deposition of monodisperse particles in a pediatric oral-extrathoracic airway was conducted. The effect of particle aerodynamic diameter (using monodisperse particles), particle charge (using uniformly charged particles), and flow rate were investigated. Two empirical relations, based on two different characteristic diameters, are developed for predicting deposition in pediatric mouth-throat airways. The results of the current study may be useful in predicting and understanding deposition in the pediatric respiratory tract.

4.2. Methods

The effect of electrostatic charge on the deposition of aerosols was studied here by using monodisperse and uniformly charged particles produced using the experimental apparatus described by Azhdarzadeh et al. (2014a), and briefly outlined below.

Particles were generated using controlled Rayleigh jet break up. This method relies on disintegration of a jet under the action of capillary waves produced by a piezo-electric transducer at optimum frequencies and amplitudes (Berglund and Liu 1973; Rayleigh 1879). An atomizer using this method was designed and built as described by Azhdarzadeh et al. (2014a). The atomizer was designed to be compatible for incorporation into a commercial spray dryer (Buchi B-190, Buchi Labortechnik AG, Flawil, Switzerland) where the volatile phase, i.e., ethanol, of the initial droplets evaporates and Di (2-ethylhexyl) sebacate (DEHS, ACROS, 269920010,

97%, USA) particles are left behind. The final size of particles depends on the solution concentration, actuation frequency and volume flow rate of the jet.

Uniform charging of droplets was achieved with an induction charging cap (Reischl et al. 1977). The charge that the particles acquire in this method has two origins as described by the following equation:

$$q = q_0 + \beta V \quad (4.1)$$

Here, q_0 is the charge from spraying (Moore 1973) and βV is the induction charge, where V is the potential difference between the orifice and the cap. The constant, β, depends on the physical properties of the working fluid and the geometry of the cap. The validity of Eq. 4.1 was confirmed previously for our experimental setup (Azhdarzadeh et al. 2014a). The other role of the cap was dispersion of the droplets, by passing a turbulent air flow through it, thus minimizing droplet coalescence in order to provide a high level of monodispersity.

The particle charge was measured by implementing a Faraday pail connected to an electrometer (Keithley 6517A, Ohio, USA) with a measurement range of 10 fC to 2 μC for charge and an accuracy of 0.4% of reading. It was assumed that the droplets were uniformly charged (Reischl et al. 1977), so the charge on each droplet can then be calculated from the total charge measured by the Faraday pail over a specific sampling time and droplet generation frequency, which is precisely controlled by a function generator (Ashgriz and Yarin 2011).

A schematic of the deposition investigation set up is depicted in Fig. 4.1. An idealized child mouth- throat model (Golshahi and Finlay 2012) represents the pediatric oral-extrathoracic

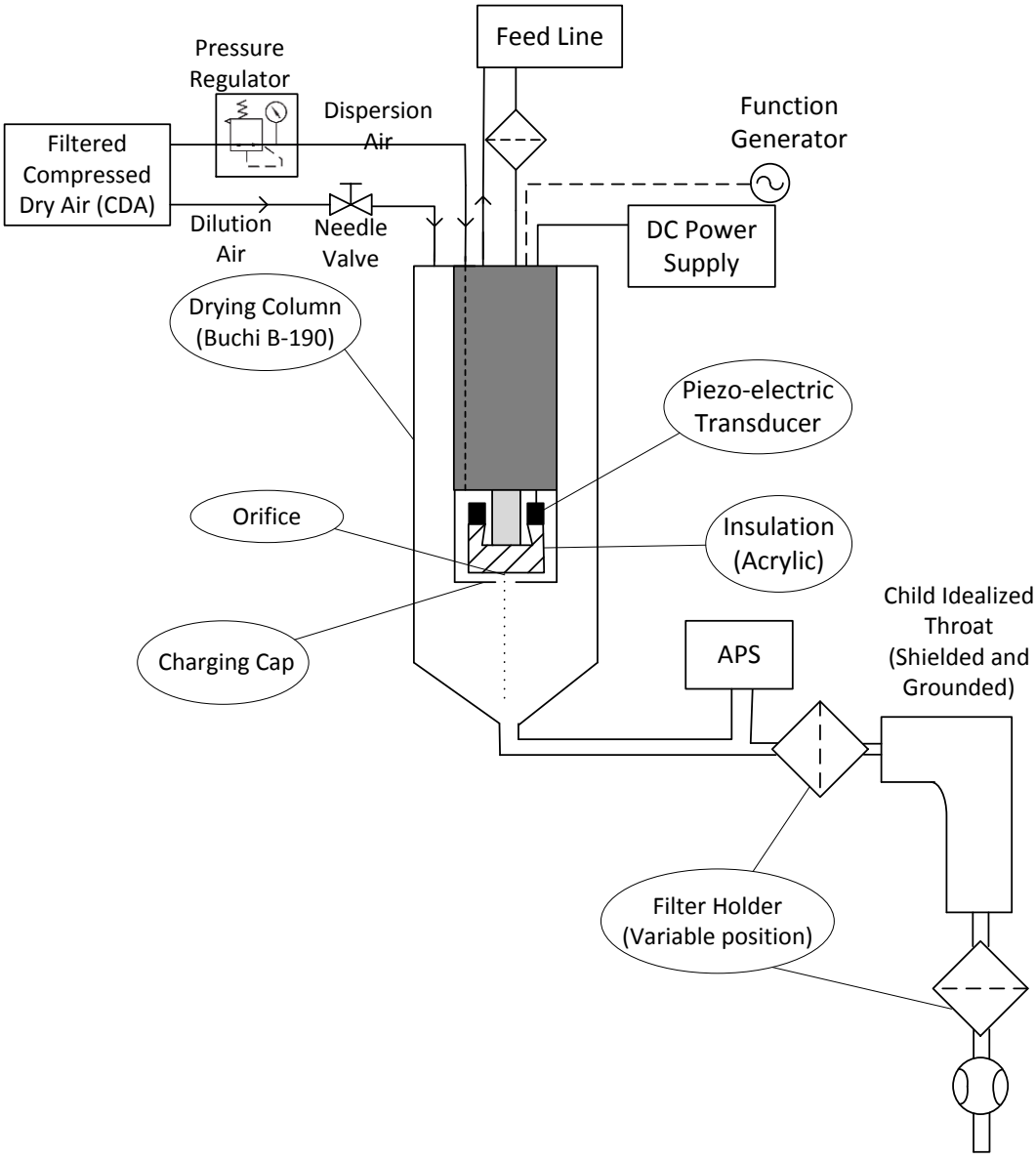

Figure 4.1. Schematic of the setup to investigate the effect of particle electrostatic charge, aerodynamic diameter and flow condition on deposition in a pediatric oral-extrathoracic airway, after Azhdarzadeh et al. (2014a)

airways. This model was built based on scaling the Alberta Idealized Throat (Stapleton et al. 2000) by a factor of 0.62 and was successful in mimicking average mouth-throat deposition in 9 realistic models of the upper airways of children aged 6-14 years (Golshahi and Finlay 2012).

Golshahi and Finlay (2012) chose the scaling factor in a way that matches the average characteristic diameter of the airway, $d_c = \frac{\bar{V}}{A_s}$, for their nine tested models. An electrically grounded aluminum version of the model was utilized to avoid any electrostatic effects between static charge on the interior walls of the throat and particles passing through the model. To prevent any possible electromagnetic effects, the mouth-throat model was also shielded. According to the findings of Melandri et al. (1983a) and Elajnaf et al. (2007b), the effect of relative humidity on the charge of particles is negligible mainly due to the short residence time of particles in the mouth-throat model, which is about 75 and 150 ms for the present model at flow rates of 20 and 10 L/min, respectively.

The deposition investigation was performed by collecting particles immediately upstream and downstream of the model with a non-hygroscopic borosilicate glass filter membrane (47 mm, TX40HI20WW, Pall, USA) mounted in a filter holder (47 mm, XX4404700, Millipore, USA) with filter mass measured by an ultra-microbalance (Mettler Toledo UMX2, USA). To avoid any electrostatic effects due to a possible charge on the filter membrane, the membranes were neutralized by a piezoelectric neutralizing device (Zerostat 3, Milty, Hertfordshire, UK) before conducting any measurement. See (Azhdarzadeh et al. 2014a) for further details.

Real time monitoring of aerodynamic particle diameter was conducted immediately after the dryer column by a time-of-flight particle sizer (APS 3321, TSI, Minneapolis, USA). Flow rate through the mouth-throat model was monitored by a digital flow-meter (Model 4000, TSI, Minneapolis, USA) immediately after the model and controlled by adjusting the amount of air entering the dryer column with a needle valve (Penutrol, N30BK, Antrim, Ireland).

4.3. Results and Discussion

Although the present setup was validated for the case of an adult idealized mouth-throat model by Azhdarzadeh et al. (2014a), it is worth examining its validity for the present pediatric deposition measurements. Figure 4.2 shows a comparison between the experimental data obtained with the present experimental setup for neutral particles and the results reported by Golshahi et al. (2013) for particle deposition in the same Alberta Idealized Child Mouth-throat model used here at volume flow rates of Q=11.5 and 16.2 L/min. Golshahi et al. (2013) used a six jet Collison atomizer (BGI, USA) along with jojoba oil (100% pure, Dessert Essence, NY, USA) with a density of 0.86 kg/m^3 as a working fluid, for producing polydisperse particles and an APS (3321, TSI, Minneapolis, USA) for investigating deposition in the model. The results are presented versus impaction parameter, $d_a^2 Q$, where d_a and Q are aerodynamic diameter of the particle and volume flow rate of inhaled gas, respectively.

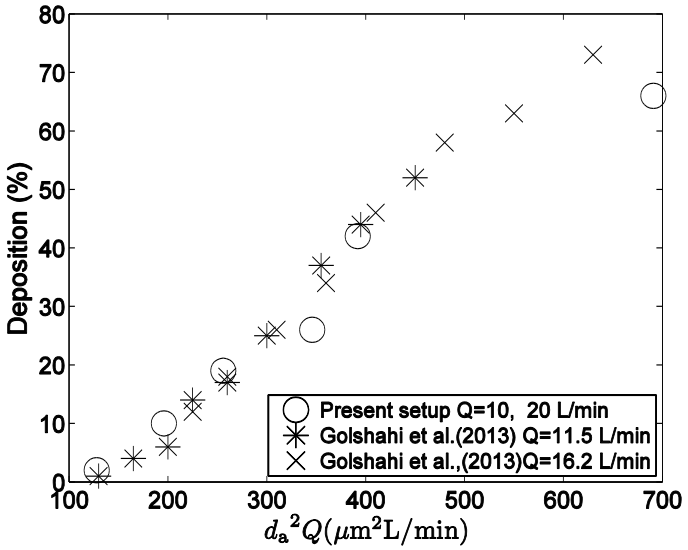

Figure 4.2. Comparison of the data from the present setup for the deposition of neutralized particles in the Idealized Child mouth-throat with the results reported by Golshahi et al. (2013)

Figures 4.3, 4.4 and 4.5 show the effect of induced charge on deposition of particles with aerodynamic diameters of 3.6, 4.4 and 5.9 μm in the Idealized Child oral-extrathoracic airway model. This range of particle sizes was chosen based on common aerodynamic diameters for inhaled pharmaceutical particles and the experimental limitations of the ultra-microbalance for very fine particles. In all the experiments the geometric standard deviation (GSD) of the generated aerosol was less than 1.1 as determined by the APS. The studied charge range was 0-10^4 e/particle which is well below the Rayleigh and electron emission limits (Hinds 1999). The Rayleigh and electron emission limits for the smallest particle in the experiments are 2×10^5 and 2×10^6 e/particle respectively. Deposition uncertainty analysis of the data was performed based on three sets of points, each including three points, and the average and maximum uncertainty values were 4% and 8%, respectively. This uncertainty also includes the variation as a result of charge variation for three adjacent points. To examine charge measurements and also charge variation during the experiment, charge measurements were made at the beginning and at the end of twelve experiments. The variation was approximately 0.045 nC for a sampling time of 10 s, which, assuming an approximate working frequency of 100 kHz for the atomizer, results in an uncertainty of approximately 140 e per particle (or approximately 2% of the maximum charge state of 10,000 e).

The data in Figures 4.3, 4.4 and 4.5 show a substantial enhancement in deposition due to induced charge effects. Note that space charge effects are unimportant here because of the low concentration of particles in the aerosol stream (i.e. lower than 10^3 cm^{-3}).

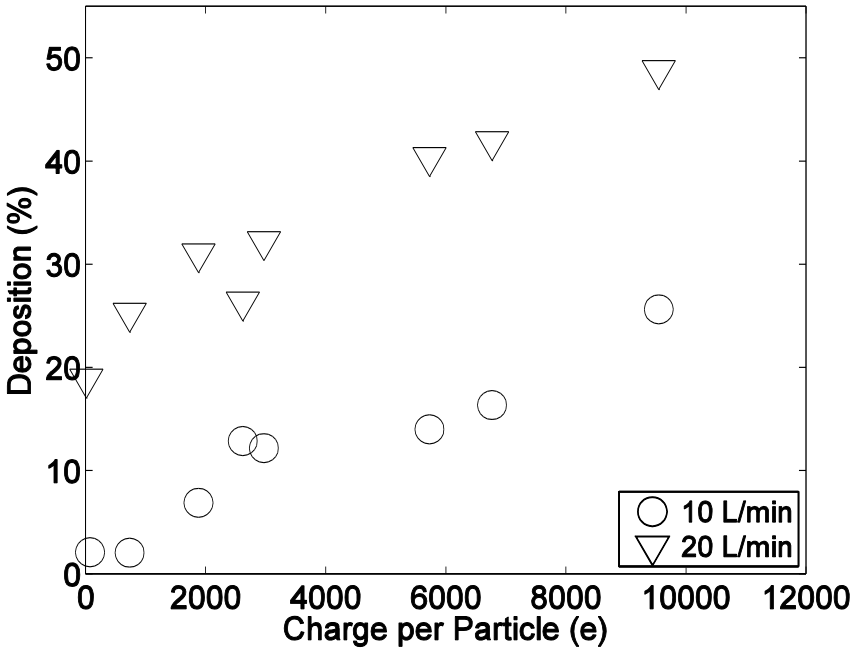

Figure 4.3. Effect of charge on deposition of particles in the idealized child oral-extrathoracic airway at two flow rates Q=10 and 20 L/min for d_a = 3.6 µm

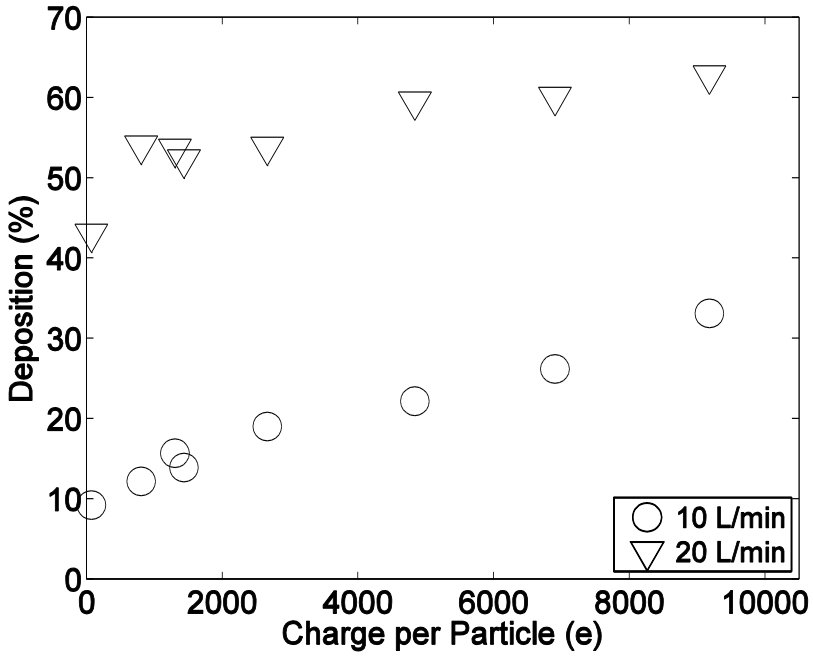

Figure 4.4. Effect of charge on deposition of particles in the idealized child oral-extrathoracic airway at two flow rates Q=10 and 20 L/min for, d_a = 4.4 µm

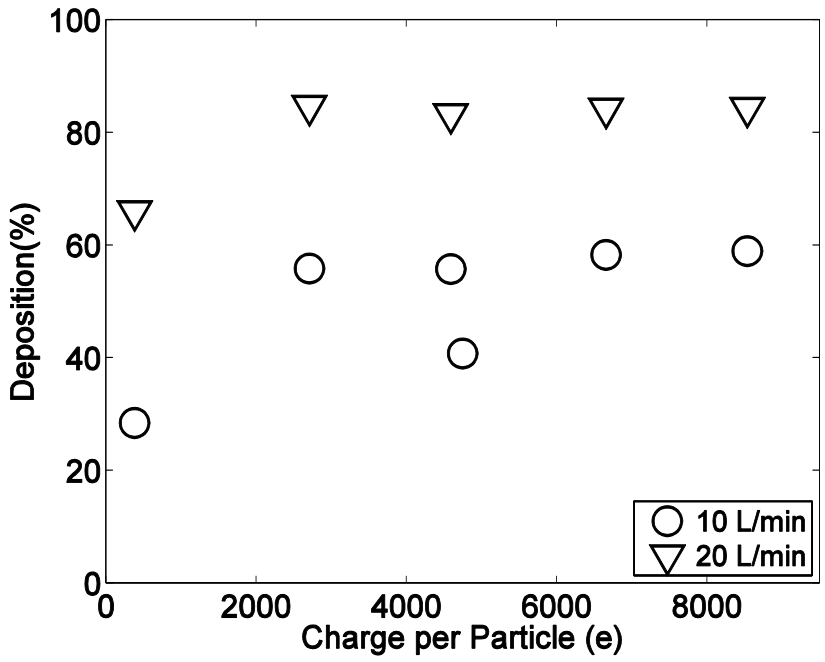

Figure 4.5. Effect of charge on deposition of particles in the idealized child oral-extrathoracic airways at two flow rates Q=10 and 20 L/min for, d_a = 5.9 µm

Comparing deposition results for the child mouth throat model in Figures 4.3, 4.4 and 4.5 with the data for the adult model in our previous study (Figure 3.3, 3.4 and 3.5, Azhdarzadeh et al. (2014a)), higher deposition values for the present child oral-extrathoracic airway are observed. This phenomenon is partly explained by higher velocities for a specific volume flow rate in the child replica, due to its smaller diameter compared to the adult model, which results in higher impaction. The smaller geometry of the child model is also a favorable parameter in increasing deposition due to induced electrostatic charges because of the smaller distance between the particles and the walls of the airway.

Golshahi et al. (2012) suggested two empirical relations for deposition, $\hat{\eta}$, of uncharged particles in the pediatric mouth-throat airways as a function of Reynolds number, Re, and Stokes number, *Stk*, as follows,

$$\eta_1(\%) = [1 - \frac{1}{1 + 2.45(Stk^{1.33}Re^{0.58})}] \times 100 \quad (4.2)$$

$$\eta_2(\%) = [1 - \frac{1}{1 + 0.000335(Stk^{1.5}Re^{0.69})}] \times 100 \quad (4.3)$$

The two characteristic diameters used in the aforementioned equations are:

$$d_{c1} = \sqrt{\frac{\bar{V}}{L}} \quad (4.4)$$

$$d_{c2} = \frac{\bar{V}}{A_s} \quad (4.5)$$

where V, L and A_s are oral airway volume, length, and surface area, respectively. The first characteristic diameter is similar to the one Grgic et al. (2004a) used for deposition in the mouth-throat of human adults. Although Golshahi et al. (2012) reported better predictions for deposition using the second characteristic diameter, Eq. (4.5), Golshahi et al. (2012) also suggested a relation as a function of the first diameter, Eq. (4.4), since it is more easily measured *in vivo* by acoustic pharyngometry. They suggested that the reason for better capture of inter-individual variability with the latter diameter may be due to more sensitivity of A_s to individual variations in geometry rather than *L*.

To include electrostatic effects, in the present work we include two new variables defined as

$$\hat{x}_1 = Stk^{1.33}Re^{0.58}\left(1 + a_1 Inc^{b_1}\right) \quad (4.6)$$

$$\hat{x}_2 = Stk^{1.5} Re^{0.69} \left(1 + a_2 Inc^{b_2}\right) \quad (4.7)$$

A MATLAB code that uses nonlinear least squares algorithm was developed to determine values of the constants *a* and *b* here. The results are as follow,

$$\hat{\eta}_1(\%) = [1 - \frac{1}{1 + 2.45\hat{x}_1}] \times 100 \quad (4.8)$$

$$\hat{x}_1 = Stk^{1.33} Re^{0.58} (1 + 31.09 Inc^{0.20}) \quad (4.9)$$

$$\hat{\eta}_2(\%) = [1 - \frac{1}{1 + 0.000335\hat{x}_2}] \times 100 \quad (4.10)$$

$$\hat{x}_2 = Stk^{1.5} Re^{0.69} (1 + 41.27 Inc^{0.20}) \quad (4.11)$$

The induced charge number, $Inc = \frac{\sqrt{\frac{\rho_p}{\rho^*}} e^2 n^2}{192\pi\mu d_a \varepsilon_0 Q \acute{x}^2}$, appearing in the above equations includes the induced charge effects where ρ_p, ρ^*, *e*, *n*, μ and ε_0 are particle density, unit density of 1000 kg/m^3, elementary charge, number of elementary charges on particle, dynamic viscosity of inhaled gas, permittivity of free space. $\acute{x}$ is a characteristic nondimensional distance of particles from the wall and to keep consistency with Finlay (2001c), a constant representative value of 0.025 was utilized. These relations were developed using nonlinear least squares data fitting. To remain consistent with Golshahi et al. (2012) the same values for characteristic diameters, $d_{c1} = 1.46$ cm and $d_{c2} = 0.27$ cm, were utilized in the current study. These diameters are the mean values for the nine children, aged 6-14 years, in their study.

Figures 4.6 and 4.7 show the experimental data obtained using the setup illustrated in Fig. 4.1, along with the suggested empirical Eq. (4.8) and Eq. (4.10). The coefficient of determination of the fitting, R^2, and root mean square error for Eq. (4.8) and Eq. (4.10) are 0.90, 6, 0.92 and 6 respectively. As is seen in the figures, Eq. (4.10) is a better fit compared to

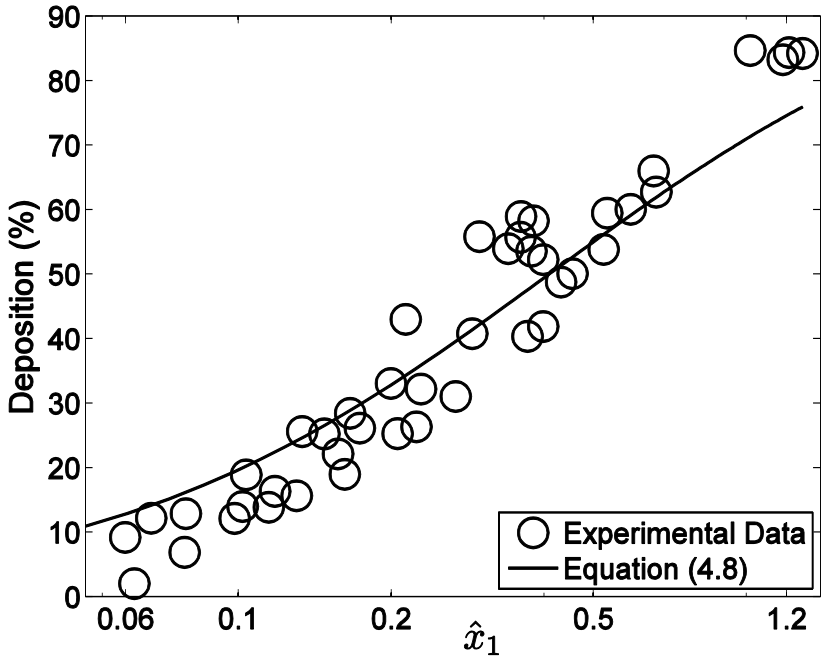

Figure 4.6. Deposition in an idealized pediatric oral-extrathoracic airway including inertial and induced charge effects along with suggested dimensionless Eq. (4.8)

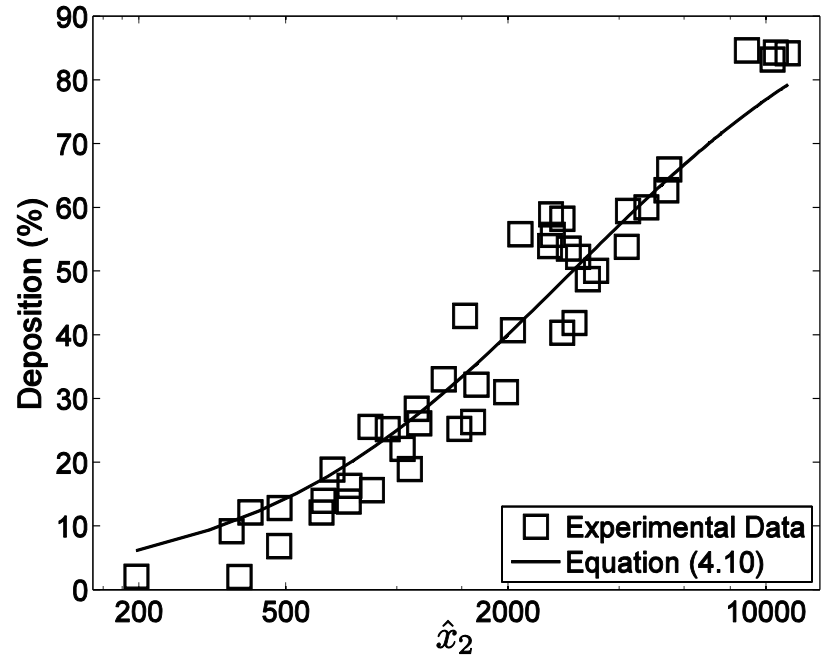

Figure 4.7. Deposition in an idealized pediatric oral-extrathoracic airway including inertial and induced charge effects along with suggested dimensionless Eq. (4.10)

Eq. (4.8), especially at very low or very high values of the parameters $\hat{x}_1$ and $\hat{x}_2$. The dimensionless nature of the suggested equations makes them potentially applicable to different gases and particle materials. For neutral particles the equations reduce to the equations proposed by Golshahi et al. (2012). Equations (4.8) and (4.10) include the two dominant deposition mechanisms for mouth-throat deposition operating in our experiments, i.e., impaction and electrostatic induction forces. For the particle diameters examined here, deposition due to diffusion is negligible and sedimentation is important only for more distal lung airways where the residence time is larger (Finlay 2001c).

The introduced correlation equations are valid only for the range of conditions of the current experiments (i.e. charged, dilute aerosols with particle diameters in the range of 3 – 6 μm and flow rates 10 – 20 L/min, for children aged 6-14 years). Extrapolation outside of these parameter ranges is expected to result in reduced accuracy.

4.4. Conclusions

The experimental results show a substantial increase in particle deposition associated with particle charge and related induced charge effects in the Idealized Alberta Child oral-extrathoracic airway. The higher slope of the deposition curve vs. charge in Fig. 4.3 for smaller particles indicates a more prominent effect of charge on deposition enhancement for smaller particles, which is explained by less dominant inertial impaction, allowing electrostatic effects to be more obviously seen.

Two empirical equations were suggested for predicting deposition of charged particles using two characteristic lengths, $d_{c1} = \sqrt{\frac{\bar{V}}{L}}$ and $d_{c2} = \frac{\bar{V}}{A_s}$. The introduced equations capture the effect of particle aerodynamic diameter, particle charge, and flow rate on pediatric oral-extrathoracic airway deposition and may be useful to those interested in predicting deposition of electrostatically charged aerosols in school age children.

Bibliography

Ali, M., Mazumder, M. K., Martonen, T. B. (2009). Measurements of electrodynamic effects on the deposition of MDI and DPI aerosols in a replica cast of human oral – pharyngeal – laryngeal airways. Journal of Aerosol Medicine, 22:35-44.

Ali, M., Reddy, R. N., Mazumder, M. K. (2008). Electrostatic charge effect on respirable aerosol particle deposition in a cadaver based throat cast replica. Journal of Electrostatics, 66:401-406.

Ashgriz, N. and Yarin, A. L. (2011). Handbook of Atomization and Sprays. Springer, New York.

Azhdarzadeh, M., Olfert, J. S., Vehring, R., Finlay, W. H. (2014). Effect of electrostatic charge on oral-extrathoracic deposition for uniformly charged monodisperse aerosols. Journal of Aerosol Science, 68:38-45.

Bailey, A. G., Hashish, A. H., Williams, T. J. (1998). Drug delivery by inhalation of charged particles. Journal of Electrostatics, 44:3-10.

Balachandran, W., Machowski, W., Gaura, E., Hudson, C. (1997). Control of drug aerosol in human airways using electrostatic forces. Journal of Electrostatics, 40-41:579-584.

Becquemin, M., Swift, D., Bouchikhi, A., Roy, M., Teillac, A. (1991). Particle deposition and resistance in the noses of adults and children. European Respiratory Journal, 4:694-702.

Below, A., Bickmann, D., Breitkreutz, J. (2013). Assessing the performance of two dry powder inhalers in preschool children using an idealized pediatric upper airway model. International Journal of Pharmaceutics, 444:169-174.

Bennett, W. D. and Zeman, K. L. (2004). Effect of body size on breathing pattern and fine-particle deposition in children. Journal of applied physiology (Bethesda, Md. : 1985), 97:821-826.

Berglund, R. N. and Liu, B. Y. H. (1973). Generation of monodisperse aerosol standards. Environmental Science & Technology, 7:147-153.

Bickmann, D., Wachtel, H., Kroger, R., Langguth, P. (2008). Examining Inhler Performance Using a Child's Throat Model, in Respiratory Drug Delivery, 565-570.

Borgström, L. (1999). In vitro, ex vivo, in vivo veritas. Allergy, 54:88-92.

Borgström, L., Olsson, B., Thorsson, L. (2006). Degree of throat deposition can explain the variability in lung deposition of inhaled drugs. Journal of Aerosol Medicine, 19:473-483.

Bowes, S. M. and Swift, D. L. (1989). Deposition of inhaled particles in the oral airway during oronasal breathing. Aerosol Science and Technology, 11:157-167.

Brancatisano, T., Collett, P. W., Engel, L. A. (1983). Respiratory movements of the vocal cords. Journal of Applied Physiology, 54:1269-1276.

Byron, P. R., Peart, J., Staniforth, J. N. (1997). Aerosol Electrostatics I: Properties of Fine Powders Before and After Aerosolization by Dry Powder Inhalers. Pharmaceutical Research, 14:698-705.

Cass, L. M. R., Brown, J., Pickford, M., Fayinka, S., Newman, S. P., Johansson, C. J., Bye, A. (1999). Pharmacoscintigraphic evaluation of lung deposition of inhaled zanamivir in healthy volunteers. Clinical Pharmacokinetics, 36:21-31.

Chan, T. L. and Lippmann, M. (1980). Experimental measurements and empirical modelling of the regional deposition of inhaled particles in humans. American Industrial Hygiene Association Journal, 41:399-409.

DeHaan, W. H. and Finlay, W. H. (2001). In vitro monodisperse aerosol deposition in a mouth and throat with six different inhalation devices. Journal of Aerosol Medicine, 14:361-367.

DeHaan, W. H. and Finlay, W. H. (2004). Predicting extrathoracic deposition from dry powder inhalers. Journal of Aerosol Science, 35:309-331.

Elajnaf, A., Carter, P., Rowley, G. (2007). The effect of relative humidity on electrostatic charge decay of drugs and excipient used in dry powder inhaler formulation. Drug development and industrial pharmacy, 33:967-974.

Emmett, P. C., Aitken, R. J., Hannan, W. J. (1982). Measurements of the total and regional deposition of inhaled particles in the human respiratory tract. Journal of Aerosol Science, 13:549-560.

Finlay, W. H. (2001). The Mechanics of Inhaled Pharmaceutical Aerosols: An Introduction:320.

Foord, N., Black, A., Walsh, M. (1978). Regional deposition of 2.5–7.5 μm diameter inhaled particles in healthy male non-smokers. Journal of Aerosol Science, 9:343-357.

Golshahi, L. and Finlay, W. H. (2012). An Idealized Child Throat that Mimics Average Pediatric Oropharyngeal Deposition. Aerosol Science and Technology, 46:i-iv.

Golshahi, L., Noga, M. L., Finlay, W. H. (2012). Deposition of inhaled micrometer-sized particles in oropharyngeal airway replicas of children at constant flow rates. Journal of Aerosol Science, 49:21-31.

Golshahi, L., Vehring, R., Noga, M. L., Finlay, W. H. (2013). In vitro deposition of micrometer-sized particles in the extrathoracic airways of children during tidal oral breathing. Journal of Aerosol Science, 57:14-21.

Grgic, B., Finlay, W. H., Burnell, P. K. P., Heenan, A. F. (2004a). In vitro intersubject and intrasubject deposition measurements in realistic mouth–throat geometries. Journal of Aerosol Science, 35:1025-1040.

Grgic, B., Finlay, W. H., Heenan, A. F. (2004b). Regional aerosol deposition and flow measurements in an idealized mouth and throat. Journal of Aerosol Science, 35:21-32.

Hall, J. E. (2011). Guyton and Hall Textbook of Medical Physiology. Saunders/Elsevier, Philadelphia, PA.

Hashish, A. H. (1992). Selective deposition of pulsed aerosols in the human lung. Journal of Aerosol Science, 23:473-476.

Hashish, A. H., Bailey, a. G., Williams, T. J. (1994). Modelling the effect of charge on selective deposition of particles in a diseased lung using aerosol boli. Physics in Medicine and Biology, 39:2247-2262.

Hinds, W. C. (1999). Aerosol Technology: Properties, Behavior, and Measurement of Airborne Particles. Wiley-Interscience, New York.

Hoe, S., Traini, D., Chan, H. K., Young, P. M. (2009). Measuring charge and mass distributions in dry powder inhalers using the electrical Next Generation Impactor (eNGI). European Journal of Pharmaceutical Sciences, 38:88-94.

Kwok, P. C. L. and Chan, H. K. (2009). Electrostatics of pharmaceutical inhalation aerosols. The Journal of Pharmacy and Pharmacology, 61:1587-1599.

Kwok, P. C. L., Glover, W., Chan, H. K. (2005). Electrostatic charge characteristics of aerosols produced from metered dose inhalers. Journal of Pharmaceutical Sciences, 94:2789-2799.

Majid, H., Madl, P., Hofmann, W., Alam, K. (2012). Implementation of Charged Particles Deposition in Stochastic Lung Model and Calculation of Enhanced Deposition. Aerosol Science and Technology, 46:547-554.

Melandri, C., Tarroni, G., Prodi, V., De Zaiacomo, T., Formignani, M., Lombardi, C. C. (1983). Deposition of charged particles in the human airways. Journal of Aerosol Science, 14:657-669.

Mitchell, J. P. and Nagel, M. (1997). In Vitro Performance Testing of Three Small Volume-Holding Chambers under Conditions That Correspond with Use by Infants and Small Children. Journal of Aerosol Medicine, 10:341-349.

Moore, A. D. (1973). Electrostatics and Its Applications. Wiley, New York.

Rayleigh, L. (1879). On the instability of jets. Proceedings of London Mathematical Society, 10:3-14.

Reischl, G., John, W., Devor, W. (1977). Uniform electrical charging of monodisperse aerosols. Journal of Aerosol Science, 8:55-65.

Saini, D., Gunamgari, J., Zulaloglu, C., Sims, R. A., Mazumder, M. K. (2004). Effect of electrostatic charge and size distributions on respirable aerosol deposition in lung model. IEEE Industry Applications Conference. 39th IAS Annual Meeting., 2:948-952.

Saini, D., Yurteri, C. U., Grable, N., Sims, R. A., Mazumder, M. K. (2002). Drug delivery studies on electrostatically charged dry powder inhaler aerosols using a glass bead lung model, in EEE Industry Applications Conference. 37th IAS Annual Meeting, 2451-2453.

Schueepp, K. G., Devadason, S. G., Roller, C., Minocchieri, S., Moeller, A., Hamacher, J., Wildhaber, J. H. (2009). Aerosol delivery of nebulised budesonide in young children with asthma. Respiratory Medicine, 103:1738-1745.

Stahlhofen, W., Gebhart, J., Heyder, J., Scheuch, G. (1983). New regional deposition data of the human respiratory tract. Journal of Aerosol Science, 14:186-188.

Stapleton, K. W., Guentsch, E., Hoskinson, M. K., Finlay, W. H. (2000). On the suitability of k–ε turbulence modeling for aerosol deposition in the mouth and throat: a comparison with experiment. Journal of Aerosol Science, 31:739-749.

Zhou, Y., Sun, J., Cheng, Y. S. (2011). Comparison of deposition in the USP and physical mouth-throat models with solid and liquid particles. Journal of Aerosol Medicine and Pulmonary Drug Delivery, 24:277-284.

Chapter 5. Effect of electrostatic charge on deposition of uniformly charged monodisperse particles in the nasal-extrathoracic airways of an infant

This chapter has been published as:

Azhdarzadeh, M., Olfert, J. S., Vehring, R., Finlay, W. H. (2014). Effect of electrostatic charge on deposition of uniformly charged monodisperse particles in the nasal-extrathoracic airways of an infant. Journal of Aerosol Medicine and Pulmonary Drug Delivery, 27:1-5.

5.1. Introduction

The study of particle deposition in extrathoracic airways is important due to its effect in controlling the amount of particles that can pass through this airway and reach the lungs (Borgström et al. 2006). Due to obligate nasal breathing in infants, (Amirav and Newhouse 2012; Sasaki et al. 1977) nasal extrathoracic airway deposition is normally more relevant to infants than oral extrathoracic airway deposition. There is little data on the deposition of aerosols in the airways of infants due to the strict ethical requirements for *in vivo* experiments on infants and due to the difficulty of achieving cooperation from infants. Deposition studies which have been completed considered uncharged particles (Janssens et al. 2001; Janssens et al. 2004; Javaheri et al. 2013; Laube et al. 2010; Mitchell and Nagel 1997; Storey-Bishoff et al. 2008a). Janssens et al. (2001) developed a model of the upper airways of an infant, the Sophia Anatomical Infant Nose Throat (SAINT) model, based on 3D computed tomography scans of the neck and head of a 9-month-old infant. Janssens et al. (2004) used the SAINT model for studying the deposition of particles emitted from four pressurized Metered Dose Inhaler spacer combinations. Javaheri et al. (2013) developed an idealized infant model whose characteristics

are explained below in the methods section. Mitchell and Nagel (1997) have conducted *in vitro* performance tests of three types of small volume-holding chambers designed to be used by children and infants. Laube et al. (2010) studied the deposition of particles generated by a pneumatic nebulizer in the SAINT airway model. Storey-Bishoff et al. (2008a) conducted *in vitro* deposition tests using replicas of the nasal geometries of eleven 3-18 month old infants. While a few studies have examined the effect of charge on the oral particle deposition in adults (Ali et al. 2008; Azhdarzadeh et al. 2014a) and children (Azhdarzadeh et al. 2014b), to the authors' knowledge there are no such studies for infants.

Studies on the charge of the particles emitted from commercial inhaled drug delivery devices (Hoe et al. 2009; Kwok et al. 2005) revealed high levels of charges on the particles. Kwok et al. (2005) observed more than 40,000 e per particle on particles with a diameter of 6 μm. These high charge levels emphasize the importance of studying the effect of electrostatic charge on deposition of inhaled particles.

An electrical charge on a particle can cause electrostatic induction in the tissue of the airway wall which gives rise to an attraction force between the wall and the charged particle. Consequently, this force will result in an increase in deposition of charged particles in the airway (Majid et al. 2012). The objective of the current *in vitro* work was to study the effect of induced electrostatic charge on deposition of particles in the nasal extrathoracic airway of an infant, and to develop an empirical equation for predicting deposition in this airway. The other charge related effect is the space charge effect which is due to repulsive force between particles carrying a unipolar charge (Finlay 2001). This effect is only important for aerosols with

a high concentration of particles and is not important in the present experiments due to the low particle concentration range, i.e., less than 10^3 cm^{-3}.

5.2. Materials and Methods

An idealized geometry developed by Javaheri et al. (2013) which mimics the infant nasal extrathoracic airways, was used for our *in vitro* deposition measurements. This replica is based on nasal computed tomography images of 10 infants aged 3-18 months (Storey-Bishoff et al. 2008a) and extends from the anterior nares to the trachea. The replica also includes the face, which is necessary to mimic actual conditions of drug delivery through a mask to the respiratory tract of infants. The idealized geometry was validated (Javaheri et al. 2013) by conducting deposition tests and comparing the results with those reported by Storey-Bishoff et al. (2008b) for 10 realistic *in vitro* replicas. This physical airway model, along with the deposition measurement setup described in Azhdarzadeh et al. (2014a) was utilized for studying deposition of particles in the airway. Figure 5.1 shows a schematic of the setup with its main components. An atomizer was designed and built to produce monodisperse droplets based on controlled Plateau-Rayleigh jet break up, (Berglund and Liu 1973; Rayleigh 1879) which essentially involves applying a disturbance with constant frequency to the jet emerging from the orifice. Optimum frequencies and amplitudes of the disturbance were obtained by monitoring the generated particles with an Aerodynamic Particle Sizer (APS) (3321, TSI, Minneapolis, USA) while sweeping the frequency and amplitude ranges.

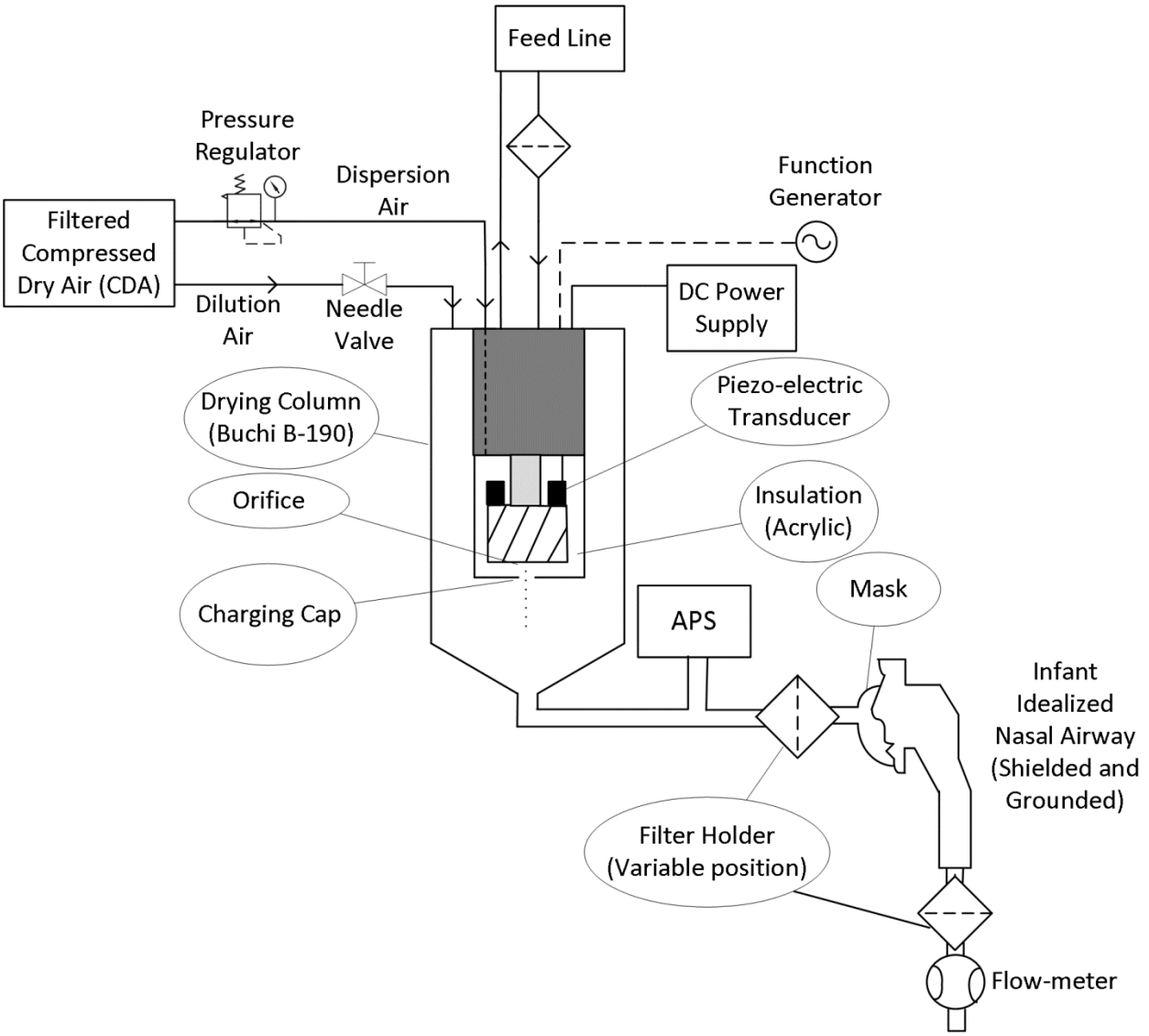

Figure 5.1. Schematic of deposition measurement setup to study effect of electrostatic charge (along with aerodynamic diameter and flow rate) on particle deposition in an infant nasal-extrathoracic airway, after (Azhdarzadeh et al. 2014a)

Charging of the generated droplets was achieved via jet induction (Moore 1973; Reischl et al. 1977) using a charging cap which was essentially a conductive plate having a constant electrical potential difference relative to the orifice. The electrical potential difference between the orifice and conductive plate establishes a constant electrical field in the gap between the orifice

and the plate, causing the droplets to carry a net charge after their disintegration. The residence time of particles in the nasal extrathoracic air way of infant is about 46 and 92 ms for volume flow rates of 15 and 7.5 L/min respectively. Due to the very short residence time of particles in the airway, compared to the time required for the humidity to alter the charge levels of particles which is in the orders of minutes (Elajnaf et al. 2007), the effect of humidity on the charge of particles was considered to be negligible. The assumption of negligible effect of humidity on particle charge in the human airways was also confirmed in experiments conducted by Melandri et al. (1983). By passing a turbulent air stream through the charging cap, coalescence is reduced and monodispersity is preserved (Liu and Frohn 1988). Droplets issuing from the jet are made from a solution of Di(2-ethylhexyl) sebacate (DEHS) (269920010, 97%, ACROS ORGANICs, New Jersey, USA), and were subsequently dried in a commercial spray dryer (Buchi B-190, Buchi Labortechnik AG, Flawil, Switzerland) to produce the particles. The diameter of the particles depends on the concentration of the feed solution and initial droplet size. To obtain sufficient conductivity needed for charging the droplets, an aqueous solution of sodium chloride, whose concentration depended on the required charge level, was added to the DEHS solution. The charge of the particles was measured using a Faraday cup immediately after the charging cap. The electric charge per particle was calculated under the assumption of uniform charging of particles (Reischl et al. 1977). The range of charge per particle studied in the present experiments was $0 - 10{,}000$ e. This range is much below the limits imposed by Rayleigh and electron emission limits (Hinds 1999), which are 2×10^5 and 2×10^6 e/particle respectively for the smallest particle in the present experiments, i.e. $d_{\mathrm{a}} = 3.55\ \mu\mathrm{m}$. Further details in design, building, and validation of the setup are given in Azhdarzadeh et al. (2014a).

The aerosol was delivered to the nasal extrathoracic infant airway through a silicone mask (041F0711, size1, PARI, Midlothian, USA) which was sealed on the face by silicone sealant (732 Multi-Purpose Sealant, DOW, Midland, USA). Particles were collected on a non-hygroscopic filter membrane made from borosilicate glass microfibers (47 mm, TX40HI20WW, Pall, USA) which was mounted in a filter holder (47 mm, XX4404700, Millipore, Billerica, USA) at the inlet of the mask and also after the model, allowing measurement of collected particle mass by an ultra-microbalance (UMX2, Mettler Toledo, Columbus, USA). This allowed calculation of the fraction of mass depositing in the airway replica. Given the common size of particles for commercial inhaled aerosols and also experimental limitations for smaller particles, the experiments were performed for particles with aerodynamic diameters of 3-6 μm. Details of the particle collection and mass measurements were reported previously by Azhdarzadeh et al. (2014a).

5.3. Results and Discussion

Figures 5.2, 5.3 and 5.4 show the deposition enhancement for particles in the nasal extrathoracic airway due to induced electrostatic effects. The experiments were conducted using particles with geometric standard deviation below 1.1 as measured by the APS. Uncertainty analysis of the present setup for deposition measurement was performed previously in a child oral airway model (Azhdarzadeh et al. 2014b) using three groups of points, with each group including three deposition measurements for the child model. The average and maximum absolute uncertainties for our deposition measurements, $\tilde{\eta}(\%)$, were noted as $\tilde{\eta} \pm 4$ and $\tilde{\eta} \pm 8$, respectively. Since the same experimental apparatus was used here, these values

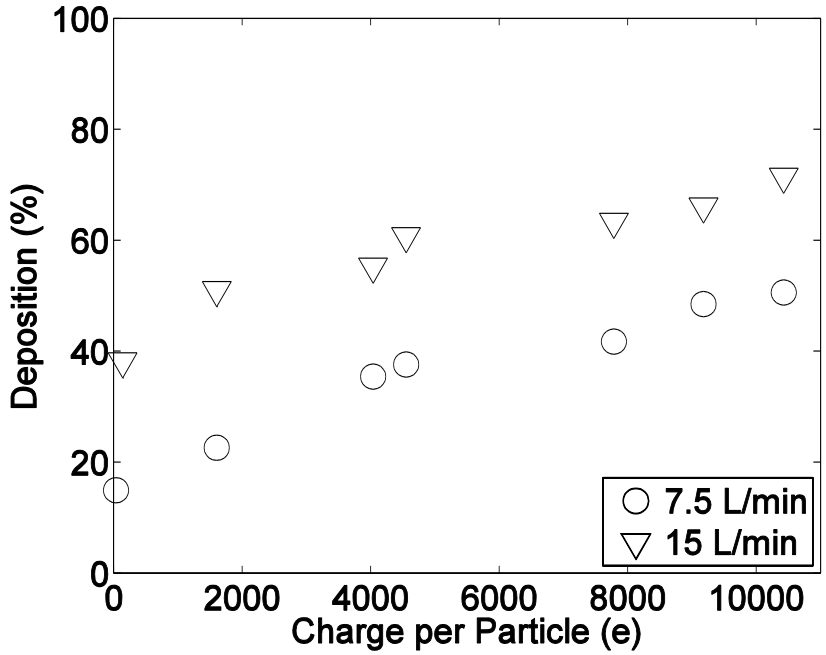

Figure 5.2. Aerosol deposition in infant nasal extrathoracic airways vs. particle charge level for particles with aerodynamic diameter of $d_{\mathrm{a}} = 3.55\ \mu\mathrm{m}$

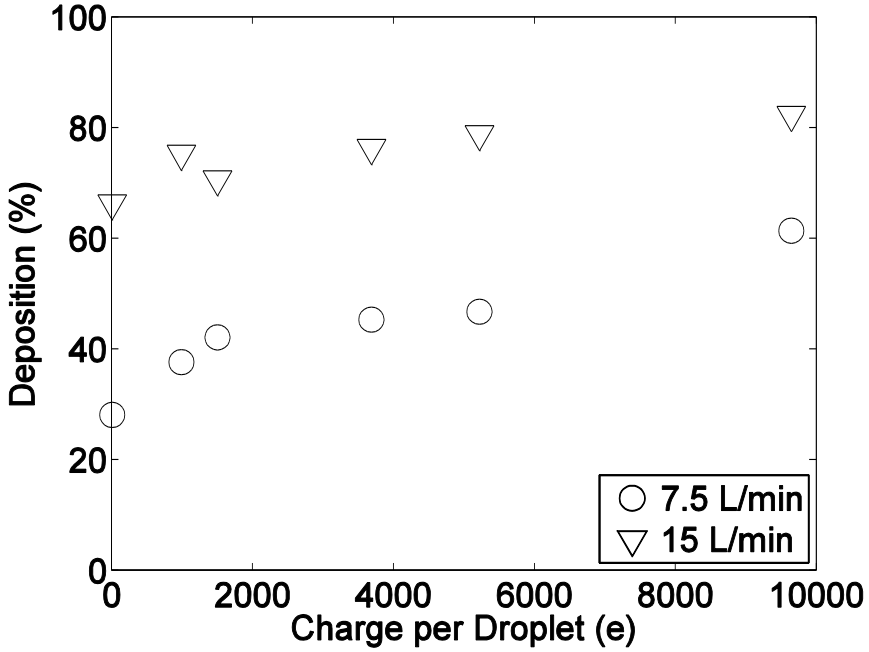

Figure 5.3. Aerosol deposition in infant nasal extrathoracic airways vs. particle charge level for particles with aerodynamic diameter of $d_{\mathrm{a}} = 4.71\ \mu\mathrm{m}$

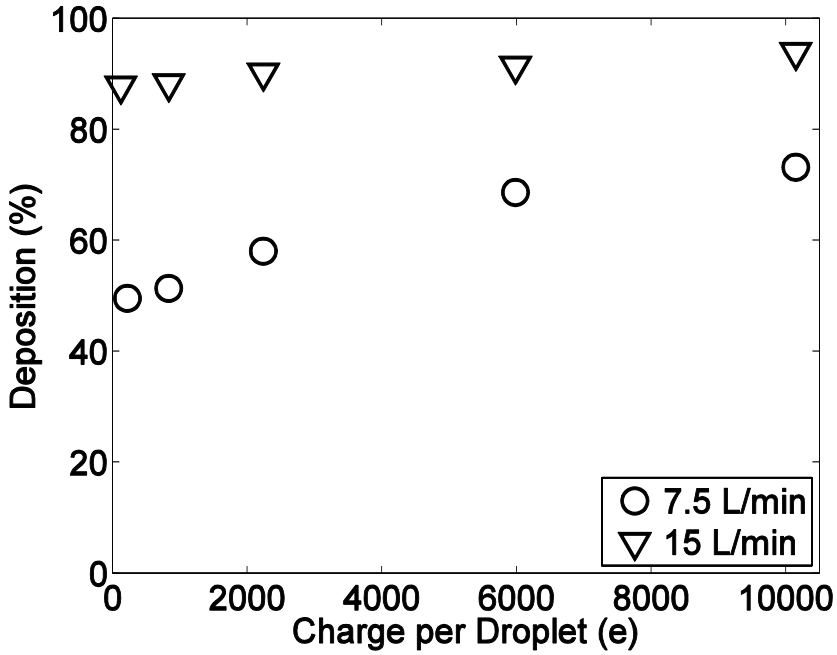

Figure 5.4. Aerosol deposition in infant nasal extrathoracic airways vs. particle charge level for particles with aerodynamic diameter of $d_{\mathrm{a}} = 6.08\ \mu\mathrm{m}$

are expected to be unchanged. Charge measurement absolute uncertainty, evaluated by measuring the charge at the beginning and the end of twelve experiments, was 140 e per particle. The reported uncertainty is the result of temporal variations over the experimental data acquisition time, which is about 1 hour for each test, and other measurement uncertainties.

As can be seen in Figs. 5.2, 5.3 and 5.4, the deposition of larger particles is enhanced to a lesser extent than that of smaller particles by the presence of electrostatic charge. For smaller particles, the deposition enhancement due to the electrostatic effect is very large. In the present experiments, impaction and electrostatic induction are the relevant deposition mechanisms. The importance of impaction can be assessed using the Stokes number which

increases with the square of the particle diameter and linearly with flow velocity. Hence, for the larger particles impaction becomes the dominant deposition mechanism, particularly at higher flow rates.

Comparing the results for the present nasal inhalation infant model with previously published data for adult (Azhdarzadeh et al. 2014a) and child oral inhalation models (Azhdarzadeh et al. 2014b) some observations can be reported. Comparing the fraction of particles deposited in the presence of electrostatic charge, it is observed that deposition is highest for the infant nasal model and lowest for the adult oral model, a result already reported for neutral particles by many previous researchers (Golshahi et al. 2012; Golshahi et al. 2011). Higher deposition rates for the nasal airway are mainly due to smaller diameter of airway and its sharper bends. A more interesting comparison is the relative increase in deposition due to electrostatic effects in the present infant model compared to child and adult oral inhalation models. This comparison shows similar deposition enhancement for all three adult, child and infant models, emphasizing the importance of electrostatic effects for inhaled therapeutic aerosols regardless of the age of subject.

It is useful to report the present data in a dimensionless equation that predicts deposition. For this purpose, the Reynolds number, $Re = 4\rho_{\mathrm{g}}Q/\pi\mu D_{\mathrm{h}}$, Stokes number, $Stk = 2C_{\mathrm{c}}\rho^{*}Qd_{\mathrm{a}}^{2}/9\pi\mu D_{\mathrm{h}}^{3}$ and induced charge number, $Inc = \sqrt{\rho_{\mathrm{p}}/\rho^{*}}\, e^{2}n^{2}/192\pi\mu d_{a}\varepsilon_{0}Q\acute{x}^{2}$, which are the relevant dimensionless numbers governing the flow in the airway, the inertia forces on

the particles, and electrostatic forces on the particles, were combined in a deposition parameter $\tilde{x}$ as follows,

$$\tilde{x} = a_1(Re^{a_2}Stk^{a_3} + a_4 Inc^{a_5})(1 + a_6\, Inc^{a_7}) \quad (5.1)$$

Here ρ_{g}, Q, μ and D_{h} are the density of inhaled gas, volume flow rate of inhaled gas, viscosity of inhaled gas and hydraulic diameter of the airway, $4\bar{V}/A_s$, where $\bar{V}$ is the volume of the airway and A_{s} is the surface area of the airway. The hydraulic diameter of the present infant replica is 4.8 mm. C_{c} is Cunningham slip correction factor which is used to compensate for non-continuum effects in very fine particles (Finlay 2001). This effect is mainly important for particles with aerodynamic diameter less than $1\mu\mathrm{m}$ (Finlay 2001). ρ^* is the reference density of 1000 kg/m^3 and d_{a} is the aerodynamic diameter of the particle which is defined as the diameter of a spherical particle with reference density of 1000 kg/m^3 and the same settling velocity (Hinds 1999). $\rho_{\mathrm{p}} = \frac{m_{\mathrm{p}}}{\bar{V}_{\mathrm{t}}}$ is the density of the particle which includes voids in the particle. Here m_{p} and V_{t} are particle mass and total volume of the particle including cavities (Brady and Weil 2007). e, n and ε_0 and are charge of elementary electron, number of elementary charges on particle and permittivity of free space. $\acute{x} = \frac{x}{D_{\mathrm{h}}}$ is the distance of the particle from the wall which is nondimensionalized by D_{h} . A constant representative value of $\acute{x} = 0.025$ as suggested by Finlay (Finlay 2001) was utilized in the equations. The coefficients and powers of these dimensionless numbers, a_{i}, that appear in the introduced parameters were obtained by curve fitting of the data using the nonlinear least square method. To assign the unknown coefficients, a code based on the "lsqnonlin" command of MATLAB was developed. The resulting empirical relation is as follows:

$$\tilde{\eta} = \left[1 - \frac{1}{1+\tilde{x}}\right] \times 100 \qquad (5.2)$$

where,

$$\tilde{x} = 0.091(Re^{0.756}Stk^{1.922} + 8.582Inc^{0.119})(1 + 203.802\, Inc^{0.531}) \qquad (5.3)$$

The coefficient of determination of the fitting, R^2, and root mean square error for deposition fraction are 0.99 and 2, respectively.

Figure 5.5 shows the developed equation versus the new introduced deposition parameter, along with the experimental data. It is recommended that the empirical equation be used only in the range of parameter variation of the present experiments, i.e., dilute aerosol, aerodynamic diameter between 3-6 μm, flow rate 7.5-15 L/min, and charge per particle of 0–

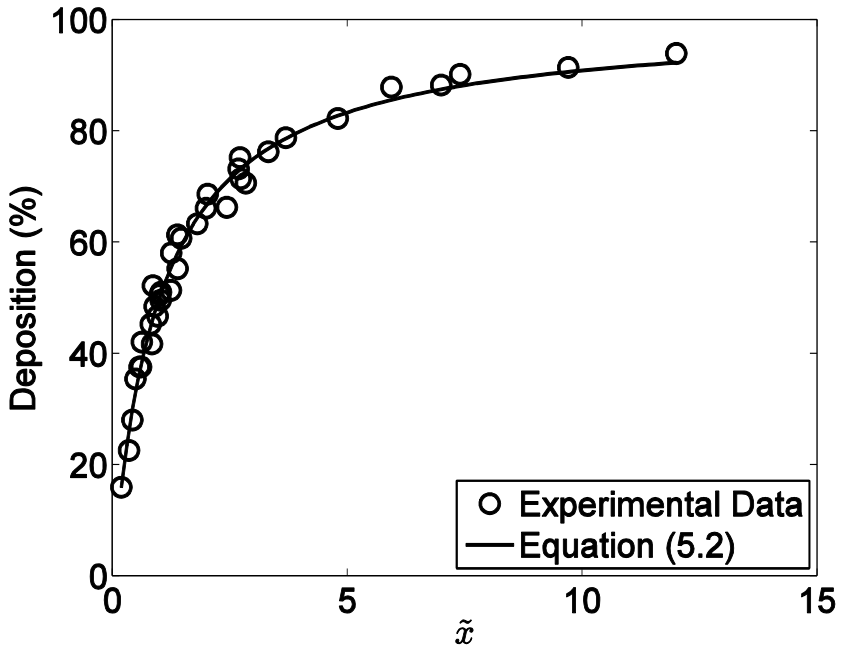

Figure 5.5. Experimental data vs. current suggested relation , Eq. (5.2) for deposition prediction of charged particles in the nasal extrathoracic airway of infant

10,000 e for nasal-extrathoracic airway of 3-18 month old infants. Use of this equation outside of this range may result in decreased accuracy as a result of extrapolation.

5.4. Conclusions

The effect of induced electrostatic charge on deposition of particles in the nasal extrathoracic airway of an infant showed enhancement in deposition as a result of particle charge. The enhancement was higher for smaller particles which is explained by the variation with particle aerodynamic diameter of deposition due to induced charge effects compared with impaction (Finlay 2001), the latter being less important for smaller particles.

Based on the data from the present experiments, a nondimensional empirical relation was developed for predicting average deposition in the nasal extrathoracic airway of an infant for charged aerosol particles.

Bibliography

Ali, M., Reddy, R. N., Mazumder, M. K. (2008). Electrostatic charge effect on respirable aerosol particle deposition in a cadaver based throat cast replica. Journal of Electrostatics, 66:401-406.

Amirav, I. and Newhouse, M. T. (2012). Deposition of small particles in the developing lung. Paediatric Respiratory Reviews, 13:73-78.

Azhdarzadeh, M., Olfert, J. S., Vehring, R., Finlay, W. H. (2014a). Effect of electrostatic charge on oral-extrathoracic deposition for uniformly charged monodisperse aerosols. Journal of Aerosol Science, 68:38-45.

Azhdarzadeh, M., Olfert, J. S., Vehring, R., Finlay, W. H. (2014b). Effect of Induced Charge on Deposition of Uniformly Charged Particles in a Pediatric Oral-Extrathoracic Airway. Aerosol Science and Technology, 48:508-514.

Berglund, R. N. and Liu, B. Y. H. (1973). Generation of monodisperse aerosol standards. Environmental Science & Technology, 7:147-153.

Borgström, L., Olsson, B., Thorsson, L. (2006). Degree of throat deposition can explain the variability in lung deposition of inhaled drugs. Journal of Aerosol Medicine, 19:473-483.

Brady, N. C. and Weil, R. R. (2007). The Nature and Properties of Soils, 14th Edition. Prentice Hall.

Elajnaf, A., Carter, P., Rowley, G. (2007). The effect of relative humidity on electrostatic charge decay of drugs and excipient used in dry powder inhaler formulation. Drug development and industrial pharmacy, 33:967-974.

Finlay, W. H. (2001). The Mechanics of Inhaled Pharmaceutical Aerosols: An Introduction. Academic Press, London.

Golshahi, L., Noga, M. L., Finlay, W. H. (2012). Deposition of inhaled micrometer-sized particles in oropharyngeal airway replicas of children at constant flow rates. Journal of Aerosol Science, 49:21-31.

Golshahi, L., Noga, M. L., Thompson, R. B., Finlay, W. H. (2011). In vitro deposition measurement of inhaled micrometer-sized particles in extrathoracic airways of children and adolescents during nose breathing. Journal of Aerosol Science, 42:474-488.

Hinds, W. C. (1999). Aerosol Technology: Properties, Behavior, and Measurement of Airborne Particles. Wiley-Interscience, New York.

Hoe, S., Traini, D., Chan, H.-K., Young, P. M. (2009). Measuring charge and mass distributions in dry powder inhalers using the electrical Next Generation Impactor (eNGI). European Journal of Pharmaceutical Sciences, 38:88-94.

Janssens, H. M., de Jongste, J. C., Fokkens, W. J., Robben, S. G., Wouters, K., Tiddens, H. A. (2001). The Sophia Anatomical Infant Nose-Throat (Saint) model: a valuable tool to study aerosol deposition in infants. Journal of aerosol medicine, 14:433-441.

Janssens, H. M., Krijgsman, A., Verbraak, T. F. M., Hop, W. C. J., de Jongste, J. C., Tiddens, H. A. W. M. (2004). Determining factors of aerosol deposition for four pMDI-spacer combinations in an infant upper airway model. Journal of aerosol medicine, 17:51-61.

Javaheri, E., Golshahi, L., Finlay, W. H. (2013). An idealized geometry that mimics average infant nasal airway deposition. Journal of Aerosol Science, 55:137-148.

Kwok, P. C. L., Glover, W., Chan, H.-K. (2005). Electrostatic charge characteristics of aerosols produced from metered dose inhalers. Journal of Pharmaceutical Sciences, 94:2789-2799.

Laube, B. L., Sharpless, G., Shermer, C., Nasir, O., Sullivan, V., Powell, K. (2010). Deposition of albuterol aerosol generated by pneumatic nebulizer in the Sophia Anatomical Infant Nose-Throat (SAINT) model. Pharmaceutical research, 27:1722-1729.

Liu, D. Y. and Frohn, A. (1988). Drag coefficients of single droplets moving in an infinite droplet chain on the axis of a tube, 14:217-232.

Majid, H., Madl, P., Hofmann, W., Alam, K. (2012). Implementation of Charged Particles Deposition in Stochastic Lung Model and Calculation of Enhanced Deposition. Aerosol Science and Technology, 46:547-554.

Melandri, C., Tarroni, G., Prodi, V., De Zaiacomo, T., Formignani, M., Lombardi, C. C. (1983). Deposition of charged particles in the human airways. Journal of Aerosol Science, 14:657-669.

Mitchell, J. P. and Nagel, M. (1997). In Vitro Performance Testing of Three Small Volume-Holding Chambers under Conditions That Correspond with Use by Infants and Small Children. Journal of Aerosol Medicine, 10:341-349.

Moore, A. D. (1973). Electrostatics and Its Applications. Wiley, New York.

Rayleigh, L. (1879). On the instability of jets. Proceedings of London Mathematical Society, 10:3-14.

Reischl, G., John, W., Devor, W. (1977). Uniform electrical charging of monodisperse aerosols. Journal of Aerosol Science, 8:55-65.

Sasaki, C. T., Levine, P. A., Laitman, J. T., Crelin, E. S. (1977). Postnatal Descent of the Epiglottis in Man: A Preliminary Report. Archives of Otolaryngology - Head and Neck Surgery, 103:169-171.

Storey-Bishoff, J., Noga, M., Finlay, W. H. (2008a). Deposition of micrometer-sized aerosol particles in infant nasal airway replicas. Journal of Aerosol Science, 39:1055-1065.

Storey-Bishoff, J., Noga, M., Finlay, W. H. (2008b). Deposition of micrometer-sized aerosol particles in infant nasal airway replicas. Journal of Aerosol Science, 39:1055-1065.

Chapter 6. Conclusions

This chapter summarizes the findings in the previous chapters. The reader can refer to the conclusion section of each chapter for more details.

6.1. Summary and Conclusions

Results of the *in vitro* tests demonstrated the substantial effect of electrostatic charge on deposition of particles with aerodynamic diameters of 3-6 μm. Induced electrostatic charge had a similar particle deposition enhancement effect in adult, child and infant models. Deposition enhancement was stronger for smaller particles due to the fact that impaction deposition is less dominant, letting the induced charge effect be seen more clearly.

The following empirical relations for particle deposition were developed by data fitting using least square methods. It is strongly recommended to use the equation with parameter values only in the range of the *in vitro* tests in order to have the highest accuracy.

6.1.1. Adult oral-extrathoracic airway

The following equations were developed based on experimental results with dilute charged aerosols, i.e. with number concentration $< 10^3 \#/\mathrm{cm}^{-3}$. The equations should be used for particle aerodynamic diameters in the range of 3-6 μm, at flow rates of 15-30 L/min, and for a

charge per particle range of 0-25,000 e. The characteristic length used in the equations is $D_{\text{mean}} = 2\sqrt{\bar{V}/\pi L}$.

$$\eta(\%) = \left[1 - \frac{1}{(1 + 11.5\bar{x}^{1.912})}\right] \times 100 \quad (3.6)$$

where,

$$\bar{x} = (0.3956\, Inc^{0.2680} + Re^{0.37} Stk)(1 + 2.4452 Inc^{0.0045}) \quad (3.7)$$

6.1.2. Child-oral extrathoracic airway

The experimental conditions for the following equations were a dilute charged aerosol with number concentration $< 10^3 \#/\text{cm}^{-3}$, particle aerodynamic diameters of 3-6 μm, and flow rates of 10-20 L/min. Particle charge was 0-10,000 e/particle and the airway model was developed based on data for children aged 6-14 years. The equations use different characteristic lengths as follows, $d_{c1} = \sqrt{\frac{\bar{V}}{L}}$ and $d_{c2} = \frac{\bar{V}}{A_s}$.

$$\hat{\eta}_1 = [1 - \frac{1}{1 + 2.45\hat{x}_1}] \times 100 \quad (4.8)$$

$$\hat{x}_1 = Stk^{1.33} Re^{0.58}(1 + 31.09 Inc^{0.20}) \quad (4.9)$$

$$\hat{\eta}_2 = [1 - \frac{1}{1 + 0.000335\hat{x}_2}] \times 100 \quad (4.10)$$

$$\hat{x}_2 = Stk^{1.5} Re^{0.69}(1 + 41.27 Inc^{0.20}) \quad (4.11)$$

6.1.3. Infant nasal-extrathoracic airway

The parameter variation range for the following relation is dilute charged aerosols, i.e. number concentration $< 10^3 \#/\text{cm}^{-3}$, and particle aerodynamic diameters of 3-6 μm at flow rates of

7.5-15 L/min. The charge per particle range of 0-10,000 e was monitored for the 3-18-month-old infant model. Hydraulic diameter of the airway, $D_{\mathrm{h}} 4\bar{V}/A_s$, is used as characteristic length in the following equations.

$$\tilde{\eta} = \left[1 - \frac{1}{1+\tilde{x}}\right] \times 100 \qquad (5.2)$$

where,

$$\tilde{x} = 0.091(Re^{0.756} Stk^{1.922} + 8.582 Inc^{0.119})(1 + 203.802\ Inc^{0.531}) \qquad (5.3)$$

6.2. Future Work

Investigating the effect of nano-sized particle electrostatic charge on deposition in human airways may be a topic for future study. The application for this study would be the deposition of nano-sized particles emitted from engines of road vehicles.

Another topic for future work may be *in vivo* tests regarding the deposition of micron-sized particles in the lung, using radio labelled particles.

Bibliography

Ali, M., Mazumder, M. K., Martonen, T. B. (2009). Measurements of electrodynamic effects on the deposition of MDI and DPI aerosols in a replica cast of human oral – pharyngeal – laryngeal airways. Journal of Aerosol Medicine, 22:35-44.

Ali, M., Reddy, R. N., Mazumder, M. K. (2008). Electrostatic charge effect on respirable aerosol particle deposition in a cadaver based throat cast replica. Journal of Electrostatics, 66:401-406.

Amirav, I. and Newhouse, M. T. (2012). Deposition of small particles in the developing lung. Paediatric Respiratory Reviews, 13:73-78.

Anders, K., Roth, N., Frohn, A. (1992). Operation Characteristics of Vibrating-Orifice Generators: The coherence length. Particle & Particle Systems Characterization, 9:40-43.

Ashgriz, N. and Yarin, A. L. (2011). Handbook of Atomization and Sprays. Springer, New York.

Azhdarzadeh, M., Olfert, J. S., Vehring, R., Finlay, W. H. (2014a). Effect of electrostatic charge on oral-extrathoracic deposition for uniformly charged monodisperse aerosols. Journal of Aerosol Science, 68:38-45.

Azhdarzadeh, M., Olfert, J. S., Vehring, R., Finlay, W. H. (2014b). Effect of Induced Charge on Deposition of Uniformly Charged Particles in a Pediatric Oral-Extrathoracic Airway. Aerosol Science and Technology, 48:508-514.

Bailey, A. G. (1997). The Inhalation and Deposition of Charged Particles Within the Human Lung. Journal of Electrostatics, 42:25-32.

Bailey, A. G., Hashish, A. H., Williams, T. J. (1998). Drug delivery by inhalation of charged particles. Journal of Electrostatics, 44:3-10.

Balachandran, W., Kulon, J., Koolpiruck, D., Dawson, M., Burnel, P. (2003). Bipolar charge measurement of pharmaceutical powders. Powder technology, 135:156-163.

Balachandran, W., Machowski, W., Gaura, E., Hudson, C. (1997). Control of drug aerosol in human airways using electrostatic forces. Journal of Electrostatics, 40-41:579-584.

Becquemin, M., Swift, D., Bouchikhi, A., Roy, M., Teillac, A. (1991). Particle deposition and resistance in the noses of adults and children. European Respiratory Journal, 4:694-702.

Beleca, R., Abbod, M., Balachandran, W., Miller, P. R. (2010). Investigation of electrostatic properties of pharmaceutical powders using phase Doppler anemometry. IEEE Transactions on Industry Applications, 46:1181-1187.

Below, A., Bickmann, D., Breitkreutz, J. (2013). Assessing the performance of two dry powder inhalers in preschool children using an idealized pediatric upper airway model. International Journal of Pharmaceutics, 444:169-174.

Bennett, W. D. and Zeman, K. L. (2004). Effect of body size on breathing pattern and fine-particle deposition in children. Journal of applied physiology (Bethesda, Md. : 1985), 97:821-826.

Berglund, R. N. and Liu, B. Y. H. (1973). Generation of monodisperse aerosol standards. Environmental Science & Technology, 7:147-153.

Bickmann, D., Wachtel, H., Kroger, R., Langguth, P. (2008). Examining Inhler Performance Using a Child's Throat Model, in Respiratory Drug Delivery, 565-570.

Borgström, L. (1999). In vitro, ex vivo, in vivo veritas. Allergy, 54:88-92.

Borgström, L., Olsson, B., Thorsson, L. (2006a). Degree of throat deposition can explain the variability in lung deposition of inhaled drugs. Journal of Aerosol Medicine, 19:473-483.

Borgström, L., Olsson, B., Thorsson, L. (2006b). Degree of throat deposition can explain the variability in lung deposition of inhaled drugs. Journal of Aerosol Medicine, 19:473-483.

Bowes, S. M. and Swift, D. L. (1989). Deposition of inhaled particles in the oral airway during oronasal breathing. Aerosol Science and Technology, 11:157-167.

Brady, N. C. and Weil, R. R. (2007). The Nature and Properties of Soils, 14th Edition. Prentice Hall.

Brancatisano, T., Collett, P. W., Engel, L. A. (1983). Respiratory movements of the vocal cords. Journal of Applied Physiology, 54:1269-1276.

Byron, P. R., Peart, J., Staniforth, J. N. (1997). Aerosol Electrostatics I: Properties of Fine Powders Before and After Aerosolization by Dry Powder Inhalers. Pharmaceutical Research, 14:698-705.

Cass, L. M. R., Brown, J., Pickford, M., Fayinka, S., Newman, S. P., Johansson, C. J., Bye, A. (1999). Pharmacoscintigraphic evaluation of lung deposition of inhaled zanamivir in healthy volunteers. Clinical Pharmacokinetics, 36:21-31.

Castle, G. S. P. (1997). Contact charging between insulators. Journal of Electrostatics, 40–41:13-20.

Chan, T. L. and Lippmann, M. (1980). Experimental measurements and empirical modelling of the regional deposition of inhaled particles in humans. American Industrial Hygiene Association Journal, 41:399-409.

Chan, T. L., Lippmann, M., Cohen, V. R., Schlesinger, R. B. (1978). Effect of electrostatic charges on particle deposition in a hollow cast of the human larynx-tracheobronchial tree. J. Aerosol Sci., 9:463-468.

Chang, K. N., Chen, Y. K., Huang, S. H., Chen, C. W., Lai, C. Y., Chen, C. C. (2012). Penetration of charged particles through metallic tubes. Journal of Aerosol Science, 48:10-17.

Cloupeau, M. and Prunet-Foch, B. (1994). Electrohydrodynamic spraying functioning modes: a critical review. Journal of Aerosol Science, 25:1021-1036.

DeHaan, W. H. and Finlay, W. H. (2001). In vitro monodisperse aerosol deposition in a mouth and throat with six different inhalation devices. Journal of Aerosol Medicine, 14:361-367.

DeHaan, W. H. and Finlay, W. H. (2004). Predicting extrathoracic deposition from dry powder inhalers. Journal of Aerosol Science, 35:309-331.

Elajnaf, A., Carter, P., Rowley, G. (2007a). The effect of relative humidity on electrostatic charge decay of drugs and excipient used in dry powder inhaler formulation. Drug development and industrial pharmacy, 33:967-974.

Elajnaf, A., Carter, P., Rowley, G. (2007b). The effect of relative humidity on electrostatic charge decay of drugs and excipient used in dry powder inhaler formulation. Drug development and industrial pharmacy, 33:967-974.

Emmett, P. C., Aitken, R. J., Hannan, W. J. (1982). Measurements of the total and regional deposition of inhaled particles in the human respiratory tract. Journal of Aerosol Science, 13:549-560.

Finlay, W. H. (2001a). The Mechanics of Inhaled Pharmaceutical Aerosols: An Introduction. Academic Press, London.

Finlay, W. H. (2001b). The Mechanics of Inhaled Pharmaceutical Aerosols: An Introduction. Academic Press, London.

Finlay, W. H. (2001c). The Mechanics of Inhaled Pharmaceutical Aerosols: An Introduction:320.

Finlay, W. H. and Martin, A. R. (2008). Recent advances in predictive understanding of respiratory tract deposition. Journal of aerosol medicine and pulmonary drug delivery, 21:189-206.

Foord, N., Black, A., Walsh, M. (1978). Regional deposition of 2.5–7.5 µm diameter inhaled particles in healthy male non-smokers. Journal of Aerosol Science, 9:343-357.

Frohn, A. and Roth, N. (2000). Dynamics of droplets. Springer.

Golshahi, L. and Finlay, W. H. (2012). An Idealized Child Throat that Mimics Average Pediatric Oropharyngeal Deposition. Aerosol Science and Technology, 46:i-iv.

Golshahi, L., Noga, M. L., Finlay, W. H. (2012). Deposition of inhaled micrometer-sized particles in oropharyngeal airway replicas of children at constant flow rates. Journal of Aerosol Science, 49:21-31.

Golshahi, L., Noga, M. L., Thompson, R. B., Finlay, W. H. (2011). In vitro deposition measurement of inhaled micrometer-sized particles in extrathoracic airways of children and adolescents during nose breathing. Journal of Aerosol Science, 42:474-488.

Golshahi, L., Vehring, R., Noga, M. L., Finlay, W. H. (2013). In vitro deposition of micrometer-sized particles in the extrathoracic airways of children during tidal oral breathing. Journal of Aerosol Science, 57:14-21.

Grgic, B., Finlay, W. H., Burnell, P. K. P., Heenan, A. F. (2004a). In vitro intersubject and intrasubject deposition measurements in realistic mouth–throat geometries. Journal of Aerosol Science, 35:1025-1040.

Grgic, B., Finlay, W. H., Heenan, A. F. (2004b). Regional aerosol deposition and flow measurements in an idealized mouth and throat. Journal of Aerosol Science, 35:21-32.

Hall, J. E. (2011). Guyton and Hall Textbook of Medical Physiology. Saunders/Elsevier, Philadelphia, PA.

Hashish, A. H. (1992). Selective deposition of pulsed aerosols in the human lung. Journal of Aerosol Science, 23:473-476.

Hashish, A. H., Bailey, a. G., Williams, T. J. (1994). Modelling the effect of charge on selective deposition of particles in a diseased lung using aerosol boli. Physics in Medicine and Biology, 39:2247-2262.

Heenan, A. F., Finlay, W. H., Grgic, B., Pollard, A., Burnell, P. K. P. (2004). An investigation of the relationship between the flow field and regional deposition in realistic extra-thoracic airways. Journal of Aerosol Science, 35:1013-1023.

Hinds, W. C. (1999). Aerosol Technology: Properties, Behavior, and Measurement of Airborne Particles. Wiley-Interscience, New York.

Hoe, S., Traini, D., Chan, H.-K., Young, P. M. (2009a). Measuring charge and mass distributions in dry powder inhalers using the electrical Next Generation Impactor (eNGI). European Journal of Pharmaceutical Sciences, 38:88-94.

Hoe, S., Traini, D., Chan, H. K., Young, P. M. (2009b). Measuring charge and mass distributions in dry powder inhalers using the electrical Next Generation Impactor (eNGI). European Journal of Pharmaceutical Sciences, 38:88-94.

Janssens, H. M., de Jongste, J. C., Fokkens, W. J., Robben, S. G., Wouters, K., Tiddens, H. A. (2001a). The Sophia Anatomical Infant Nose-Throat (Saint) model: a valuable tool to study aerosol deposition in infants. Journal of aerosol medicine, 14:433-441.

Janssens, H. M., de Jongste, J. C., Fokkens, W. J., Robben, S. G., Wouters, K., Tiddens, H. A. (2001b). The Sophia Anatomical Infant Nose-Throat (Saint) model: a valuable tool to study aerosol deposition in infants. Journal of aerosol medicine, 14:433-441.

Janssens, H. M., Krijgsman, A., Verbraak, T. F. M., Hop, W. C. J., de Jongste, J. C., Tiddens, H. A. W. M. (2004). Determining factors of aerosol deposition for four pMDI-spacer combinations in an infant upper airway model. Journal of aerosol medicine, 17:51-61.

Javaheri, E., Golshahi, L., Finlay, W. H. (2013). An idealized geometry that mimics average infant nasal airway deposition. Journal of Aerosol Science, 55:137-148.

Kulkarni, P., Baron, P. A., Willeke, K. (2011). Aerosol Measurement: Principles, Techniques, and Applications, . John Wiley & Sons. Inc.

Kulon, J. and Balachandran, W. (2001). The measurement of bipolar charge on aerosols. Journal of Electrostatics, 51:552-557.

Kulon, J., Malyan, B. E., Balachandran, W. (2003). Simultaneous measurement of particle size and electrostatic charge distribution in DC electric field using phase Doppler anemometry. IEEE Transactions on Industry Applications, 39:1522-1528.

Kwetkus, B. A. (1998). Particle triboelectrification and its use in the electrostatic separation process. Particulate Science and Technology, 16:55-68.

Kwok, P. C. L. and Chan, H. K. (2009). Electrostatics of pharmaceutical inhalation aerosols. The Journal of Pharmacy and Pharmacology, 61:1587-1599.

Kwok, P. C. L., Glover, W., Chan, H.-K. (2005a). Electrostatic charge characteristics of aerosols produced from metered dose inhalers. Journal of Pharmaceutical Sciences, 94:2789-2799.

Kwok, P. C. L., Glover, W., Chan, H.-K. (2005b). Electrostatic charge characteristics of aerosols produced from metered dose inhalers. Journal of Pharmaceutical Sciences, 94:2789-2799.

Kwok, P. C. L., Glover, W., Chan, H. K. (2005c). Electrostatic charge characteristics of aerosols produced from metered dose inhalers. Journal of Pharmaceutical Sciences, 94:2789-2799.

Kwok, P. C. L., Trietsch, S. J., Kumon, M., Chan, H.-K. (2010). Electrostatic charge characteristics of jet nebulized aerosols. Journal of aerosol medicine and pulmonary drug delivery, 23:149-159.

Laube, B. L., Sharpless, G., Shermer, C., Nasir, O., Sullivan, V., Powell, K. (2010a). Deposition of albuterol aerosol generated by pneumatic nebulizer in the Sophia Anatomical Infant Nose-Throat (SAINT) model. Pharmaceutical research, 27:1722-1729.

Laube, B. L., Sharpless, G., Shermer, C., Nasir, O., Sullivan, V., Powell, K. (2010b). Deposition of albuterol aerosol generated by pneumatic nebulizer in the Sophia Anatomical Infant Nose-Throat (SAINT) model. Pharmaceutical research, 27:1722-1729.

Lin, H. B., Eversole, J. D., Campillo, A. J. (1990). Vibrating orifice droplet generator for precision optical studies. Review of Scientific Instruments, 61:1018-1018.

Liu, D. Y. and Frohn, A. (1988a). Drag coefficients of single droplets moving in an infinite droplet chain on the axis of a tube, 14:217-232.

Liu, D. Y. and Frohn, A. (1988b). Drag coefficients of single droplets moving in an infinite droplet chain on the axis of a tube, 14:217-232.

M. Cloupeau and Prunet-Foch, B. (1989). Electrostatic spraying of liquids in cone-jet mode. Journal of Electrostatics, 22:135-159.

Majid, H., Madl, P., Hofmann, W., Alam, K. (2012a). Implementation of Charged Particles Deposition in Stochastic Lung Model and Calculation of Enhanced Deposition. Aerosol Science and Technology, 46:547-554.

Majid, H., Madl, P., Hofmann, W., Alam, K. (2012b). Implementation of Charged Particles Deposition in Stochastic Lung Model and Calculation of Enhanced Deposition. Aerosol Science and Technology, 46:547-554.

Masters, K. (1991). Spray drying handbook:725.

May, K. R. (1949). An Improved Spinning Top Homogeneous Spray Apparatus. Journal of Applied Physics, 20:932.

McCarthy, M. J. and Molloy, N. A. (1974). Review of stability of liquid jets and the influence of nozzle design. The Chemical Engineering Journal, 7:1-20.

Melandri, C., Tarroni, G., Prodi, V., De Zaiacomo, T., Formignani, M., Lombardi, C. C. (1983a). Deposition of charged particles in the human airways. Journal of Aerosol Science, 14:657-669.

Melandri, C., Tarroni, G., Prodi, V., De Zaiacomo, T., Formignani, M., Lombardi, C. C. (1983b). Deposition of charged particles in the human airways. Journal of Aerosol Science, 14:657-669.

Melandri, C., Tarroni, G., Prodi, V., Zaiacomo, T. D., Formignani, M., Lombardi, C. C. (1983c). Deposition of charged particles in the human airways. Journal of Aerosol Science, 14:657-669.

Mitchell, J. P. (1984). The production of aerosols from aqueous solutions using the spinning top generator. Journal of aerosol Science, 15:35-45.

Mitchell, J. P. and Nagel, M. (1997a). In Vitro Performance Testing of Three Small Volume-Holding Chambers under Conditions That Correspond with Use by Infants and Small Children. Journal of Aerosol Medicine, 10:341-349.

Mitchell, J. P. and Nagel, M. (1997b). In Vitro Performance Testing of Three Small Volume-Holding Chambers under Conditions That Correspond with Use by Infants and Small Children. Journal of Aerosol Medicine, 10:341-349.

Moore, A. D. (1973). Electrostatics and Its Applications. Wiley, New York.

O'Leary, M., Balachadran, W., Rogueda, P., Chambers, F. (2008). The bipolar nature of charge resident on supposedly unipolar aerosols, in Journal of Physics: Conference Series, IOP Publishing, 012022.

O'Leary, M., Blachandran, W., Chambers, F. (2008). Electrical mobility profiling used to illustrate the bipolar nature of pharmaceutical aerosol charge. Respiratory Drug Delivery.

Ohnesorge, W. v. (1936). Formation of drops by nozzles and the breakup of liquid jets. Z. Angew. Math. Mech, 16:355-358.

Orme, M. and Muntz, E. P. (1990). The manipulation of capillary stream breakup using amplitude-modulated disturbances: A pictorial and quantitative representation. Physics of Fluids A: Fluid Dynamics, 2:1124.

Paschen, F. (1889). Ueber die zum Funkenübergang in Luft, Wasserstoff und Kohlensäure bei verschiedenen Drucken erforderliche Potentialdifferenz (On the potential difference required for spark initiation in air, hydrogen, and carbon dioxide at different pressures). Annalen der Physik, 273:69-75.

Plateau, J. A. F. (1873). Statique expérimentale et théorique des liquides soumis aux seules forces moléculaires. Gauthier-Villars.

Pradip, Nandiyanto, A. B. D., Okuyama, K. (2011). Progress in developing spray-drying methods for the production of controlled morphology particles: From the nanometer to submicrometer size ranges. Advanced Powder Technology, 22:1-19.

Rayleigh, L. (1879). On the instability of jets. Proceedings of London Mathematical Society, 10:3-14.

Reischl, G., John, W., Devor, W. (1977). Uniform electrical charging of monodisperse aerosols. Journal of Aerosol Science, 8:55-65.

Rosell-Llompart, J. and Mora, J. F. d. l. (1994). Generation of monodisperse droplets 0.3 to 4 μm in diameter from electrified cone-jets of highly conducting and viscous liquids. Journal of Aerosol Science, 25:1093-1119.

Saini, D., Biris, a. S., Srirama, P. K., Mazumder, M. K. (2007). Particle size and charge distribution analysis of pharmaceutical aerosols generated by inhalers. Pharmaceutical Development and Technology, 12:35-41.

Saini, D., Gunamgari, J., Zulaloglu, C., Sims, R. A., Mazumder, M. K. (2004a). Effect of electrostatic charge and size distributions on respirable aerosol deposition in lung model. IEEE Industry Applications Conference. 39th IAS Annual Meeting., 2:948-952.

Saini, D., Gunamgari, J., Zulaloglu, C., Sims, R. A., Mazumder, M. K. (2004b). Effect of electrostatic charge and size distributions on respirable aerosol deposition in lung model, in Industry Applications Conference, 2004. 39th IAS Annual Meeting, Seattle, 948-952.

Saini, D., Yurteri, C. U., Grable, N., Sims, R. A., Mazumder, M. K. (2002a). Drug delivery studies on electrostatically charged dry powder inhaler aerosols using a glass bead lung model, in EEE Industry Applications Conference. 37th IAS Annual Meeting, 2451-2453.

Saini, D., Yurteri, C. U., Grable, N., Sims, R. A., Mazumder, M. K. (2002b). Drug delivery studies on electrostatically charged dry powder inhaler aerosols using a glass bead lung model, in Industry Applications Conference, 2002. 37th IAS Annual Meeting, Pittsburgh, PA, 2451-2453.

Sasaki, C. T., Levine, P. A., Laitman, J. T., Crelin, E. S. (1977a). Postnatal Descent of the Epiglottis in Man: A Preliminary Report. Archives of Otolaryngology - Head and Neck Surgery, 103:169-171.

Sasaki, C. T., Levine, P. A., Laitman, J. T., Crelin, E. S. (1977b). Postnatal Descent of the Epiglottis in Man: A Preliminary Report. Archives of Otolaryngology - Head and Neck Surgery, 103:169-171.

Savart, F. (1833). Mémoire sur la constitution des veines liquides lancées par des orifices circulaires en mince paroi. Ann. Chim. Phys, 53:1833.

Schneider, J. M. and Hendricks, C. D. (1964). Source of Uniform-Sized Liquid Droplets. Review of Scientific Instruments, 35:1349-1350.

Schueepp, K. G., Devadason, S. G., Roller, C., Minocchieri, S., Moeller, A., Hamacher, J., Wildhaber, J. H. (2009). Aerosol delivery of nebulised budesonide in young children with asthma. Respiratory Medicine, 103:1738-1745.

Stahlhofen, W., Gebhart, J., Heyder, J. (1980). Experimental determination of the regional deposition of aerosol particles in the human respiratory tract. American Industrial Hygiene Association journal, 41:385-398a.

Stahlhofen, W., Gebhart, J., Heyder, J., Scheuch, G. (1983). New regional deposition data of the human respiratory tract. Journal of Aerosol Science, 14:186-188.

Stahlhofen, W., Gebhart, J., Heyder, J., Scheuch, G., Juraske, P. (1984). Particle deposition in extrathoracic airways of healthy subjects and of patients with early stages of laryngeal carcinoma. Journal of Aerosol Science, 15:215-217.

Stapleton, K. W., Guentsch, E., Hoskinson, M. K., Finlay, W. H. (2000). On the suitability of k–ε turbulence modeling for aerosol deposition in the mouth and throat: a comparison with experiment. Journal of Aerosol Science, 31:739-749.

Storey-Bishoff, J., Noga, M., Finlay, W. H. (2008a). Deposition of micrometer-sized aerosol particles in infant nasal airway replicas. Journal of Aerosol Science, 39:1055-1065.

Storey-Bishoff, J., Noga, M., Finlay, W. H. (2008b). Deposition of micrometer-sized aerosol particles in infant nasal airway replicas. Journal of Aerosol Science, 39:1055-1065.

Tang, K. and Gomez, A. (1994). Generation by electrospray of monodisperse water droplets for targeted drug delivery by inhalation. Journal of Aerosol Science, 25:1237-1249.

Tolman, R. C. (1938). The Principles of Statistical Mechanics. Dover Publications.

Tomaides, M., Liu, B. Y. H., Whitby, K. T. (1971). Evaluation of the condensation aerosol generator for producing monodispersed aerosols. Journal of Aerosol Science, 2:39-46.

Tu, K.-W. (1982). A condensation aerosol generator system for monodisperse aerosols of different physicochemical properties. Journal of Aerosol Science, 13:363-371.

Vehring, R., Foss, W. R., Lechuga-Ballesteros, D. (2007). Particle formation in spray drying. Journal of Aerosol Science, 38:728-746.

Walton, W. H. and Prewett, W. C. (1949). The Production of Sprays and Mists of Uniform Drop Size by Means of Spinning Disc Type Sprayers. Proceedings of the Physical Society. Section B, 62:341-350.

Yu, C. P. (1985). Theories of electrostatic lung deposition of inhaled aerosols. Annals of Occupational Hygiene, 29:219-227.

Zhang, Y., Gilbertson, K., Finlay, W. H. (2007). In vivo–in vitro comparison of deposition in three mouth–throat models with Qvar® and turbuhaler® inhalers. Journal of Aerosol Medicine:227-235.

Zhou, Y., Sun, J., Cheng, Y. S. (2011). Comparison of deposition in the USP and physical mouth-throat models with solid and liquid particles. Journal of Aerosol Medicine and Pulmonary Drug Delivery, 24:277-284.

Appendix A

A.1. Drawings of the Atomizer and Charging Cap

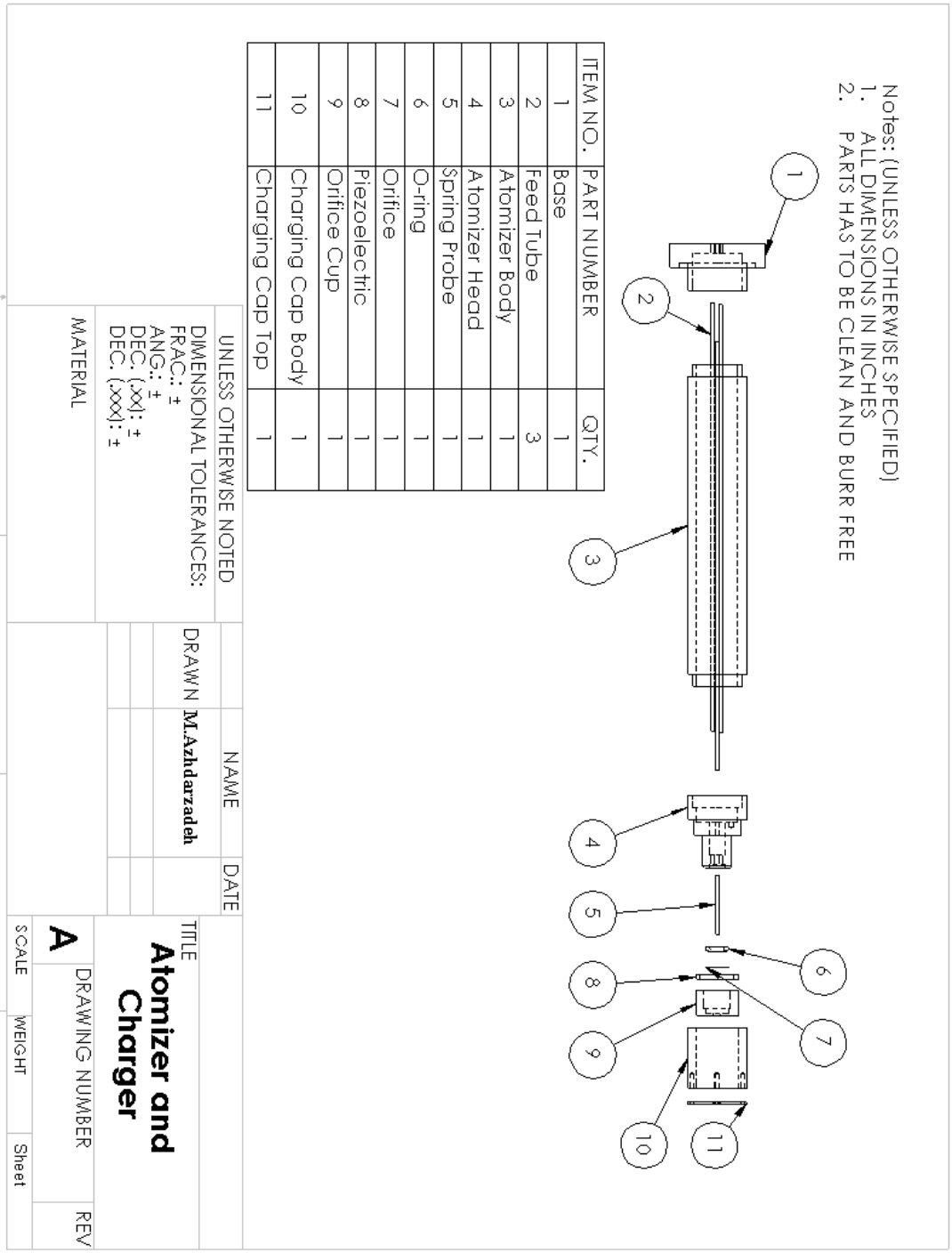

Notes: (UNLESS OTHERWISE SPECIFIED)
1. ALL DIMENSIONS IN INCHES
2. PARTS HAS TO BE CLEAN AND BURR FREE
3. CLEARANCE FIT APPLIES TO ALL MATING PARTS

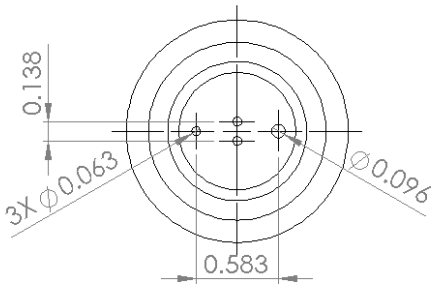

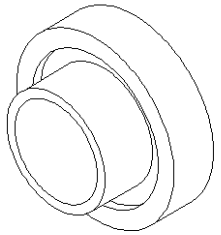

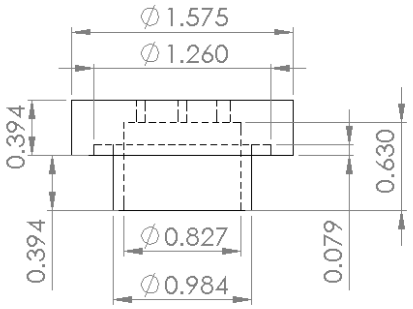

UNLESS OTHERWISE NOTED		NAME	DATE	
DIMENSIONAL TOLERANCES: FRAC.: ±1/32 ANG.: ±0.5 deg DEC. (.xx): ±0.01 DEC. (.xxx): ±0.005	DRAWN	M.Azhdarzadeh		TITLE
MATERIAL: **Stainless Steel**				A DRAWING NUMBER **Base** REV
				SCALE WEIGHT Sheet

5 4 3 2 1

Notes: (UNLESS OTHERWISE SPECIFIED)
1. ALL DIMENSIONS IN INCHES
2. PARTS HAS TO BE CLEAN AND BURR FREE
3. CLEARANCE FIT APPLIES TO ALL MATING PARTS

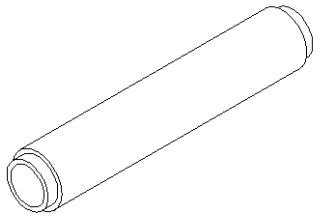

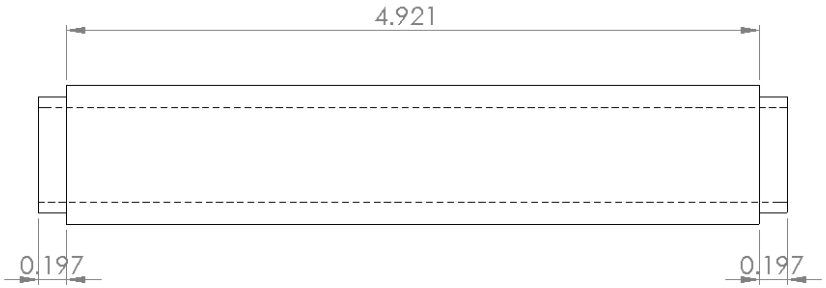

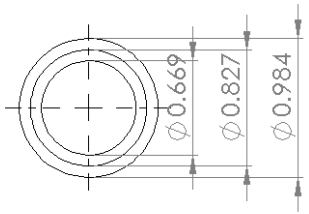

UNLESS OTHERWISE NOTED		NAME	DATE	
DIMENSIONAL TOLERANCES: FRAC.: ±1/32 ANG.: ±0.5 deg DEC. (.xx): ±0.01 DEC. (.xxx): ±0.005	DRAWN	M.Azhdarzadeh		TITLE: **Atomizer Body**
MATERIAL: **Stainless Steel**				A — DRAWING NUMBER — REV
				SCALE — WEIGHT — Sheet

5 4 3 2 1

Notes: (UNLESS OTHERWISE SPECIFIED)
1. ALL DIMENSIONS IN INCHES
2. PARTS HAS TO BE CLEAN AND BURR FREE
3. CLEARANCE FIT APPLIES TO ALL MATING PARTS

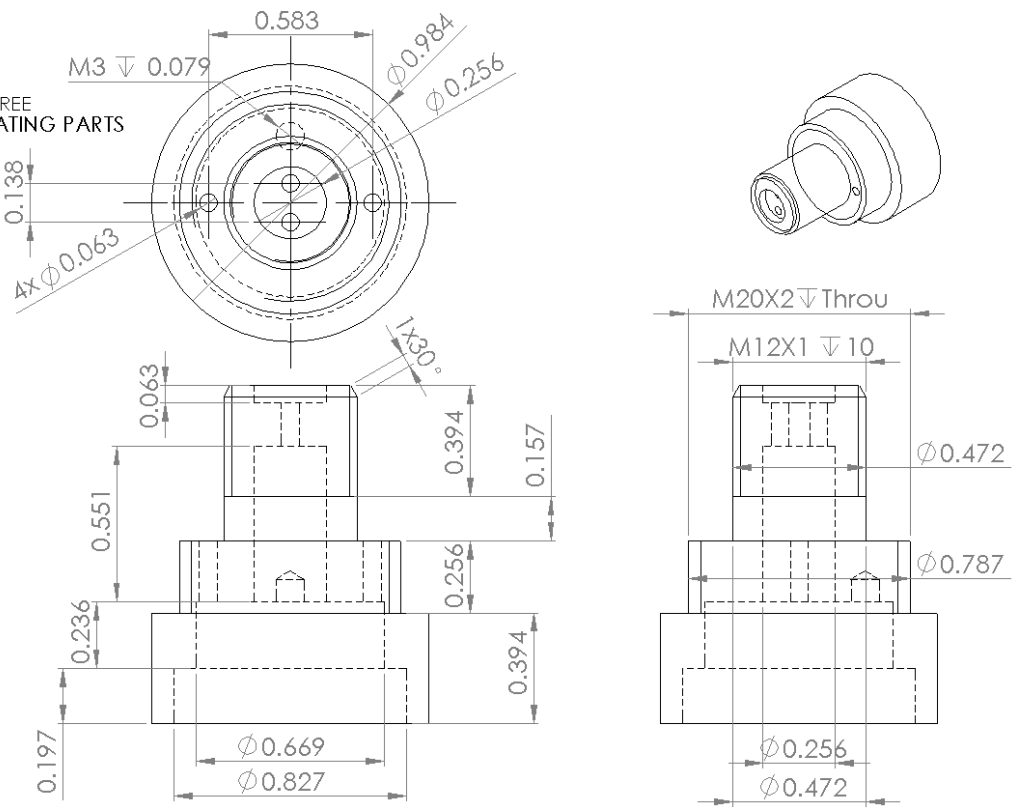

UNLESS OTHERWISE NOTED		NAME	DATE
DIMENSIONAL TOLERANCES: FRAC.: ±1/32 ANG.: ±0.5 deg DEC. (.xx): ±0.01 DEC. (.xxx): ± 0.005	DRAWN	M.Azhdarzadeh	
MATERIAL: **Stainless Steel**			

TITLE
Atomizer Head

A	DRAWING NUMBER	REV
SCALE	WEIGHT	Sheet

5 4 3 2 1

Notes: (UNLESS OTHERWISE SPECIFIED)
1. ALL DIMENSIONS IN INCHES
2. PARTS HAS TO BE CLEAN AND BURR FREE
3. CLEARANCE FIT APPLIES TO ALL MATING PARTS

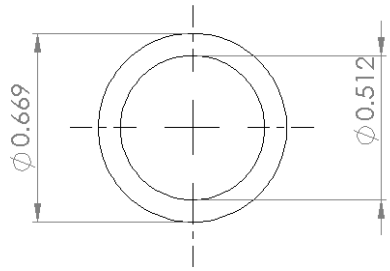

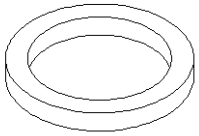

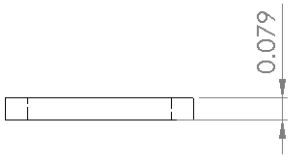

UNLESS OTHERWISE NOTED		NAME	DATE	
DIMENSIONAL TOLERANCES: FRAC.: ±1/32 ANG.: ±0.5 deg DEC. (.xx): ±0.01 DEC. (.xxx): ±0.005	DRAWN	M.Azhdarzadeh		TITLE **Piezoelectric**
MATERIAL: **Ferroperm PiezoCeramics, 105261, Pz26**				A DRAWING NUMBER REV
				SCALE WEIGHT Sheet

5 4 3 2 1

Notes: (UNLESS OTHERWISE SPECIFIED)
1. ALL DIMENSIONS IN INCHES
2. PARTS HAS TO BE CLEAN AND BURR FREE
3. CLEARANCE FIT APPLIES TO ALL MATING PARTS

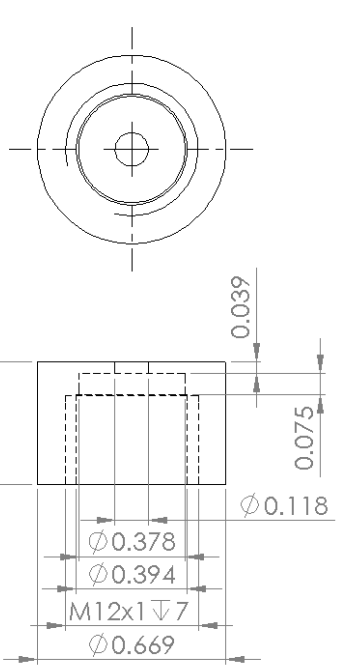

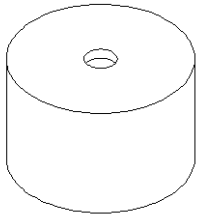

UNLESS OTHERWISE NOTED		NAME	DATE	
DIMENSIONAL TOLERANCES: FRAC.: ±1/32 ANG.: ±0.5 deg DEC. (.xx): ±0.01 DEC. (.xxx): ±0.005	DRAWN	M.Azhdarzadeh		TITLE: **Orifice Cup**
MATERIAL: **Stainless Steel**				A — DRAWING NUMBER — REV
				SCALE — WEIGHT — Sheet

5 4 3 2 1

Notes: (UNLESS OTHERWISE SPECIFIED)
1. ALL DIMENSIONS IN INCHES
2. PARTS HAS TO BE CLEAN AND BURR FREE
3. CLEARANCE FIT APPLIES TO ALL MATING PARTS

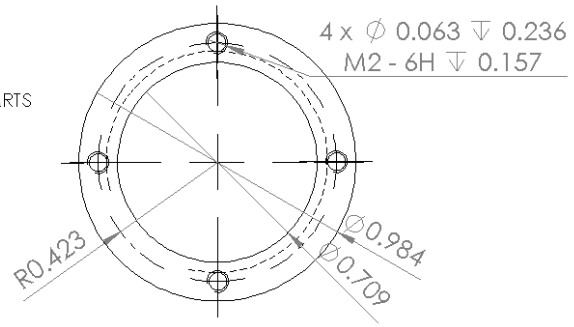

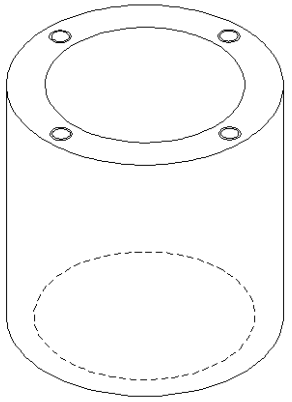

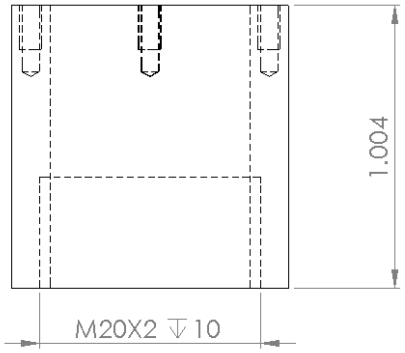

UNLESS OTHERWISE NOTED		NAME	DATE	
DIMENSIONAL TOLERANCES: FRAC.: ±1/32 ANG.: ±0.5 deg DEC. (.xx): ±.01 DEC. (.xxx): ±0.005	DRAWN	M.Azhdarzadeh		TITLE: **Charging Cap Body**
MATERIAL: **Cast Acrylic**				A — DRAWING NUMBER — REV
				SCALE — WEIGHT — Sheet

5 4 3 2 1

Notes: (UNLESS OTHERWISE SPECIFIED)
1. ALL DIMENSIONS IN INCHES
2. PARTS HAS TO BE CLEAN AND BURR FREE
3. CLEARANCE FIT APPLIES TO ALL MATING PARTS

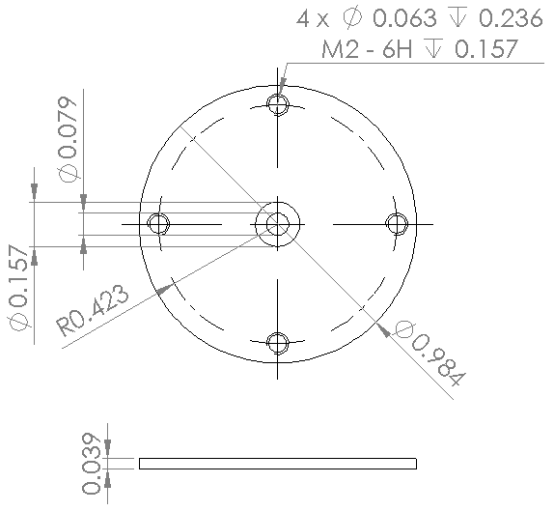

UNLESS OTHERWISE NOTED		NAME	DATE	
DIMENSIONAL TOLERANCES: FRAC.: ±1/32 ANG.: ±0.5 deg DEC. (.xx): ±0.01 DEC. (.xxx): ±0.005	DRAWN	M.Azhdarzadeh		TITLE: Charging Cap Top
MATERIAL: **Stainless Steel**				A — DRAWING NUMBER — REV
				SCALE — WEIGHT — Sheet

5 4 3 2 1

A.2. Parts supplied by manufacturer

- Mini-coaxial cable (Alpha wire, P/N: 9174, USA)
- Piezoelectric (Ferroperm Piezoceramics, 105261, Pz26), modified to the required size by water jet cutting
- 10 μm orifice (TSI, 393520, USA)
- 20 μm orifice (TSI, 393530, USA)
- O-ring (McMaster, Viton® Fluoroelastomer, 2857T116, USA)
- Conductive epoxy glue (EPO-TEK® H20E, PAISLEY, Canada)
- Glue (Henkel, Loctite® 603™ Retaining Compound, Press Fit/Oil Tolerant, 21441, Düsseldorf, Germany)
- Stainless steel seamless tube 1/16 in. (Swagelok, SS-T1-S-014-6ME, USA)
- Metric Viton® Fluoroelastomer O-ring, 1.9 mm width, 5.8 mm ID (McMaster, 9263K639, USA)
- ICT-075 Lead Free Probe (IDI interconnect devices)

A.3. Assembling Parts

	Part A	Part B	Connection Type
1	Base (1)	Atomizer Body (3)	Glued
2	Atomizer Body (3)	Atomizer Head (4)	Glued
3	Spring Probe (5)	Atomizer Head (4)	Insulated by heat shrink tubing and glued to the atomizer head
4	Feed Tubes (2)	Atomizer Head (4)	Silver soldered
5	Feed Tubes (2)	Base (1)	Glued
6	Orifice Cup	Atomizer Head (4)	Threaded connection
7	Charging Cap Body (10)	Atomizer Head (4)	Threaded connection
8	Charging Cap Top (11)	Charging Cap Body (10)	Screw connection
9	Coaxial Cable	Spring Probe (5)	Soldered
10	Coaxial Cable	Atomizer Head (4)	Screw connection (from inside)
11	Piezoelectric (8)	Orifice Cup (9)	Conductive Glue

A.4. Operation, Troubleshooting and Maintenance

Note: This section is prepared based on my observations and personal experience of work with the atomizer and charger and may be updated.

A.4.1. Atomizer

The first step in running the atomizer is choosing the proper orifice size, *D*, and preparing a solution with the right concentration for achieving a given particle size, which depends on the desired particle diameter, d_{p} , and diameter of the orifice. Considering frequent clogging of small orifices, a $20\mu\mathrm{m}$ orifice is recommend for the atomizer. A rough estimate of the initial droplet size is $d_{\mathrm{d}} = 1.89D$ (for more details refer to section 2.2.1 of this thesis), so if a $20\mu\mathrm{m}$ orifice is chosen, the initial droplets would have a geometric diameter of about 37.8 $\mu\mathrm{m}$. As an example, for a particle with desired geometric diameter of 4 $\mu\mathrm{m}$ the diameter reduction for the droplet, after drying, would be $\frac{37.8}{4} = 9.45$. The volume of a spherical droplet is proportional to the cube of the particle diameter, hence the relative volume concentration of the nonvolatile phase to the volatile phase for the required solution would be $(1/9.45)^3 = 1/844$. As already mentioned, these are rough estimates for particle geometric diameter and the required solution concentration. This is due to the fact that these are the values at optimum frequency suggested by Rayleigh (1879). All the reported values in the experiments are measured by an aerodynamic particle sizer (APS 3321, TSI, Minneapolis, USA).

After filling the reservoir with the prepared solution and pressurizing it, open the ball valve before the atomizer and let the jet build up. After successfully establishing the jet, it is required to adjust working parameters of the atomizer, i.e. frequency, amplitude of function generator,

dispersion air and sheath flow (volume flow-rate of spray dryer). To adjust these parameters, a device for monitoring diameter of generated particles such as APS (APS 3321, TSI, Minneapolis, USA) is suggested. The following range of parameters are typical values which were used in this project based on our solution (DEHS in reagent alcohol), orifice size and pressure of the reservoir and should be adjusted for different solutions and working conditions. After setting the amplitude of the function generator to about 2-5 Volt peak to peak and choosing a sinusoidal wave form, try to adjust the frequency of the atomizer (for our cases between 80-140 kHz) and the dispersion air (for our cases between 20-80 psi) until you achieve monodisperse particles while real time monitoring of particles diameter. Keep the sheath flow rate in a range such that the sizer can sample your aerosol close to isokinetic conditions (To avoid biasness in sampling). At high flow rates, due to higher inertial effects (high Stoke numbers) for large particles, they may not be able to follow the stream lines for sampling flow and may hit the wall of the sampling T or avoid being sampled, hence the APS would not show the right distribution. Be advised that finding the working conditions may take a lot of patience and effort. If still the distribution is polydisperse, it can be due to any of the following reasons:

- The function generator is off
- Check the concentration of your solution
- Orifice is half blocked: clean the orifice using the approach which is explained in the maintenance section.
- Failure of electrical connections: Check the connections up to the conductive surface of the piezoelectric by an ohmmeter.
- Make sure the wave form is on sinus wave

- Check the dispersion air and make sure it is not due to droplet coalescence since **dispersion of droplets is a key factor in the process**
- By adjusting sheath flow make sure the problem is not due to a sampling problem
- Check to be sure the piezoelectric is not separated from the head of the atomizer. Some glues may lose their functionality after a long time of being exposed to heat, alcohol and vibration.
- Use high volatile substances such as ethanol as solvent to avoid drying problems (low vapor pressure substances such as water is not recommended)

A.4.2. Charger

To charge particles, it is required to have a conductive solution. To give the required conductivity to the solution of DEHS in reagent alcohol, it is enough to add a very small amount of sodium chloride (NaCl) solution in water to the DEHS solution. The amount of this added solution depends on the desired charge level for particles, electrical potential difference of charger, and the concentration of DEHS solution. As a typical amount, it is preferred to keep the relative volume of NaCl to DEHS as small as possible, i.e. 1/1000 or less to avoid affecting the final particle size. To facilitate drying of particles it is also recommended to keep the volume fraction of NaCl solution in the final solution to about 1% or less. This is mainly because of the lower vapor pressure of water compared to ethanol which makes drying of droplets difficult.

The easiest approach to control the charge of particles is to adjust the voltage of the DC power supply while measuring charge of particles using a Faraday cup. It is highly

recommended to measure charge for each test since many parameters can affect the charge of particles, hence predicting the charge of particles is not usually very accurate.

If the charger stops working, check the following possibilities:

- DC power supply is off
- Failure of electrical connections, check the connections with ohmmeter
- Change your solution

A.4.3. Cautions

- **Never ever touch atomizer before turning DC power supply off.**
- **Charger should not come in contact with any conductive apparatus such as spray dryer body**
- Keep working voltage as low as possible, i.e. 0-20 V, as a safety precaution.

A.4.4. Cleaning a clogged orifice

Note: It is recommended to flush the system to bring down the possibility of orifice blockage

First remove the O-ring holding the orifice in the orifice cup using a pair of tweezers. Then, carefully remove the orifice using a needle, and soak it in a beaker of detergent solution in Deionized Ultra Filtered (DIUF) water. After soaking for a couple of minutes transfer it to another beaker containing DIUF water and soak it again, and finally soak it in ethanol. You can soak the O-ring along with the orifice to keep any contamination away from the system. If the problem persists you can try a sonic bath. To perform the sonic bath, put the orifice in a beaker containing ethanol and expose it very shortly to a sonic bath (approximately less than 6 sec). The sonic bath may cause damages to the orifice, so keep sonication time as short as possible. If

the problem still persists, checking the orifice under the microscope may help to find out the possible problem.

Appendix B

B.1. Drawings of the Faraday Cup

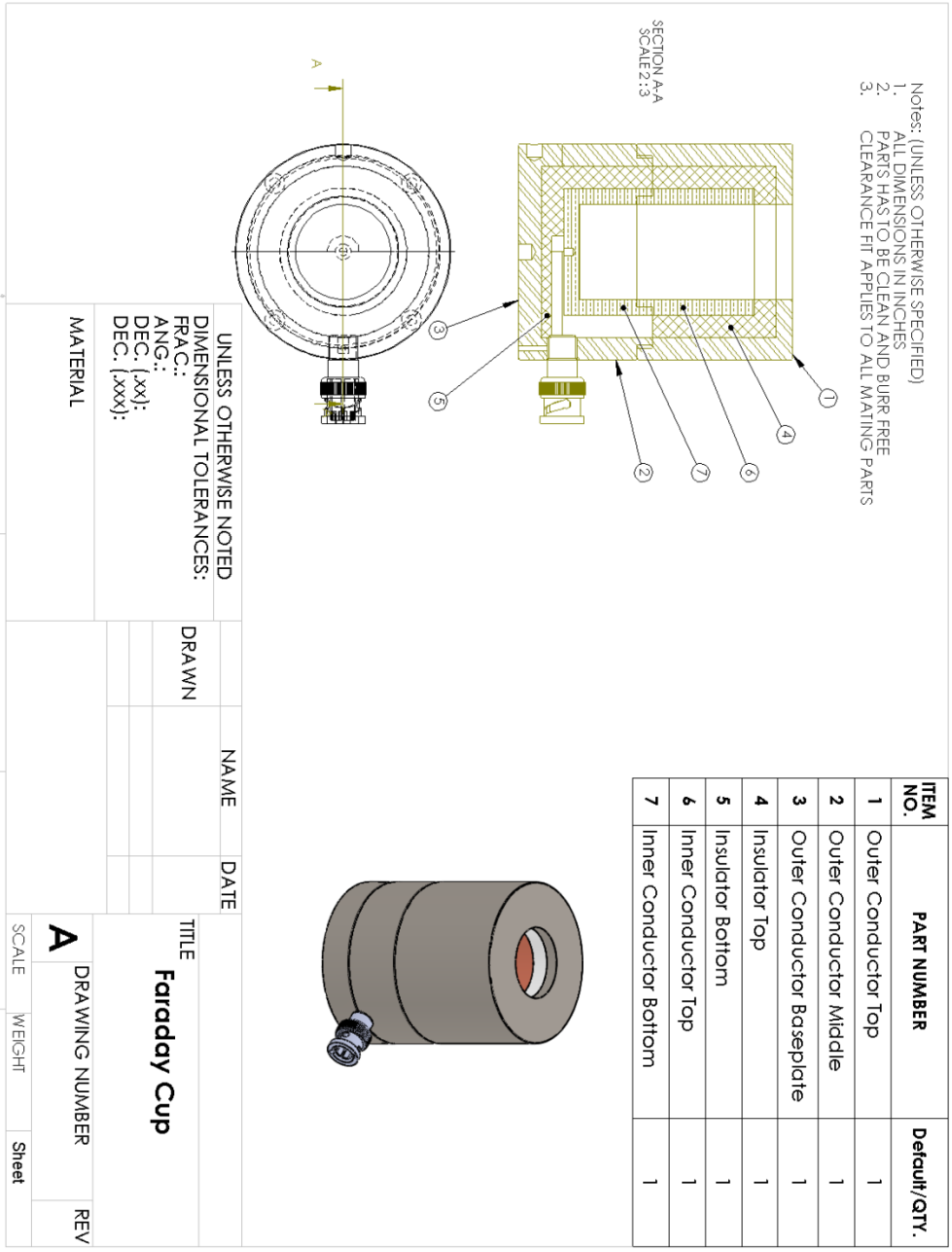

Notes: (UNLESS OTHERWISE SPECIFIED)
1. ALL DIMENSIONS IN INCHES
2. PARTS HAS TO BE CLEAN AND BURR FREE
3. CLEARANCE FIT APPLIES TO ALL MATING PARTS

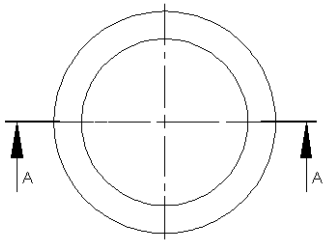

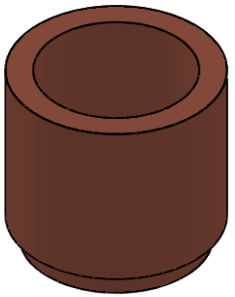

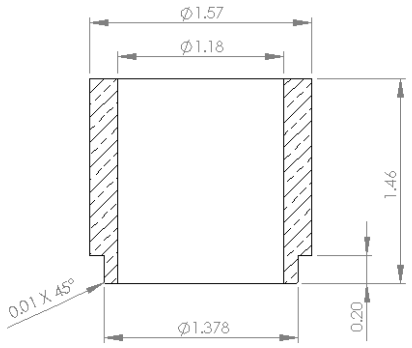

SECTION A-A

UNLESS OTHERWISE NOTED		NAME	DATE	
DIMENSIONAL TOLERANCES: FRAC.: ±1/32 ANG.: ±0.5 deg DEC. (.xx): ±0.01 DEC. (.xxx): ±0.005	DRAWN			TITLE **Inner Conductor Top**
MATERIAL: **Copper**				A DRAWING NUMBER REV
				SCALE WEIGHT Sheet

5 4 3 2 1

Notes: (UNLESS OTHERWISE SPECIFIED)
1. ALL DIMENSIONS IN INCHES
2. PARTS HAS TO BE CLEAN AND BURR FREE
3. CLEARANCE FIT APPLIES TO ALL MATING PARTS

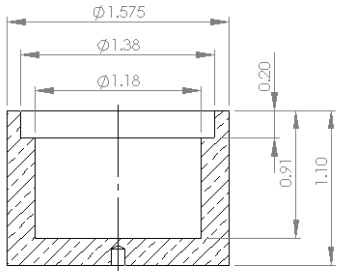

SECTION A-A

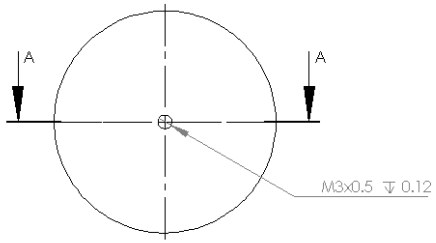

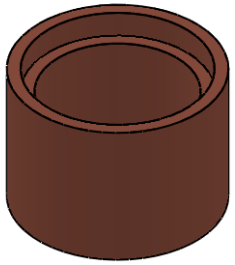

UNLESS OTHERWISE NOTED		NAME	DATE	
DIMENSIONAL TOLERANCES: FRAC.: ±1/32 ANG.: ±0.5 deg DEC. (.xx): ±0.01 DEC. (.xxx): ±0.005	DRAWN			TITLE **Inner Conductor Bottom**
MATERIAL: **Copper**				A DRAWING NUMBER REV
				SCALE WEIGHT Sheet

5 4 3 2 1

Notes: (UNLESS OTHERWISE SPECIFIED)
1. ALL DIMENSIONS IN INCHES
2. PARTS HAS TO BE CLEAN AND BURR FREE
3. CLEARANCE FIT APPLIES TO ALL MATING PARTS

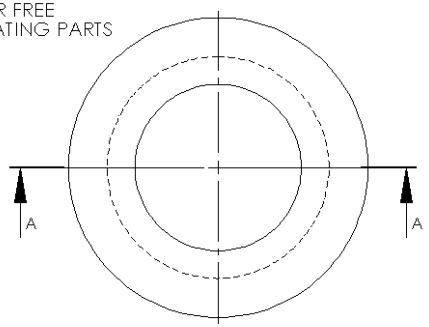

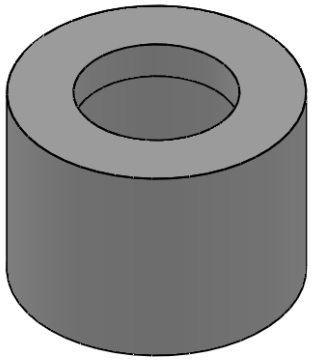

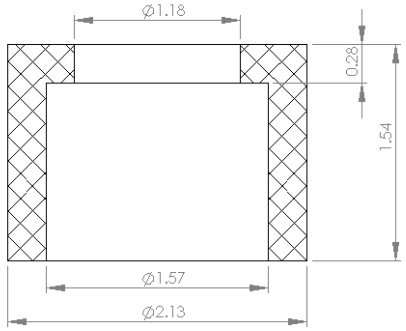

SECTION A-A

UNLESS OTHERWISE NOTED		NAME	DATE	
DIMENSIONAL TOLERANCES: FRAC.: ±1/32 ANG.: ±0.5 DEC. (.xx): ±0.01 DEC. (.xxx): ±0.005	DRAWN			TITLE **Insulator Top**
MATERIAL: **PVC**				A DRAWING NUMBER REV
				SCALE WEIGHT Sheet

5 4 3 2 1

Notes: (UNLESS OTHERWISE SPECIFIED)
1. ALL DIMENSIONS IN INCHES
2. PARTS HAS TO BE CLEAN AND BURR FREE
3. CLEARANCE FIT APPLIES TO ALL MATING PARTS

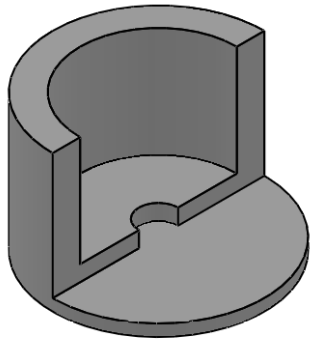

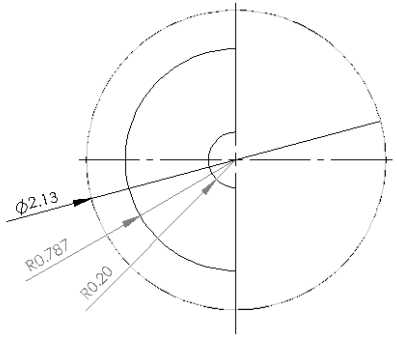

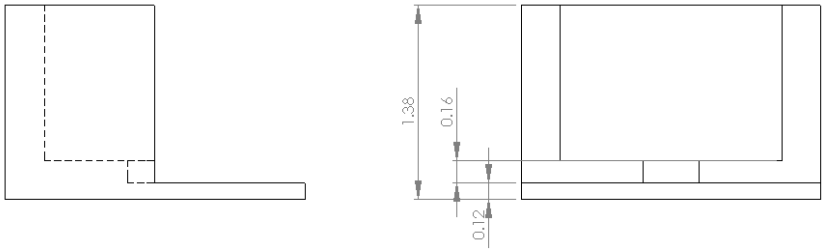

UNLESS OTHERWISE NOTED		NAME	DATE	
DIMENSIONAL TOLERANCES: FRAC.: ±1/32 ANG.: ±0.5 deg DEC. (.xx): ±0.01 DEC. (.xxx): ±0.005	DRAWN			TITLE **Insulator Bottom**
MATERIAL: **PVC**				A DRAWING NUMBER REV
				SCALE WEIGHT Sheet

5 4 3 2 1

Notes: (UNLESS OTHERWISE SPECIFIED)
1. ALL DIMENSIONS IN INCHES
2. PARTS HAS TO BE CLEAN AND BURR FREE
3. CLEARANCE FIT APPLIES TO ALL MATING PARTS

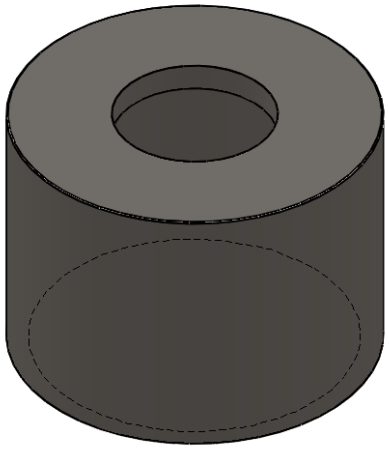

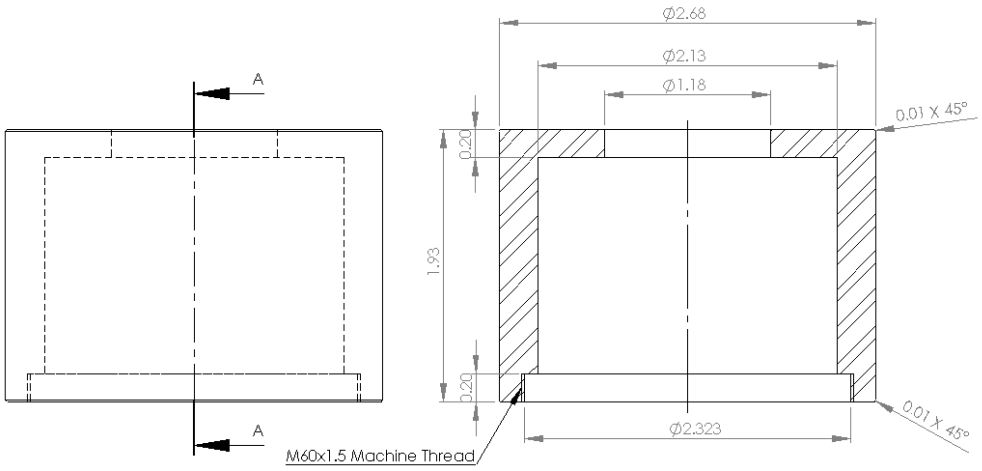

SECTION A-A

UNLESS OTHERWISE NOTED		NAME	DATE	
DIMENSIONAL TOLERANCES: FRAC.: ±1/32 ANG.: ±0.5 deg DEC. (.xx): ±0.01 DEC. (.xxx): ±0.005	DRAWN			TITLE **Outer Conductor Top**
MATERIAL: **Stainless Steel**				**A** DRAWING NUMBER REV
				SCALE WEIGHT Sheet

5 4 3 2 1

Notes: (UNLESS OTHERWISE SPECIFIED)
1. ALL DIMENSIONS IN INCHES
2. PARTS HAS TO BE CLEAN AND BURR FREE
3. CLEARANCE FIT APPLIES TO ALL MATING PARTS

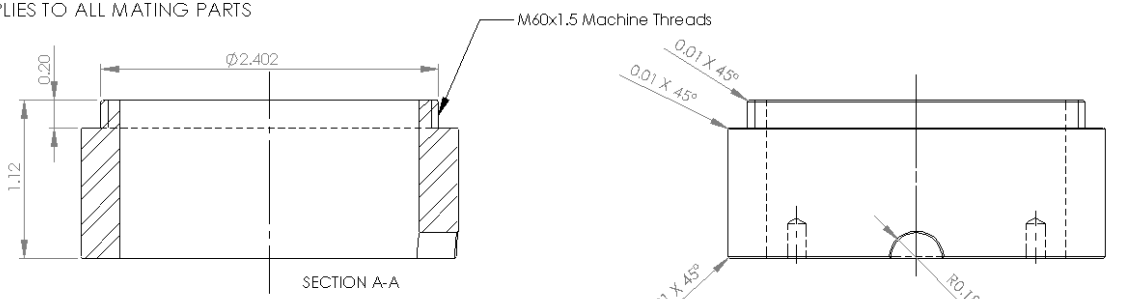

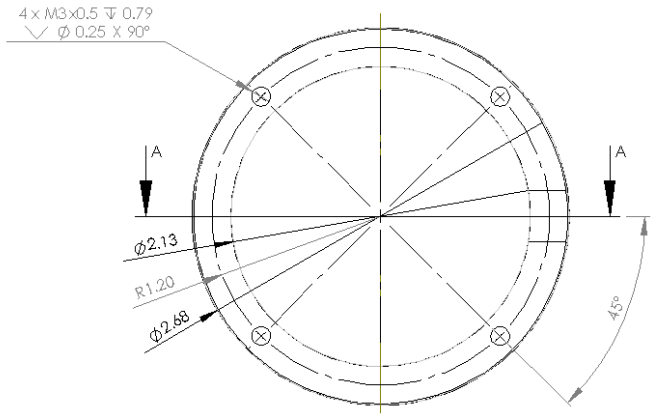

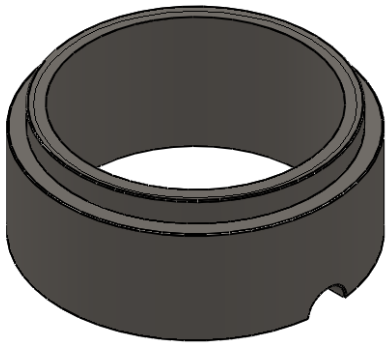

UNLESS OTHERWISE NOTED		NAME	DATE	
DIMENSIONAL TOLERANCES: FRAC.: ±1/32 ANG.: ±0.5 deg DEC. (.xx): ±0.01 DEC. (.xxx): ±0.005	DRAWN			TITLE **Outer Conductor Middle**
MATERIAL: **Stainless Steel**				**A** DRAWING NUMBER REV
				SCALE WEIGHT **Sheet**

5 4 3 2 1

Notes: (UNLESS OTHERWISE SPECIFIED)
1. ALL DIMENSIONS IN INCHES
2. PARTS HAS TO BE CLEAN AND BURR FREE
3. CLEARANCE FIT APPLIES TO ALL PARTS

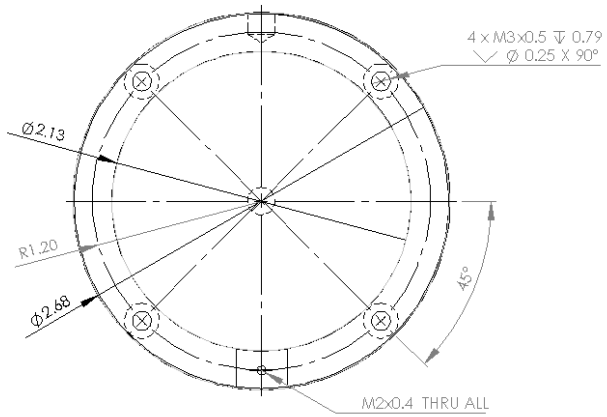

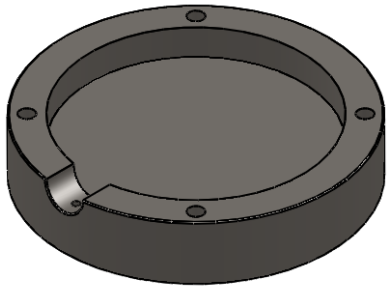

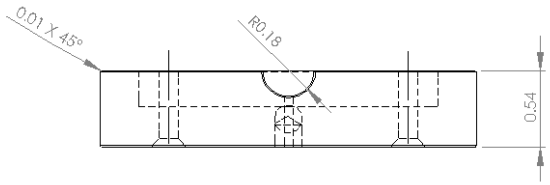

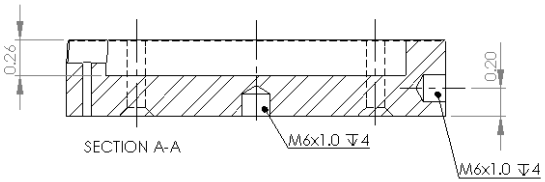

UNLESS OTHERWISE NOTED		NAME	DATE
DIMENSIONAL TOLERANCES: FRAC.: ±1/32 ANG.: ±0.5 deg DEC. (.xx): ±0.01 DEC. (.xxx): ±0.005	DRAWN		
MATERIAL: **Stainless Steel**			

TITLE
Outer Conductor Base

A	DRAWING NUMBER	REV
SCALE	WEIGHT	Sheet

5 4 3 2 1

B.2. Assembling Parts

	Part A	Part B	Connection Type
1	Outer Conductor Top (1)	Outer Conductor Middle (2)	Threaded connection
2	Outer Conductor Middle (2)	Outer Conductor Base (3)	Screw connection
3	Insulator Top (4)	Insulator Bottom (5)	Sliding on inner conductor
4	Inner Conductor Top (6)	Inner Conductor Bottom (7)	Sliding connection
5	BNC Connector Male	Outer Conductor (2) and (3)	Set screw
6	BNC Connector Male	Inner Conductor Bottom (7)	Soldered wire